Model Predictive Control of Power Converters – Theory and Practice

Ricardo Patricio Aguilera Echeverría, MSc

A thesis submitted in fulfilment of the requirements for the degree of

Doctor of Philosophy

School of Electrical Engineering
and Computer Science

The University of Newcastle
Callaghan, N.S.W. 2308
Australia

August, 2012

The UNIVERSITY *of* NEWCASTLE
AUSTRALIA

Declaration

This thesis contains no material which has been accepted for the award of any other degree or diploma in any university or other tertiary institution and, to the best of my knowledge and belief, contains no material previously published or written by another person, except where due reference has been made in the text. I give consent to this copy of my thesis, when deposited in the University Library, being made available for loan and photocopying subject to the provisions of the Copyright Act 1968.

I hereby certify that this thesis is submitted in the form of a series of published papers of which I am a joint author. I have included as part of the thesis a written statement from each co-author; and endorsed by the Faculty Assistant Dean (Research Training), attesting to my contribution to the joint publications.

Ricardo Patricio Aguilera Echeverría

March, 2012

Acknowledgements

This thesis is the product of my research carried out during my Ph.D. studies. This work was accomplished with the help and support of several people.

Firstly, I would like to acknowledge the unconditional love of my wife, Katherine. She has put her dreams on hold to be with me while I pursue mine. In the end it was her support and encouragement that made this thesis possible.

Secondly, I would like to thank the love and suport of my wonderful family: my parents Ricardo and Miroslava and my siblings Ricardo, Martha, Carlos, José, and Cristian. They have always been concerned about my progress and I feel that this achievement belongs to them as well.

I would like to express my most sincere gratitude to my supervisor, Dr. Daniel E. Quevedo for his investment of patience, time, and effort in my work. His patient guidance, encouragement, and advice that he provided throughout my Ph.D studies were key in achieving this thesis. I am also grateful to my co-supervisor Prof. Graham C. Goodwin. He always provided me with very useful advice, especially during some difficult moments which helped me out of the darkness. I thank also to Dr. Terrence Summers for his support with my experimental work.

I cannot forget to mention my good friend and colleague Dr. Pablo Lezana (Universidad Técnica Federico Santa María). Most of my research was possible thanks to his deep knowledge on power electronics. I hope we can keep working together in the future.

Special thanks to Dr. Damián Marelli and Dr. Juan Carlos Agüero for their valuable time to discuss some mathematical issues related to my research.

I also want to thank to Hope Sneddon for the time she dedicated to the editing of the

thesis and her patience when explaining to me some English grammar. I will never forget the Oxford comma.

Throughout this journey, I have made several friends who have made my PhD experience much more enjoyable. Special thanks to Aaron Hector, Alain Yetendje, Alejandro Donaire, Ali Mohammadi, Anthony Laskovski, Aurélio Salton, Boris Godoy, Diego Carrasco, Eduardo Rohr, Erik Henriksson, Fernando López-Caamal, Germán Castellanos, He Messi Kong, Isabel Jurado, Marcus Reble, Mauricio Cea, Pierre de Lamberterie, Raheleh Nazari, Ramón Delgado, Rodrigo Carvajal, Sonja Stüdli, Steffi Knorn, and Xin Tai.

Finally, I thank the University of Newcastle, the Australian Government, and the Chilean Government for the financial support that allowed me to come to Australia and pursue a Ph.D. degree.

A mi amada Katherine,
por su incondicional amor.

List of Publications Included as Part of the Thesis

This thesis is presented in the form of a series of published and submitted publications which are listed below in order of appearance in the thesis.

[P1] P. Lezana, R. P. Aguilera, and D. E. Quevedo, "Model Predictive Control of an Asymmetric Flying Capacitor Converter," *IEEE Transactions on Industrial Electronics,* vol. 56, no. 6, pp. 1839–1846, 2009.

[P2] D. E. Quevedo, R. P. Aguilera, M. Pérez, P. Cortés, and R. Lizana, "Model Predictive Control of an AFE Rectifier with Dynamic References," *IEEE Transactions on Power Electronics,* vol. 27, no. 7, pp. 3128–3136, 2012.

[P3] R. P. Aguilera, P. Lezana, and D. E. Quevedo, "Finite-Control-Set Model Predictive Control with Improved Steady-State Performance," *IEEE Transactions on Industrial Informatics,* to appear on 2013.

[P4] R. P. Aguilera, D. E. Quevedo, T. J. Summers, and P. Lezana, "Predictive control algorithm robustness for achieving fault tolerance in multicell converters," *in the 34th Annual Conference of IEEE Industrial Electronics Society, IECON 2008,* Orlando, Florida, Nov. 2008.

[P5] R. P. Aguilera and D. E. Quevedo, "Stability Analysis of Quadratic MPC with a Discrete Input Alphabet," submitted for journal publication.

[P6] R. P. Aguilera and D. E. Quevedo, "Finite Control Set MPC for Power Converters: Stability and Performance," submitted for journal publication.

Contents

Abstract

This thesis studies the use of model predictive control (MPC) to handle power converters. The focus is on technical and theoretical issues regarding the use of a particular class of predictive strategy called Finite Control Set MPC (FCS-MPC). The main advantage of this predictive strategy comes from the fact that switching actions are explicitly taken into account as constraints on the control input of the system in the problem formulation. Consequently, modulation stages (to handle the converter switches) are not required.

Throughout this thesis, we illustrate how to implement this predictive technique to improve the performance, in terms of power quality and dynamic response, in some classes of power converters. We show that FCS-MPC allows power converters to operate near to their limits of achievable performance when.

In this thesis we also show that the benefits of using FCS-MPC can be obtained not only to handle power converters under normal operating conditions but also to achieve fault tolerance of these devices.

Additionally, in this thesis we present a presented a stability analysis of MPC for linear time-invariant (LTI) systems with discrete input alphabets. Based on our theoretical results, we also analysed stability and performance of power converters when governed by FCS-MPC. The latter study is focused on power converters that can be modelled as LTI systems with quantised inputs.

1

Introduction

Advances in the field of power electronics have allowed engineers to manipulate electrical energy like no other power source. This flexibility has allowed the use of electrical power to spread to different industrial and residential applications, becoming a vital element of modern society [1].

In general, standard electrical power sources provide energy with constant voltage amplitude and constant frequency. However, some applications require this kind of energy with different electrical parameters. In power electronics, the process to adapt the electrical characteristic of the power supply in order to meet the application necessities is called *power conversion*, while the technology which makes this possible is called *power converter*. More precisely, power converters are electronic devices which transfer energy from an available electrical power source to the electrical load changing the electrical characteristic (voltage magnitude and/or frequency) of the source to satisfy the electrical load requirements. The power range that power converters cover is from a few milliwatts (e.g., in mobile phones) to megawatts (e.g., for high voltage DC transmission) [2,3]. It is for this reason that power converters have played an important role in the expansion of the use of electrical power in a wide variety of application areas, including energy, transportation, communication, medicine, mining (see [4–9]).

To meet dynamic load requirements, it is necessary to handle the power converter automatically. Thus, a key element in the power conversion, in terms of power quality and dynamic response, is the choice of a suitable automatic controller. It is in this area that

predictive control has emerged as a promising control strategy [10, 11].

Model Predictive Control (MPC) has been, for several decades, a fertile area of research reaching significant success in industry. This popularity comes from the fact that constraints and non-linearities are explicitly taken into account in the problem formulation, thereby allowing processes to operate close to their limits of achievable performance [12,13].

The focus of this thesis is on the control of power converters using a particular class of predictive strategy called *Finite Control Set MPC* (FCS-MPC) [10, 11, 14]. Throughout this thesis, we will show that this predictive control formulation can improve the performance of power converters when compared to traditional modulation based control techniques.

Despite the good performance that FCS-MPC potentially offers, there still remains several open problems; one of the most important being the lack of stability guarantees. Motivated by this problem, this thesis also presents a theoretical analysis to establish stability of FCS-MPC. This study is addressed for MPC of linear time-invariant (LTI) systems with quantized inputs. Therefore, these results can also be used in other areas where quantisations are present.

To put the work in context, we next give a brief review on the main control techniques used to handle power converters focusing primarily on standard modulation based control and MPC.

1.1 Control of Power Converters

To adapt the electrical characteristic of the power source, modern power converters utilise solid-state switches to synthesize the desired voltage to be applied to the electrical load. The quality of the electrical power generated by the power converter depends on the electrical topology (i.e., the array of power switches) and the commutation strategy used to handle the switches. It is for this reason that power converters have been in constant development not only to obtain new advantageous architectures, but also to improve the control techniques used [15–17].

1.1.1 Traditional Control of Power Converters

In standard approaches, the power converter is considered as the actuator which applies the required voltage given by the controller to achieve the control targets. However, due to the nature of these systems, power converters can provide only a finite number of voltage levels. For this reason, a modulation stage to synthesize the required converter output voltage, in an average fashion, is normally included. The standard modulation based control loop for power converters is depicted in Fig 1.1.

The most common switching strategy utilised to synthesize the required converter output voltage, $v(k)$, is the so-called pulse width modulation (PWM) technique [18,19]. Here, the controller provides a modulation index, $m(k)$, which is used by the modulator to handle the converter switches, $S(k)$, in order to obtain an average value of the required voltage, $v(k)$, in a switching period.

The main advantage of using a modulation stage comes from the fact that control targets related to the electrical load and the manipulation of the converter switches to achieve these goals are decoupled. Here, one can assume that the power converter can provide any voltage inside a range, i.e., $v(k) \in [v_{\min}, v_{\max}]$. Therefore, one can implement any control technique capable to deal with bounded inputs. Nevertheless, the control goals will only be achieved in terms of average values.

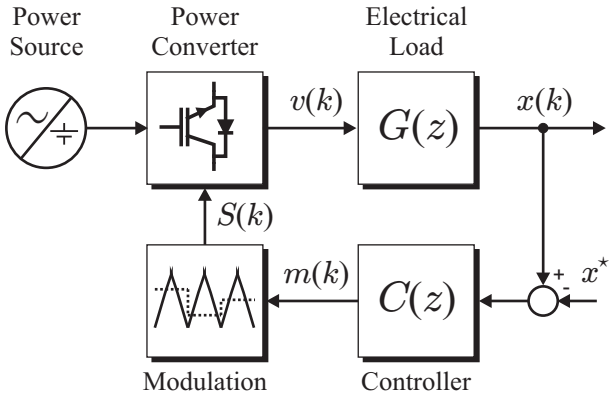

Figure 1.1: Standard modulation based control scheme for power converters.

In regards to the controller, several control techniques have been implemented in order to obtain good performance in terms of dynamic response and power quality. The most popular being the proportional-integral (PI) controller. This is due to the fact that, since it is a well established controller with a solid underpinnings, there exist several tools to design it in order to obtain a desired performance. However, in cases where multivariable control is required and constraints and non-linearities are present, performance losses are inevitable.

To improve the performance obtained by the classic approach presented above, several classes of control techniques have been proposed to handle power converters, such as fuzzy logic, neural networks, sliding mode, and predictive control [10, 20–23]. In particular, the latter has attracted significant attention in the power electronics community, as evidenced by the several predictive control techniques proposed, showing that these methods can outperform traditional PWM based control strategies in several applications [10,14,24–26].

1.1.2 Model Predictive Control

MPC or Receding Horizon Control (RHC) [12, 13] is a control technique which calculates the control action by solving, at each sampling instant, an optimal control problem over a finite horizon. To do this, MPC uses a dynamic model of the system to forecast the future system behaviour from the current system state. This generates an optimal control sequence. Finally, the control action to be applied to the plant is the first element of this sequence. The main advantage of MPC is that constraints and non-linearities can be included in the optimisation. Nevertheless, a large amount of calculation is required to obtain the optimal control sequence. For this reason, MPC is not yet used widely in practical power converters [14]. We next show some variations of MPC which have been considered for the control of power convertes.

Generalised Predictive Control

To overcome difficulties in obtaining the optimal input, the so-called Generalised Predictive Control (GPC) method can be used [27]. Here, the optimal problem is solved in two parts. First, a predicted *free response* is obtained assuming that a constant control action of *zero* is applied during the whole prediction horizon. Then, a *forced response* is obtained by solving the optimisation problem considering the free response predictions. Thus, the optimal input is obtained (for the linear case) by combining both results. However, solving the optimal problem when constraints and non-linearities are included can result in a formidable task. Additionally, GPC provides a non-quantised voltage as a solution, thus in practice, a modulation stage is still required.

Piecewise Affine MPC

An interesting alternative approach for MPC for power converters can be found in [28, 29]. Here, the authors proposed to model the converter as a hybrid system by deriving a piecewise affine (PWA) model. This is carried out by using a so-called ν-resolution approximation of the switch commutation within a switching period. Afterwards, based on this model, a constrained MPC problem is solved offline using dynamic programming [30]. The benefit of this approach comes from the fact that the optimal controller is implemented through a lookup table. Nonetheless, deriving the optimal controller is rather complex and the lookup table can easily comprise 50 or more entries making it unattractive for some applications.

Finite Control Set MPC

One of the most popular predictive algorithms for power converters is FCS-MPC [10, 14] (sometimes also referred to as *Direct MPC*, see [25]). The main advantage of this predictive strategy comes from the fact that switching actions are explicitly taken into account as constraints on the control input of the system. Consequently, modulation stages (to handle

the converter switches) are not required. In Fig 1.2 a closed-loop block diagram of this class of predictive strategy is presented.

To obtain the optimal switching action to be applied to the converter, a cost function which considers the future predictive behaviour of the system as a function of the inputs (converter switches) is used. These forecasts are obtained from a discrete-time model of the converter along with the electrical load. Thus, the cost function is evaluated at each sampling instant by exploring all the allowable switch combinations. Finally, the optimal switching action to be applied in the next sampling instant is the one that minimises the proposed cost function. The popularity of this predictive strategy comes from the fact that when a one-step horizon is considered, the optimal problem can be easily solved online, making this strategy one of the most attractive predictive strategies in practice [11, 14]. It is well known that choosing lager prediction horizons, in general, gives better closed-loop performance than choosing short ones [12, 13]. Unfortunately, for FCS-MPC, obtaining the optimal input sequence requires one to solve a combinatorial optimisation problem. This limits the use of larger horizons in practical applications.

As evidenced in the literature, FCS-MPC has proved to be an interesting alternative to handling power converters. Nevertheless, there still remain some unsolved issues. They are as follows:

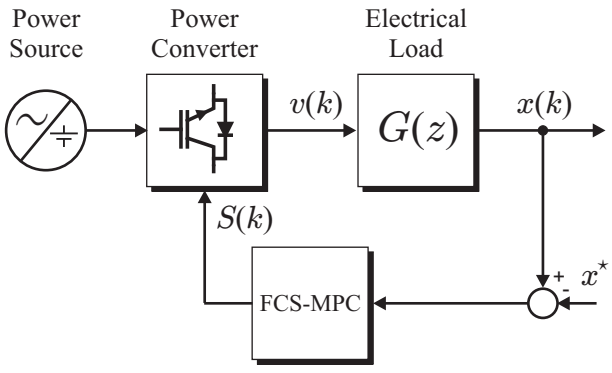

Figure 1.2: FCS-MPC scheme for power converters.

1. MPC has the potential to drive processes near limits of achievable performance. For some applications, this has not been achieved yet.

2. So far, the literature has shown the benefits of using FCS-MPC to control power converters under normal operating conditions. Nonetheless, the use of FCS-MPC to achieve fault tolerance in power converters has not been investigated.

3. One of the main open problems for FCS-MPC is the lack of stability guarantees. This constitutes a major weakness of this control paradigm.

1.2 Main Contribution of this Thesis

This thesis focuses on the technical and theoretical issues regarding the use of FCS-MPC in power electronics. We will illustrate how to implement this predictive technique to improve the performance, in terms of power quality and dynamic response, in some classes of power converters. Additionally, we present a stability analysis of MPC for LTI systems with quantised inputs. Our results can be used as a framework to develop stabilising predictive strategies for power converters.

1.2.1 Extending the Performance of Power Converters

To illustrate the benefits of using FCS-MPC, we implement this predictive control strategy to two different kind of topologies.

Multicell Converters

This class of power converters belongs to the *Multilevel Converter* family. In order to generate the different output voltage levels, this converter utilises electrically floating capacitors. It is for this reason that this topology is also known as *Flying Capacitor Converter (FCC)*. To achieve the multilevel characteristic it is necessary to control not only the output current, but also the internal floating capacitor voltages. The dominant strategy to handle FCCs is the so-called phase-shifted PWM (PS-PWM). This modulation

technique allows floating capacitors to achieve a *voltage balance* in a natural manner. However, since this is an open-loop strategy, the obtained dynamics, in general, are too slow [31, 32]. In this thesis we will show that using FCS-MPC allows one to achieve this control goal with a faster dynamic response than those obtained using standard PWM based strategies. Additionally, we also show that with this predictive strategy one can extend the number of output voltage levels by changing the *traditional ratio* of the floating capacitor voltages obtained with PS-PWM. This allows one to increase the number of output voltages levels without adding more cells.

Active Front End Rectifiers

When compared to traditional diode-based rectifiers, Active Front End (AFE) rectifiers allow one to obtain sinusoidal input currents with low harmonic distortion, whilst at the same time providing a regulated dc-voltage. In the literature, several predictive strategies have been proposed to control the active and reactive power in the ac-side of the rectifier. However, to regulate the dc-link voltage, a second control loop based on a PI controller is still used [33, 34]. In this thesis we propose to derive compatible dynamic references for the dc-voltage and the active power in order to smoothly achieve the control goals. This allows one to implement the FCS-MPC strategy without requiring additional control loops.

Continuos-Time Performance

As already stated, the control target of FCS-MPC is to minimize the system tracking error produced at each sampling instant. Consequently, the predictive controller will optimize the *at sample response* of the converter. However, since the system states are continuous, e.g., output current, the converter may achieve a poor continuous-time performance. Therefore, it is important to analyse the continuous-time response of the controlled converter when using the discrete-time control laws such as FCS-MPC. To address this problem, in this thesis we propose to incorporate the predicted continuos-time sys-

tem behaviour in the cost function. To facilitate the understanding of the problem and the proposed solution, a simple architecture consisting in the output current control of a four-quadrant chopper converter is considered.

1.2.2 Fault Tolerant FCS-MPC for FCCs

An important feature of FCCs is their ability to contain internal faults, due to the fact that the associated capacitors seek voltage balance [35]. In this thesis we propose to use FCS-MPC for achieving fault tolerance in FCC. The fault is identified through the measurement of the output voltage. To do this, a suitable constraint on the switch sequence transition is imposed. Whenever faults are detected, the proposed controller isolates the faulty cell and adapts capacitor voltage references in order to maintain the number of output voltage levels. The results obtained show that the proposed FCS-MPC strategy provides output voltage characteristics, which closely resemble those obtained under normal operating conditions. This is an important result which shows that FCS-MPC can outperform standard PWM control strategies by achieving fault tolerance.

1.2.3 Closed Loop Stability of FCS-MPC for Linear Systems

While stability of convex MPC formulations is relatively well understood, less is known in the finite alphabet case. In [36], stability analysis of a receding-horizon formulation for LTI systems with quantised inputs has been presented. The focus of [36] is on characterising the region of attraction of the predictive controller. The stability analysis in [37] is based on designing a *final state weighting* term using an algebraic Lyapunov equation. The main disadvantage of the stability analyses in [36, 37] is their limitation to open-loop stable systems. Moreover, the origin is required to belong to the control alphabet. Nonetheless, as will be shown in this thesis, this is not the case for most power electronics applications. Therefore, the analyses presented in [36, 37] can not be, in general, applied in power electronic.

Motivated by the lack of stability guarantees of FCS-MPC, in this thesis we present a

stability analysis of MPC for LTI systems with a discrete (finite) input alphabet. A key observation is that when system inputs are restricted to belong to a discrete (finite) set, in general, the best one can hope for is to obtain bounded state trajectories. Therefore, we will focus on practical stability, i.e., ultimate boundedness of solutions. To do this, we consider the (quadratic) MPC cost function as a candidate practical-Lyapunov function and design the terminal cost by using an algebraic Riccati equation. As will be shown in this thesis, our analysis can be applied to both open-loop stable and open-loop unstable LTI systems. It is important to emphasise that our results are not limited only to power converters; in fact, they can be used in any application where the inputs are affected by a quantisation process.

Furthermore, we show how to design a quadratic cost function in order to guarantee the stability of FCS-MPC when it is applied to a specific class of power converters. The key idea of our proposal is to model power converters as LTI systems with a quantised input. Thus, our stability results of MPC for LTI systems with discrete (finite) set can be applied to guarantee practical stability and characterize the performance of the controlled converter.

1.3 Thesis Overview

This thesis is presented in the form of a series of published and submitted manuscripts where each chapter is self-contained. This work is comprised of two major parts: (i) applications of FCS-MPC in power converters (Chapters 2, 3, and 4) and (ii) stability analysis of MPC with discrete (finite) control set (Chapters 5 and 6). The chapters are summarised as follows:

Chapter 2

In this chapter, FCS-MPC strategy is implemented to control a three-cell FCC in order to extend the output voltage levels. This is achieved by changing the traditional ratio of the flying capacitor voltages. For this configuration, one can obtain 4 different voltage levels

when using the standard phase-shifted PWM technique. With our proposal, it is possible to extend this to a maximun of 8 different voltage levels, even for high power factor loads. Experimental results are provided to illustrate the benefits of our proposal.

Chapter 3

In this chapter a predictive control strategy for of AFE is proposed. The diference of our proposal when compared to previous predictive algorithms for AFEs is the fact that it does not require a second control loop to regulate the dc-voltage. The key novelty of our approach lies in the way that compatible dynamic references for the dc-voltage and the active power are derived in order to smoothly achieve the control goals. To validate the proposed predictive strategy, experimental results are provided.

Chapter 4

The continuous-time performance obtained when power converters are governed by FCS-MPC is analysed in this chapter. Here, it is shown that FCS-MPC, in general, provides a non-zero steady-state error. This is due to the fact that this predictive strategy only seeks to minimise the system tracking error at the sampling instants. To overcome this problem, we propose to modify the cost function in order to take into account the continuous-time behaviour of the system also during the inter-sampling times. As an illustrative example, we analyse the continuous-time behaviour of a four-quadrant chopper when governed by FCS-MPC. Experimental and simulation results are provided to illustrate the benefits our proposal.

Chapter 5

Here, a predictive formulation for achieving fault tolerance in FCC is presented. The idea of this application is to detect and identify internal cell faults by only taking measurement of the converter output voltage. To make the internal fault observable, a suitable constraint on the switch sequence transition is imposed in the optimal problem. This allows the controller to identify and isolate the faulty cell. As a remedial action, the proposed

controller adapts the capacitor voltage references in order to maintain the original number of output voltage levels. The results obtained show that the proposed predictive strategy provides output voltage characteristics which closely resemble those obtained under normal operating conditions.

Chapter 6

As already summarised in Chapters 2, 3, 4, and 5, throughout this thesis we show that FCS-MPC is an interesting alternative to handle power converters. However, stability of this strategy still remains as an open problem. Motivated by this issue, in this chapter we present a stability study of MPC with a quadratic cost function for LTI systems with a discrete input alphabet. Since these kinds of systems may present a steady-state error, the focus is on practical stability, i.e., ultimate boundedness of solutions. To derive sufficient conditions for practical stability and characterise the ultimately invariant set, we adapt tools used for convex MPC formulations.

Chapter 7

Here, a stability and performance analysis of FCS-MPC for power converters is presented. This study is based on the results presented in Chapter 6. The key idea of our analysis is to model power converters as LTI systems with quantised inputs. Therefore, it is possible to use Lyapunov stability concepts to design the MPC cost function in order to guarantee practical stability and characterise the performance of the controlled converter. In addition, we also establish bounds on the steady state behaviour of such systems. As illustrative examples, we apply our results to two converters topologies, namely, a buck dc-dc converter, and a two-level dc-ac inverter.

Chapter 8

A summary of the contributions of this thesis and a discussion on future directions for the research are presented in this chapter.

1.4 Publications

The following list presents the author's contributions to the literature in the area of power electronics as a result of the research carried out to produce this thesis.

Journal Papers

[JP1] P. Lezana, R. P. Aguilera, and D. E. Quevedo, "Model Predictive Control of an Asymmetric Flying Capacitor Converter," *IEEE Transactions on Industrial Electronics,* vol. 56, no. 6, pp. 1839–1846, 2009.

[JP2] D. E. Quevedo, R. P. Aguilera, M. Pérez, P. Cortés, and R. Lizana, "Model Predictive Control of an AFE Rectifier with Dynamic References," *IEEE Transactions on Power Electronics,* vol. 27, no. 7, pp. 3128–3136, 2012.

[JP3] R. P. Aguilera, P. Lezana, and D. E. Quevedo, "Finite-Control-Set Model Predictive Control with Improved Steady-State Performance," *IEEE Transactions on Industrial Informatics,* to appear on 2013.

[JP4] R. P. Aguilera and D. E. Quevedo, "Stability Analysis of Quadratic MPC with a Discrete Input Alphabet," submitted for journal publication.

[JP5] R. P. Aguilera and D. E. Quevedo, "Finite Control Set MPC for Power Converters: Stability and Performance," submitted for journal publication.

Peer-Reviewed Conference Papers

[CP1] R. P. Aguilera, D. E. Quevedo, T. J. Summers, and P. Lezana, "Predictive control algorithm robustness for achieving fault tolerance in multicell converters," *in the 34th Annual Conference of IEEE Industrial Electronics Society, IECON 20008,* Orlando, Florida, Nov. 2008.

[CP2] P. Lezana, R. P. Aguilera, and D. E. Quevedo, "Steady-state issues with finite control set model predictive control," *in the 35th Annual Conference of IEEE Industrial Electronics Society, IECON 2009,* Porto, Portugal, Nov. 2009.

[CP3] R. P. Aguilera and D. E. Quevedo, "Predictive control formulation for achieving a reduced finite control set in flying capacitor converters," *in Proceedings of the 10th European Control Conference,* Budapest, Hungary, 2009.

[CP4] R. P. Aguilera and D. E. Quevedo, "Capacitor voltage estimation for predictive control algorithm of flying capacitor converters," *in the IEEE International Conference on Industrial Technology, ICIT 2009,* Melbourne, Australia, 2009.

[CP5] R. P. Aguilera, D. E. Quevedo, and P. Lezana, "Predictive control of an Asymmetric Multicell Converter with floating cells," *in the IEEE International Symposium on Industrial Electronics, ISIE 2010,* Bari, Italy, 2009.

[CP6] R. P. Aguilera and D. E. Quevedo, "On stability of Finite Control Set MPC strategy for Multicell Converters," *in the IEEE International Conference on Industrial Technology, ICIT 2010,* Viña del Mar, Chile, 2010.

[CP7] D. E. Quevedo, R. P. Aguilera, M. A. Pérez, and P. Cortés, "Finite control set MPC of an AFE rectifier with dynamic references," *in the IEEE International Conference on Industrial Technology, ICIT 2010,* Viña del Mar, Chile, 2010.

[CP8] R. P. Aguilera and D. E. Quevedo, "On the stability of MPC with a Finite Input Alphabet," *in Proceedings of the 18th IFAC World Congress,* Milano, Italy, 2011.

[CP9] R. P. Aguilera and D. E. Quevedo, "On stability and performance of finite control set MPC for power converters," *Workshop on Predictive Control of Electrical Drives and Power Electronics (PRECEDE) 2011,* Munich, Germany, 2011.

[CP10] R. P. Aguilera and D. E. Quevedo, "A Switched Model Predictive Control Formulation for Flying Capacitor Converters," accepted to be presented *in the 15th International Power Electronics and Motion Control Conference, EPE-PEMC 2012,* Novi Sad, Serbia, 2012.

2

Model Predictive Control of an Asymmetric FCC

2.1 Introduction

By using medium voltage semiconductors, Multilevel converters are capable of attaining the high power levels required by nowadays industrial applications, see, e.g., [38–41] and the many applications reported in [42–47]. One of the most important Multilevel converter topologies is the Flying Capacitor Converter (FCC), also known as Multicell [40]. This topology and its derivations have been the focus of many works [31, 48, 49], most of them related with flying capacitor voltage balance (or control). For example, in [31] it has been demonstrated that in steady-state operation, and using Phase-Shifted Pulse-Width-Modulation (PS-PWM), the capacitor voltage of cell n tends to stabilize its value at n p.u., where 1 p.u. corresponds to the voltage of cell 1 capacitor (see Fig. 2.1).

In [50] it has recently been shown how the natural balancing process can be significantly accelerated by actively controlling the capacitor voltages using Finite-Control-Set Model Predictive Control (FCS-MPC). As in other MPC algorithms, see, e.g., [51–54], in [50] the actuation signal is chosen to minimize a cost function, which quantifies a tracking error. A key aspect of FCS-MPC, as used in [50, 55–57], is that the fact that force-commutated converters can generate a finite number of actuation values is explicitly taken into account. Thus, the optimal switching combination, i.e., that which minimizes the cost function, can be found by searching over a finite set. An advantage of FCS-MPC methods is that

the cost function can merge in a single expression electrical and non-electrical variables, e.g., tracking of currents, balancing of capacitor voltages and semiconductor switching frequency [58].

While most work on the FCC topology deals with balancing of the flying capacitor voltages, in [59] it was shown that, if the flying capacitors are replaced by dc-sources with a non-traditional ratio, then the number of output voltage levels can be increased. This opens the possibility to design output voltages with lower distortion. Another consequence of operating FCC in non-balanced modes lies in that redundant states decrease and the currents provided by the floating dc-sources have a non-zero average value. This characteristic is analyzed in [48] where the dc-sources are replaced by capacitors. More precisely, in [48] it is established that, for a three-cell inverter, the operation can be sustained only if the output voltage levels are 4 or 5, while the operation with 6, 7 and 8 levels is suitable only for reactive power compensation.

In the present work we develop an FCS-MPC technique for the FCC topology. In our approach, floating capacitor voltages are controlled. In particular, the strategy enables one to force non-traditional voltage ratios and increase the number of levels up to 8 (the theoretical maximum). At the same time, the FCS-MPC controls the output currents obtaining good tracking and a high output power factor. Experimental results for a 2 kW prototype illustrate the performance of the proposed algorithm.

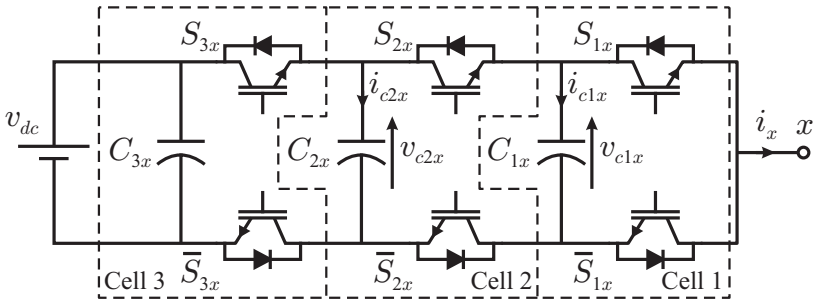

Figure 2.1: Three-cell Flying Capacitor inverter leg.

Nomenclature

y^j Variable y at instant j.

y_x Variable y of the respective x output phase, where $x \in \{a, b, c\}$.

$\mathbf{y}$ Measured value of variable y.

Y Constant or average value of y.

s_{ij} Switch state under evaluation, where $s_{ij} \in \{0, 1\}$.

S_{ij} Switch state applied, where $S_{ij} \in \{0, 1\}$.

2.2 The Flying Capacitor Converter

FCCs have emerged as an attractive multilevel topology for medium voltage application. The main reason is that, unlike cascade multicell converters [41], these converters do not require isolated dc sources, and hence bulky multi-secondary transformers. FCCs also exhibit good performance when operating under internal fault conditions [35].

The present work is focused on a three-phase FCC feeding a resistive-inductive load, as depicted in Fig. 2.2. Each output phase is based on a three-cell FCC topology, see Fig. 2.1. Each cell is a modular structure composed of one capacitor C_{jx} and two switches S_{jx} and $\overline{S}_{jx}$, which work in a complementary way. This avoids short circuits between the flying capacitors of different cells and open circuiting the load.

The internal FC equations per phase can be expressed as:

$$v_{xn}(t) = S_{3x}(t)v_{dc} - \Big(S_{3x}(t) - S_{2x}(t)\Big)v_{c2x}(t) - \Big(S_{2x}(t) - S_{1x}(t)\Big)v_{c1x}(t) \tag{2.1}$$

$$i_{c1x}(t) = i_x(t)\Big(S_{2x}(t) - S_{1x}(t)\Big) \tag{2.2}$$

$$i_{c2x}(t) = i_x(t)\Big(S_{3x}(t) - S_{2x}(t)\Big) \tag{2.3}$$

$$v_{c1x}(t) = \frac{1}{C_1}\int_{-\infty}^{t} i_{c1x}(\tau)\, d\tau \tag{2.4}$$

$$v_{c2x}(t) = \frac{1}{C_2}\int_{-\infty}^{t} i_{c2x}(\tau)\, d\tau, \tag{2.5}$$

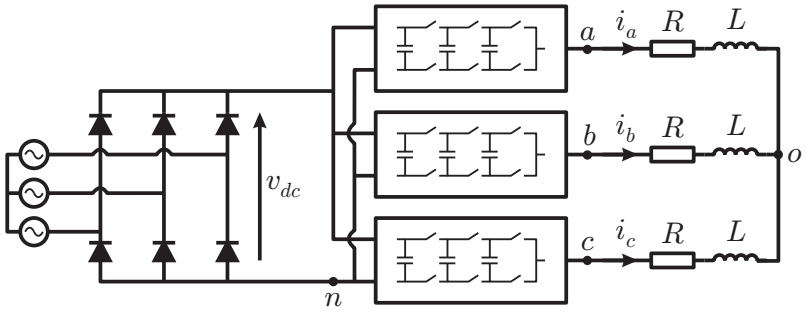

Figure 2.2: Three-phase three-cell FCC.

whereas the load equations are given by:

$$Ri_x(t) + L\frac{di_x(t)}{dt} = v_{xn} - v_{on} \tag{2.6}$$

$$v_{on}(t) = \frac{v_{an}(t) + v_{bn}(t) + v_{cn}(t)}{3}. \tag{2.7}$$

In the above expressions, v_{xn}, i_{c1x} and i_{c2x} are discontinuous functions, which depend on the switching state of the converter, as detailed in Table 2.1.

Table 2.1: Switching Combinations for a Three-cell Inverter Leg.

S_{3x}	S_{2x}	S_{1x}	$v_{xn}(t)$	$i_{c1x}(t)$	$i_{c2x}(t)$
0	0	0	0	0	0
0	0	1	$v_{c1x}(t)$	$-i_x$	0
0	1	0	$v_{c2x}(t) - v_{c1x}(t)$	i_x	$-i_x(t)$
0	1	1	$v_{c2x}(t)$	0	$-i_x(t)$
1	0	0	$v_{dc} - v_{c2x}(t)$	0	$i_x(t)$
1	0	1	$v_{dc} - v_{c2x}(t) + v_{c1x}(t)$	$-i_x(t)$	$i_x(t)$
1	1	0	$v_{dc} - v_{c1x}(t)$	$i_x(t)$	0
1	1	1	v_{dc}	0	0

The most commonly used capacitor voltage ratio is $v_{dc} : v_{c2x} : v_{c1x} = 3{:}2{:}1$. In this case, and according to Table 2.1, the inverter output voltage per phase reaches a maximum of 4 levels, using the eight possible switch combinations. It is worth noting that some voltage levels can be generated by multiple switch combinations, i.e, there is a certain degree of redundancy in the switching state combinations. These redundant states can be used to control the capacitor voltages, and hence to keep them at the desired ratio.

In [59] is is proposed to use different ratios in order to increase the number of levels (not the power), and hence increase the quality of the output currents. The main disadvantage of this approach is that the redundancy decreases (see Table 2.2), so the control of the capacitor voltages requires additional control effort.

In [48] a simple algorithm to control the capacitor voltages is proposed. First, a PWM modulator selects a desired voltage level, and taking into account the output current, the redundant switch combination which reduces the capacitor voltages error is applied. This

Table 2.2: Number of Redundant States per Voltage Level for Different Capacitor Voltages Ratios.

	Voltage ratio $v_{dc} : v_{c2x} : v_{c1x}$				
Level	3:2:1	4:2:1	5:3:1	6:3:1	7:3:1
0	1	1	1	1	1
1	3	2	1	1	1
2	3	2	2	1	1
3	1	2	2	2	1
4	–	1	1	1	1
5	–	–	1	1	1
6	–	–	–	1	1
7	–	–	–	–	1

allows operation with 4 and 5 output voltage levels for a wide range of output power factor (PF). However, for 6, 7 and 8 output voltage levels, the PF is below 0.5. Thus, the technique of [48] is mainly applicable for highly reactive loads. Overcoming these limitations constitutes the main motivation for developing the controller to be presented in the following section.

2.3 FCS-MPC of an Asymmetric FCC

In this section, we present a model predictive control method for the three-phase FCC topology depicted in Fig. 2.2. Key to our proposal is the fact that not only output currents, but also capacitor voltages are controlled. In particular, the ratios of capacitor voltages can be regulated to non traditional values. This increases the number of output voltage levels and, thus, reduces the harmonic content in the output current.

2.3.1 Overview

The proposed controller fits into the general framework of *Finite-Control-Set Model Predictive Control*, as described, e.g., in [10,37,55–57]. It operates in discrete time with fixed sampling period Δ and directly provides the switching states to be implemented at the converter. Consequently, no intermediate modulation stages are needed, cf., [51–53].

At each discrete time instant k, first measurements of the capacitor voltages, $\mathbf{v}_{c1x}^k$ and $\mathbf{v}_{c2x}^k$, and output currents, $\mathbf{i}_x^k$, of each phase $x \in \{a, b, c\}$ are taken. These measurements are then used by the controller to decide upon the switch states which are to be implemented at time $k+1$. We note that the effect of the latter will be observed only at time $k+2$.

2.3.2 Optimization Criterion

As foreshadowed in the introduction, the proposed controller chooses the switch states to be implemented at time $k+1$, namely S_{ix}^{k+1}, $i \in \{1, 2, 3\}$, through minimization of the following cost function:

$$g^k = g_a^k + g_b^k + g_c^k, \tag{2.8}$$

where:

$$g_x^k = \left(i_x^* - i_x^{k+2}\right)^2 + W_{vc1}\left(v_{c1}^* - v_{c1x}^{k+2}\right)^2 + W_{vc2}\left(v_{c2}^* - v_{c2x}^{k+2}\right)^2, \quad x \in \{a, b, c\}. \tag{2.9}$$

In (2.9), variables with superscript * are reference values *corresponding to time* $k+2$, whereas the weighting factors W_{vc1} and W_{vc2} give the control designer two degrees of freedom to improve tracking of capacitor voltages and/or output currents.

2.3.3 Control Calculations

To minimize the cost function g^k defined above, the model predictive controller examines all possible switching states S_{ix}^{k+1} explicitly. As the FCS-MPC requires an important number of calculations, the associated delay must be taken in to account. Therefore, it is convenient to separate control calculations as follows:

1. Given measurements and switching states S_{ix}^k at time k, calculate capacitor voltages and output currents at time $k+1$. We will call this the *Estimation Step*.

2. Given the results of the Estimation Step, evaluate the effect of switching states S_{ix}^{k+1} on g^k. We will refer to this as the *Prediction Steps*.

Fig. 2.3 depicts the situation. Both the Estimation Step and the Prediction Steps use discrete time recursions which are derived from the FCC model presented in Section 2.2. We will next give further details on the control calculations.

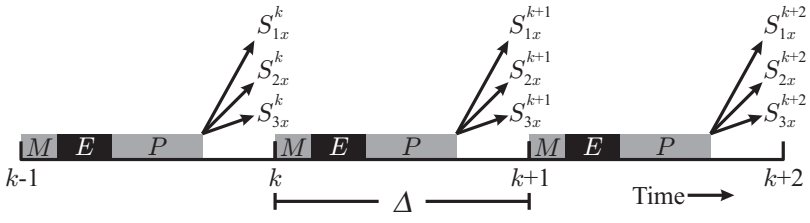

Figure 2.3: Control Calculations Timeline: measurement, estimation and prediction.

Estimation Step

The switch values S_{ix}^k (which were calculated at time $k-1$) are kept constant during the sampling period Δ. Thus, the capacitor voltages and output currents at instant $k+1$ can be approximated by the following discretization of (2.1)-(2.7):[1]

$$v_{xn}^{k+1} = S_{3x}^k V_{dc} - (S_{3x}^k - S_{2x}^k)\mathbf{v}_{c2x}^k - (S_{2x}^k - S_{1x}^k)\mathbf{v}_{c1x}^k \tag{2.10}$$

$$v_{on}^{k+1} = \frac{v_{an}^{k+1} + v_{bn}^{k+1} + v_{cn}^{k+1}}{3} \tag{2.11}$$

To obtain an expression for the output currents at $k+1$, it is assumed that the capacitor voltages change slowly, when compared to the output currents. This gives:

$$i_x^{k+1} = K_a \mathbf{i}_x^k + K_b(v_{xn}^k - v_{on}^k), \tag{2.12}$$

where the constants K_a and K_b are given by:

$$K_a = e^{-\Delta\frac{R}{L}}, \quad K_b = (1-K_a)\frac{1}{R},$$

in accordance with (2.6). Finally, a trapezoidal discretization of (2.4) and (2.5) is used:

$$\begin{aligned} v_{c1x}^{k+1} &= \mathbf{v}_{c1x}^k + \frac{\Delta}{2C_1}\left(i_x^{k+1} + \mathbf{i}_x^k\right)\left(S_{2x}^k - S_{1x}^k\right) \\ v_{c2x}^{k+1} &= \mathbf{v}_{c2x}^k + \frac{\Delta}{2C_2}\left(i_x^{k+1} + \mathbf{i}_x^k\right)\left(S_{3x}^k - S_{2x}^k\right) \end{aligned} \tag{2.13}$$

The above values are used as a starting point for the Prediction Steps described below.

Prediction Steps

In the Prediction Steps, the effect of the decision variables S_{ix}^k on g^k, is evaluated. To minimize g^k, in principle, all possibilities for S_{ix}^k need to be examined. Each three-cell FCC output phase can generate up to eight different switching states. Since the output phases interact through the load neutral point by v_{on}, this leads to a total of $8^3 = 512$ possible combinations. The associated predictions need to be evaluated for all possibilities on-line and at every discrete time instant. Thus, the computational burden may be too high for many practical applications.

[1] Note that the main dc-link voltage v_{dc} is assumed as a constant value and is not included as a measured quantity.

To reduce computation times, in this work we propose to ignore the interaction through the load neutral point in the Prediction Steps (note that these interactions are are explicitly taken into account in the Estimation Step). Consequently, to quantify the impact of the future switch combinations, we regard each output phase as an isolated unit. This gives a search space having only $3 \cdot 8 = 24$ elements.

The same discretization used in the Estimation Step is also used for the predictions. The only difference is that v_{on} is set to zero, yielding:

$$\begin{aligned} v_{xn}^{k+2} &= s_{3x}^{k+1} V_{dc} - (s_{3x}^{k+1} - s_{2x}^{k+1}) v_{c2x}^{k+1} - (s_{2x}^{k+1} - s_{1x}^{k+1}) v_{c1x}^{k+1} \\ i_x^{k+2} &= K_a i_x^{k+1} + K_b v_{xn}^{k+1} \\ v_{c1x}^{k+2} &= v_{c1x}^{k+1} + \frac{\Delta}{2C_1} \left(i_x^{k+1} + i_x^{k+2} \right) \left(s_{2x}^{k+1} - s_{1x}^{k+1} \right) \\ v_{c2x}^{k+2} &= v_{c2x}^{k+1} + \frac{\Delta}{2C_2} \left(i_x^{k+1} + i_x^{k+2} \right) \left(s_{3x}^{k+1} - s_{2x}^{k+1} \right). \end{aligned} \tag{2.14}$$

Resultant Optimization Algorithm

The FCS-MPC proposed requires evaluating the estimation equations (2.12) and (2.13) once, and the prediction equations (2.14) eight times per phase. The switch combination which gives the lowest value of g^k will be applied at the beginning of the next sampling time, i.e., at $k+1$. Fig. 2.4 shows a flow diagram of the resultant optimization algorithm.

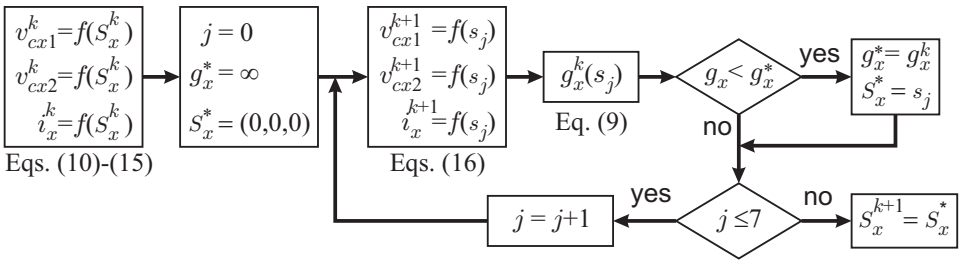

Figure 2.4: Flow diagram for the x phase ($x = a, b, c$).

2.4 Experimental Results

To test the FCS-MPC strategy developed in Section 2.3, a 2 kW prototype of the topology of Fig. 2.2 was built based on discrete IGBTs IRG4PC30KD. The most relevant prototype parameters are presented in Table 2.3. The converter was controlled by a digital platform which uses a TMS320C6713 DSP for the proposed control algorithm and an XC3s400 FPGA for driving the peripheral devices, including ADC and trigger pulses. This digital system performs the complete FCS-MPC algorithm in 18μs. However, the sampling time was set to only 15 kHz in order to reduce the commutation frequency of the converter IGBTs. This is comparable with traditional sinusoidal PWM schemes, which requiere a lower calculation power but can not control the dc-link voltages ratio. A deeper comparison is available in [57].

2.4.1 Design of Capacitor Voltage Ratio

Fig. 2.5 shows the converter behavior at different voltage ratios. As the number of levels increases the number of redundant states decreases, as mentioned before. In order to keep the capacitor voltages controlled, the FCS-MPC controller uses some unexpected switch combinations, or spikes, introducing additional high frequency components. However, due to the low-pass filter characteristic of the load, those components have only a minor effect in the output currents, see Fig. 2.5(c). As can be observed in Fig. 2.5(b1), there are no spikes for the 3:2:1 operation, since all levels used by the flying capacitors have redundant

Table 2.3: Main Prototype Parameters

Param.	Value	Param.	Value
V_{dc}	400 V	R	35 Ω
C_1	750 μF	L	20 mH
C_2	750 μF	PF@50 Hz	0.98
C_3	900 μF	$f_m = 1/\Delta$	15 kHz

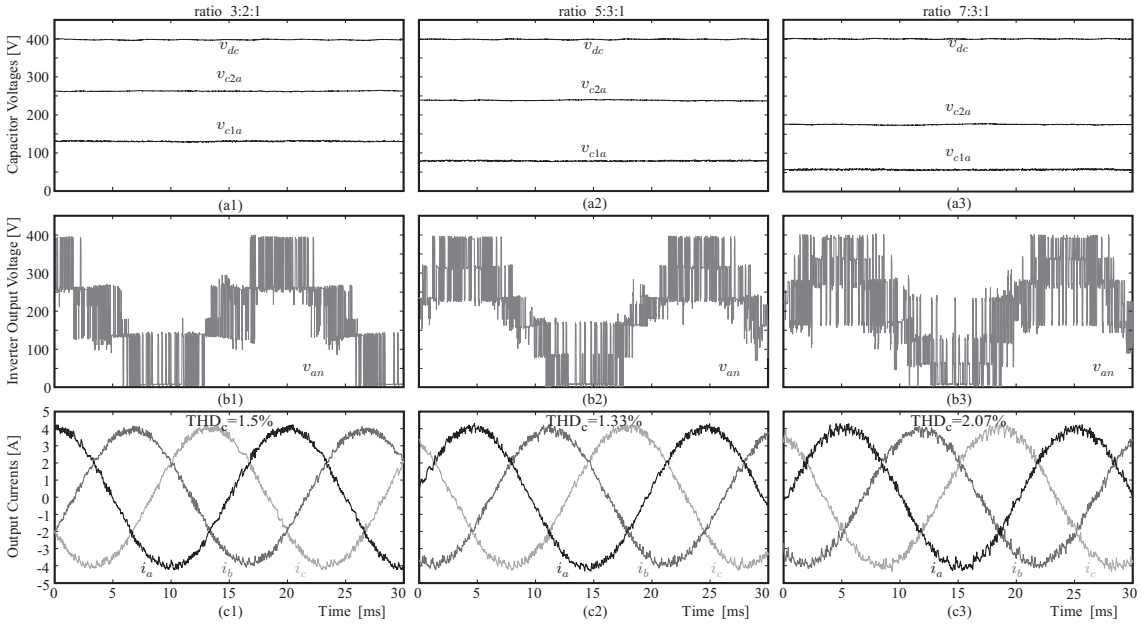

Figure 2.5: Operation at different capacitor voltages ratios: (a) Capacitor voltages; (b) Inverter output voltage; (c) Output currents.

combinations. When operating with ratio 5:3:1, the spikes appear around levels 1 and 5 [Fig. 2.5(b2)], which, according to Table 2.2, do not have redundant states. Finally, when operating with ratio 7:3:1, where no redundant states exist for any level, the spikes are equally distributed along the v_{an} waveform, see Fig. 2.5(b3).

Table 2.4 summarizes the capacitor voltage references used to achieve the different operation ratios.

Table 2.4: Comparison of the FCS-MPC at Different Capacitor Voltages Ratios.

ratio	v_{dc}	v_{c1x}	v_{c2x}	$v_{dc} - v_{c1x}$	$v_{c2x} - v_{c1x}$
3:2:1	400 V	133 V	266 V	133 V	133 V
5:3:1	400 V	80 V	240 V	160 V	160 V
7:3:1	400 V	57 V	171 V	229 V	114 V

It is worth noticing that operation with a non-traditional ratio allows one to use flying capacitors rated at a lower voltage. However, switches must be rated at a higher value, as given by the voltage difference between capacitors of adjacent cells. Thus, from a converter construction point of view, the selection of the voltage ratio will depends on the cost of semiconductors vs. capacitors. For example, when comparing 5:3:1 operation with 3:2:1 operation, we have that the capacitor voltage rate is reduced by 40% and by 10% for C_1 and C_2, respectively, whereas semiconductors voltage rate is increased by 20%.

Finally, Fig. 2.5(c) shows the current waveforms obtained for the different operation ratios. It can be observed that the currents are overall very similar. However, as the number of output levels increases, the high-frequency distortion increases, too. On the other hand, as the number of voltage levels decreases, the low-frequency distortion increases. The calculated THD_c confirms that, with the present strategy, the best current waveform is obtained by setting the capacitor voltage ratio to 5:3:1.

The current spectra for the three operation ratios are shown in Fig. 2.6 and confirm that the currents are very similar. However with a larger number of levels, the distortion at lower frequencies tends to be lower and the distortion at higher frequencies tends to increase. Interestingly, the spectra are not concentrated as with traditional PWM modulators, the latter having a higher concentration around $f_m/2$ and f_m. It is also worth noting that all the harmonics have a magnitude lower than 1%, most of them being below 0.3%.

We emphasize that previous works only allow for a maximum operative power factor of 0.3 for 6-level and 0.05 for 8-level operation [48]. The present results where obtained with a load power factor of 0.98. This represents an increase of 320% and of 1960% for 6-level and 8-level operation, respectively.

2.4.2 Parameters Sensitivity

It follows from (2.10)–(2.14) that the FCS-MPC requires information about the converter parameters to carry out the estimation and prediction calculations needed for finding the

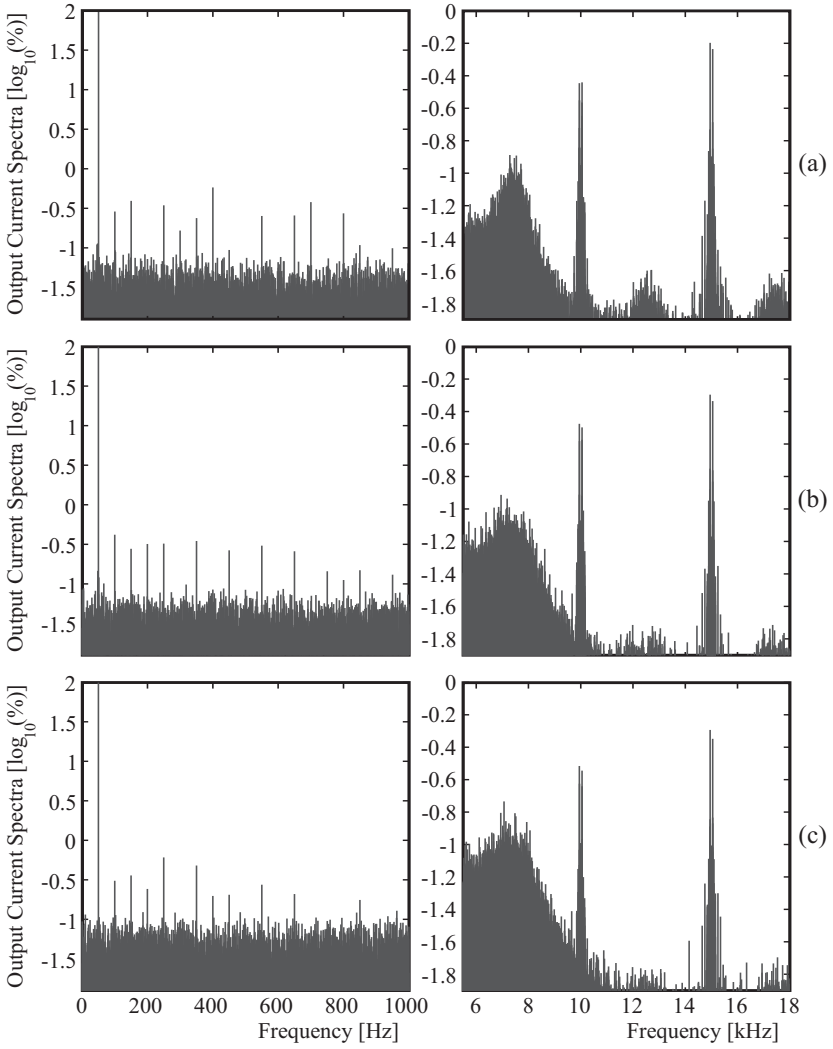

Figure 2.6: Output current spectra for voltage ratios: (a) 3:2:1; (b) 5:3:1; (c) 7:3:1.

optimal switching combination for the next step. Therefore, it is important to test the controller behavior under parameter changes.[2]

Fig. 2.7 shows the converter operation for a large distortion in the main dc-link voltage v_{dc}.

[2]Even though it is possible to extend the proposed algorithm in order to work with resistive-inductive-active loads *R-L-e*, for the sake of brevity, tests are applied only to a resistive-inductive load *R-L*. Mismatch in the load voltage parameter did not affect in a significant way the overall behavior of the converter.

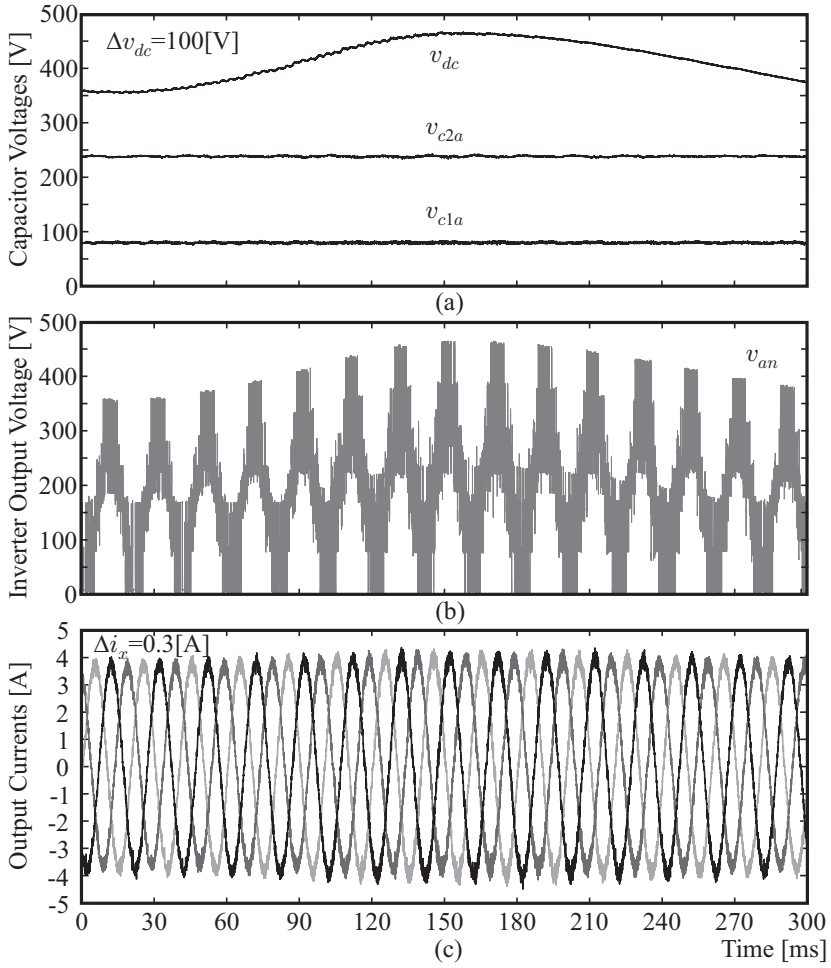

Figure 2.7: Control performance for a large v_{dc} distortion: (a) Capacitor voltages; (b) Output voltage; (c) Output currents.

This value is not measured by the control system. Consequently, even if v_{dc} has a ripple of ± 50 V, the FCS-MPC algorithm assumes that $V_{dc} = 400$ V. This amounts to a mismatch of 12.5%. As shown in Fig. 2.7(b), the ripple in v_{dc} does significantly affect the inverter output voltage waveform. Nevertheless, the controller is able to keep the flying capacitor voltages at their reference values without any perceptible ripple, see Fig. 2.7(a). The output currents show a minor distortion of ± 0.15 A, which corresponds to a tracking error of only 3.75%.

A usual problem in electrical machines is to estimate the load resistor R, since it changes,

e.g., with the temperature. Fig. 2.8 shows the behaviour of the converter for a change on the resistive component of the load from 35Ω to 47Ω, i.e., the controller works with an underestimated value about 35%. As can be seen in Fig. 2.8(a), no significant changes are observed in the dc-link voltages. The inverter output voltage, shown in Fig. 2.8(b), automatically increases its modulation index, in order to keep the currents controlled, see Fig. 2.8(c). A minor reduction in the output current magnitude of about 5% (less than 0.2A) can be noticed. This effect is small, when compared to the parameter mismatch.

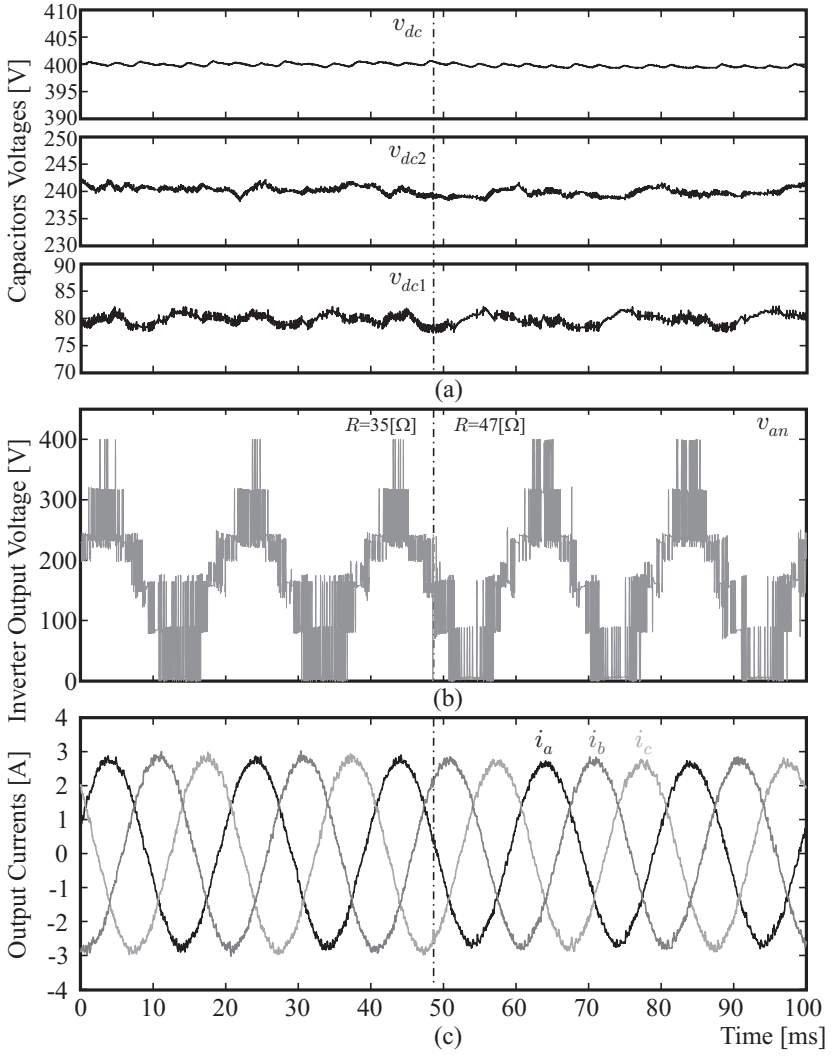

Figure 2.8: Waveforms with 35% mismatch in the load resistor value: (a) Capacitor voltages; (b) Output voltage; (c) Output currents.

Finally, the mismatch parameter estimation effect on the inductive component of the load is investigated. The MPC algorithm uses an estimated inductor value of L=15mH. On the right hand side of Fig. 2.9, the real inductor value is 50% lower than that used for control calculations, while on the left hand side of Fig. 2.9 an inductor which is 50% higher is used. As expected when a lower inductance value is used, a higher ripple in the load current is observed. However, the fundamental component of the current is the same in both cases. Similarly, the capacitor voltages do not present any significant difference. The inverter output voltages are accommodated to keep the output current to the desired values.

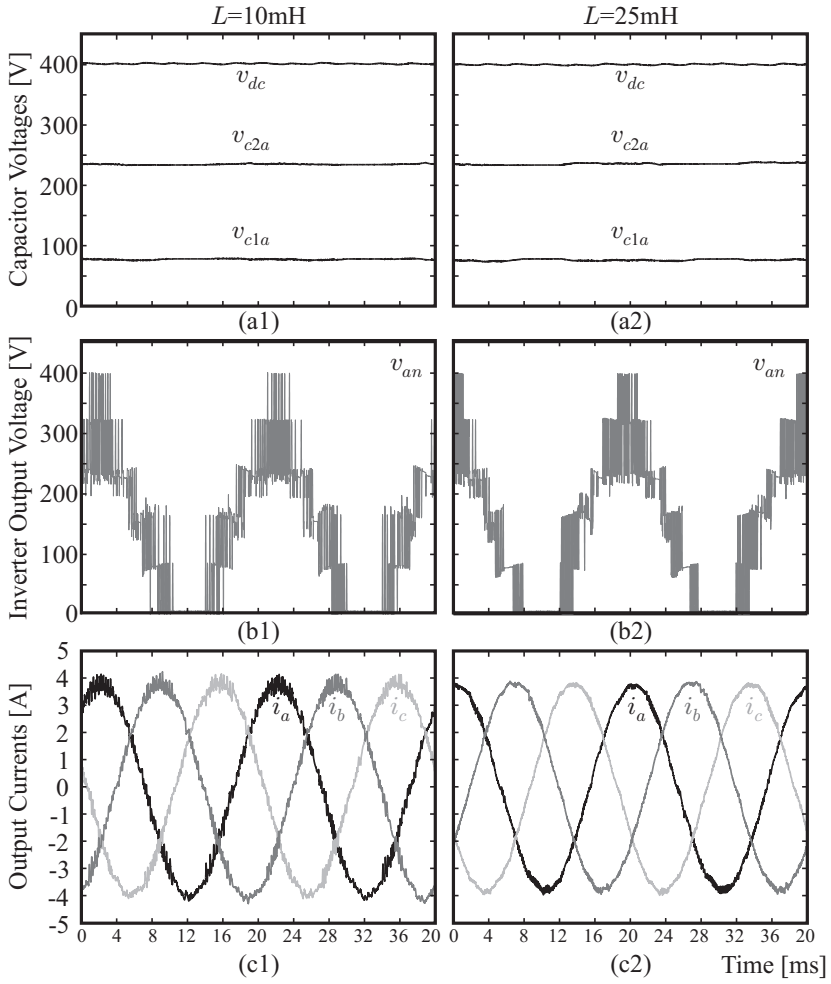

Figure 2.9: Operation with a mismatch in the load inductor value: (a) Capacitor voltages; (b) Output voltage; (c) Output currents.

2.4.3 Dynamic Performance

An important aspect of any control system is its dynamic response to reference changes. Fig. 2.10 shows the system behavior for a current reference step from 4 A to 2 A peak. As in results documented above, although the main dc-link voltage v_{dc} slightly increases its value due to the reduction in the output power, the proposed control algorithm manages to keep the flying capacitor voltages at the desired values, see Fig. 2.10(a). The inverter output voltage reduces its RMS value and the number of levels used, as can be observed in Fig. 2.10(b). This change clearly affects the output currents, which rapidly change their

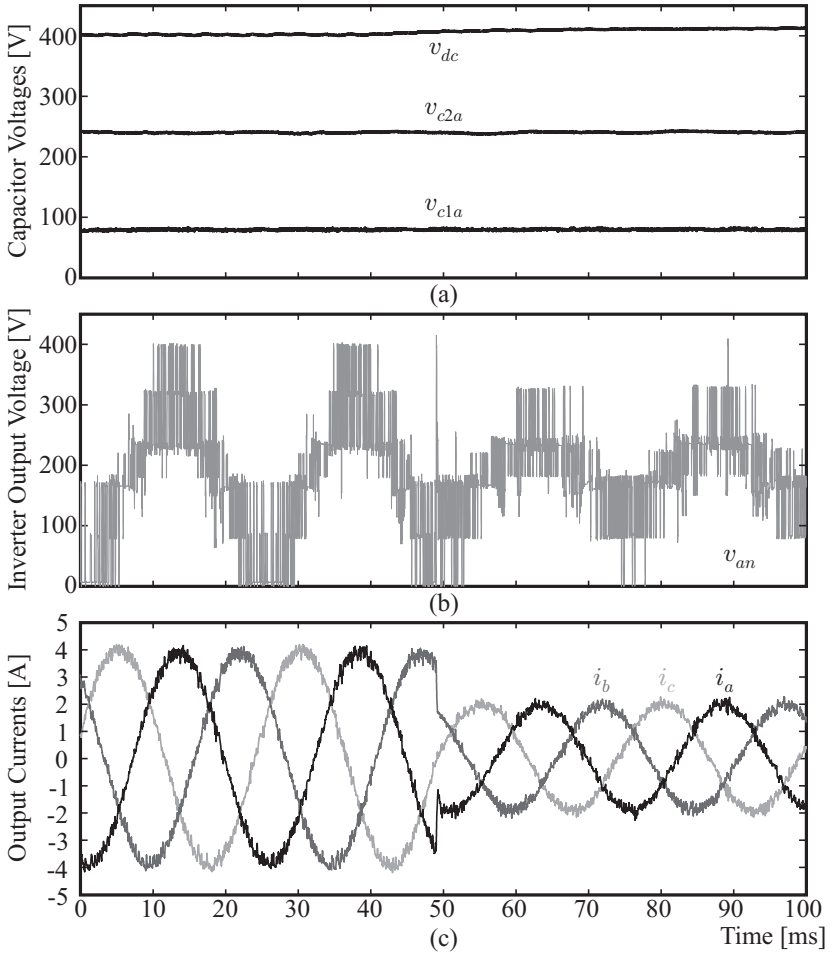

Figure 2.10: Waveforms for a current reference step from 4 A peak to 2 A peak: (a) Capacitor voltages; (b) Output voltage; (c) Output currents.

values in order to follow the new reference. Moreover, it is possible to see, how at the step instant, the inverter applies the maximum voltage v_{dc} to the inverter output voltage v_{an} forcing the current i_a to decrease its value at maximum speed, see Fig. 2.10(c).

Changing the flying capacitor voltages is not usual in traditional applications. However,

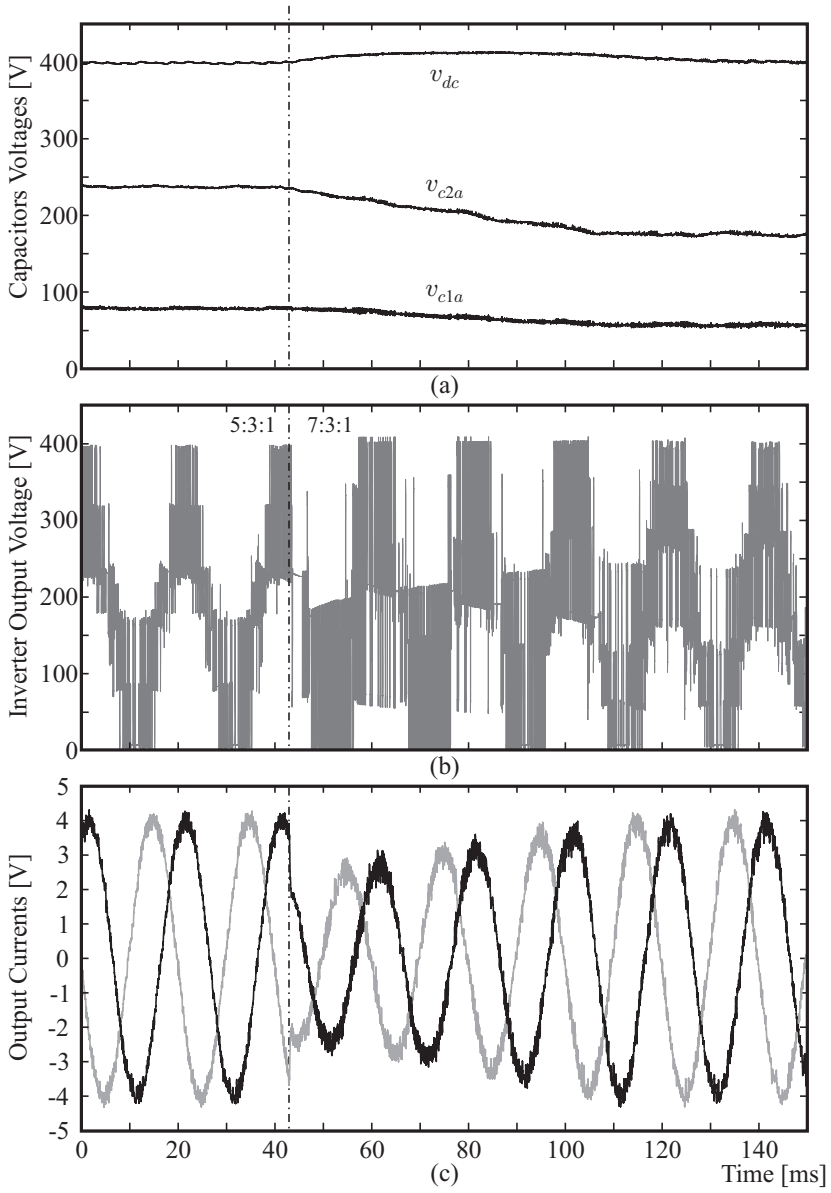

Figure 2.11: Transition from 5:3:1 to 7:3:1 capacitor voltage ratio: (a) Capacitor voltages; (b) Output voltage; (c) Output currents.

it illustrates how flexible the proposed controller can be. Fig. 2.11 shows the transition from the 5:3:1 to 7:3:1 ratio. In absolute values, v_{c1x} changes from 80 V to 57 V while v_{c2x} changes from 240 V to 171 V, in approximately 80ms. The output voltage v_{ao} in Fig. 2.11(b) reflects the change in the capacitor voltages, when changing the number of levels from 6 to 8. Note that, in the transient, the levels are not clearly defined. While the output currents change their magnitude forcing the capacitor voltages to their new values, the currents stay sinusoidal, see Fig. 2.11(c). Once the capacitor voltages reach the new reference values, the output currents reach their references, too.

2.5 Conclusions

FCC are complex systems due to the high number of semiconductors and electrical relationships. In this work we have proposed an FCS-MPC strategy to achieve an increase in the possible output voltage levels and, thus, obtain better output waveforms. To keep the computational burden low, in our formulation we have used a simplified converter model. Nevertheless, the FCS-MPC method developed gives excellent performance, even when large parameter mismatch occurs. Indeed, a significant advantage of the algorithm presented is the reduction of the output current distortion, and the good dynamic behaviour of the output currents and the flying capacitor voltages under reference changes.

The proposed controller gives good performance with a high load power factor even for 8-level operation of the converter. This clearly improves upon previously reported operation limits. To reach these new FCC operation modes, the FCS-MPC applies brief voltage spikes which allow one to control the capacitor voltages levels. Those spikes have only a minor effect on the output currents, due to the low-pass frequency characteristic of the load. The best output currents were obtained for the 6-level operation (5:3:1 voltage ratio), where voltage waveforms have fewer spikes than with 8-level operation. Also, from a constructive point of view, operating at a 5:3:1 voltage ratio seems to constitute a good compromise between required capacitor voltage rates and IGBT blocking capability rates.

3

MPC of an AFE Rectifier with Dynamic References

3.1 Introduction

In many industrial applications active front-end rectifiers (AFEs) have emerged as an attractive topology. When compared to traditional diode-based rectifiers, AFEs allow one to obtain sinusoidal input currents with low harmonic distortion, whilst at the same time providing an regulated rectifier voltage. Moreover, the amount of reactive power drawn from the source can be manipulated in order to reach a unity power factor at the input (see, e.g., [60–62]), or also to compensate lack of reactive power in the source grid; see [63] and the references therein. Another area where AFEs play an important role is when a reduction of harmonic distortion is sought. In fact, this converter is of widespread use as an active filter in which case the AFE is connected in parallel to the non-linear load thereby generating the harmonic currents necessary to reduce the pollution in the source; see, e.g., [64].

For the control of AFEs, different methods based on pulse-width modulation (PWM) techniques exist. The most popular algorithms use voltage-oriented control (VOC), and various forms of direct power control (DPC), see, e.g., [33, 65–67]. The VOC approach works in the d-q reference frame using two control loops: The external loop is based on a Proportional Integral (PI) controller which seeks to compensate the dc-voltage error by generating the direct current reference. The internal loop reduces the dq-current error

by using two PI controllers. These generate dq-voltages which are utilised to produce the associated space vector modulation. DPC techniques also require two control loops, but in a different manner: With DPC, the external controller seeks to compensate the dc-voltage error by directly generating the power reference for an internal control loop. In the standard approach, as described, e.g., in [65], the switching actions are obtained from a table lookup, which takes into account not only the dc-voltage error, but also active and reactive power estimates. Other types of DPC are based on the use of external modulators, see [33, 66, 67].

The main drawback of both VOC and DPC methods is the need for local linearizations for the linear control design part. The latter issue was investigated recently in [68].

Over the last decade, model predictive control (MPC) strategies have emerged as a promising control technique for power electronics applications; see, e.g., [10, 26, 28, 69, 70]. The main advantage of these predictive strategies, when compared to traditional PWM methods, derive from the fact that switching effects can explicitly be considered without approximations. For example, so called *Finite Control Set* MPC formulations (sometimes also referred to as *Direct MPC*, see [25]) have been presented, for example, in [14, 71, 72]. Here a switching model of the converter is used to minimize a running cost function through exploration of the different switch combinations. The switching action to be applied at the next sampling instant is that which minimizes the cost function. The latter can be chosen to reflect various control objectives. In addition to input currents, one can focus on other issues including current spectra [57] and number of commutations; see, e.g., [73].

An MPC-based direct power control method for AFEs was presented in [34]. A key issue which arises when controlling an AFE is that, unavoidably, dc-voltage and active power levels are coupled. Thus, is is necessary to find compatible references for these variables. For that purpose, in [34] the active power reference is obtained from an external PI-controller which is designed to compensate dc-voltage errors. The predictive controller then provides switching actions to track the desired active and reactive power references at the input. Not surprisingly, tuning the external PI controller needed in [34] becomes a difficult task, due to the discrete-time switching nature of the converter.

The present work proposes an MPC formulation for closed loop control of AFEs. The key novelty of our method is that it is capable of providing suitable references for the source active power and the rectified voltage, without requiring additional control loops. The method presented is formulated in discrete-time, uses a state-space model of the converter and directly provides the switching action to be applied. As documented by experimental results on a lab-prototype of 500[W], our formulation allows one to incorporate restrictions on maximum power levels, without incurring any loss of performance due to windup issues, which are typical in PI-control loops, see also [74].

The remainder of this manuscript is organized as follows: In Section 3.2 we give a dynamic model of the AFE rectifier. Section 3.3 presents the cost function chosen. In Section 3.4 we show how a compatible reference can be formulated. Simulation studies and experimental results are included in Section 3.5. Section 7.7 draws conclusions.

3.2 AFE Rectifier

In the present work, we focus on the AFE rectifier shown in Fig. 3.1. As can be seen in that figure, the rectifier is a three-phase fully-controlled bridge consisting of 6 power transistors connected to a three-phase power source v_s by means of a filter. The latter is represented by an inductance L_s and the parasitic resistance r_s. The neutral point is electrically floating.

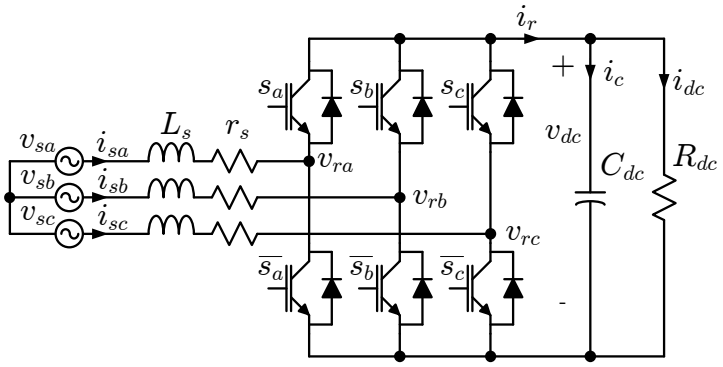

Figure 3.1: Active front-end rectifier with floating neutral point

3.2.1 Continuous Time Model

We will adopt an *abc*-frame, as presented in [75], and suppose that the three-phase source voltages v_{sa}, v_{sb} and v_{sc} are symmetric, so that in the AFE, we have:

$$v_{sa}(t) + v_{sb}(t) + v_{sc}(t) = 0 \tag{3.1}$$

$$i_{sa}(t) + i_{sb}(t) + i_{sc}(t) = 0 \tag{3.2}$$

at all times $t \in \mathbb{R}$. Thus, the source current obeys

$$\begin{aligned} \frac{di_{sa}(t)}{dt} &= \frac{1}{L_s} v_{sa}(t) - \frac{r_s}{L_s} i_{sa}(t) - \frac{1}{3L_s}\big(2s_a(t) - s_b(t) - s_c(t)\big) v_{dc}(t) \\ \frac{di_{sb}(t)}{dt} &= \frac{1}{L_s} v_{sb}(t) - \frac{r_s}{L_s} i_{sb}(t) - \frac{1}{3L_s}\big(-s_a(t) + 2s_b(t) - s_c(t)\big) v_{dc}(t), \end{aligned} \tag{3.3}$$

for all $t \in \mathbb{R}$ and where the switch variables $s_a(t)$, $s_b(t)$ and $s_b(t)$ are equal to 1, if at time t the associated switch is conducting, and equal to zero, if it is blocking current. Consequently, the active source power can be expressed via:

$$P_s(t) = v_{sa}(t)(2i_{sa}(t) + i_{sb}(t)) + v_{sb}(t)(2i_{sb}(t) + i_{sa}(t)). \tag{3.4}$$

To obtain a dynamic model for the rectified voltage $v_{dc}(t)$, we note that the currents on the rectifier side are described via:

$$\begin{aligned} i_r(t) &= (s_a(t) - s_c(t)) i_{sa}(t) + (s_b(t) - s_c(t)) i_{sb}(t) \\ i_{dc}(t) &= \frac{v_{dc}(t)}{R_{dc}} \\ i_c(t) &= i_r(t) - i_{dc}(t). \end{aligned} \tag{3.5}$$

Consequently, the dynamics of $v_{dc}(t)$ is characterized via:

$$\frac{dv_{dc}(t)}{dt} = \frac{1}{C_{dc}}\Big(\big(s_a(t) - s_c(t)\big) i_{sa}(t) + \big(s_b(t) - s_c(t)\big) i_{sb}(t) - \frac{1}{R_{dc}} v_{dc}(t)\Big), \quad \forall t \in \mathbb{R}. \tag{3.6}$$

Finally, the active power in the rectifier side can be expressed as follows:

$$P_r(t) = \left((s_a(t) - s_c(t)) i_{sa}(t) + (s_b(t) - s_c(t)) i_{sb}(t)\right) v_{dc}(t). \tag{3.7}$$

3.2.2 Discrete Time Model

The MPC algorithm to be developed operates in discrete time with fixed sampling period $h > 0$. To obtain a discrete time model of the system, we introduce

$$\mathbf{i}_s(k) \triangleq \begin{bmatrix} i_{sa}(k) \\ i_{sb}(k) \end{bmatrix}, \quad \mathbf{v}_s(k) \triangleq \begin{bmatrix} v_{sa}(k) \\ v_{sb}(k) \end{bmatrix}, \quad \mathbf{s}(k) \triangleq \begin{bmatrix} s_a(k) \\ s_b(k) \\ s_c(k) \end{bmatrix},$$

where $k \in \mathbb{N}$ refers to the sampling instants kh. An Euler approximation of the continuous time model represented by (3.3) and (3.6) then provides:[1]

$$\begin{aligned} \mathbf{i}_s(k+1) &= \Big(1 - \frac{r_s h}{L_s}\Big)\mathbf{i}_s(k) + \frac{h}{L_s}\big(\mathbf{v}_s(k) - \mathbf{M}\mathbf{s}(k)v_{dc}(k)\big) \\ v_{dc}(k+1) &= \Big(1 - \frac{h}{C_{dc}R_{dc}}\Big)v_{dc}(k) + \frac{h}{C_{dc}}(\mathbf{s}(k))^T\mathbf{F}\mathbf{i}_s(k), \end{aligned} \tag{3.8}$$

where $k \in \mathbb{N}$ and where

$$\mathbf{M} \triangleq \frac{1}{3}\begin{bmatrix} 2 & -1 & -1 \\ -1 & 2 & -1 \end{bmatrix}, \quad \mathbf{F} \triangleq \begin{bmatrix} 1 & 0 \\ 0 & 1 \\ -1 & -1 \end{bmatrix}. \tag{3.9}$$

If we now introduce the state-vector of the AFE rectifier,

$$x(k) \triangleq \begin{bmatrix} \mathbf{i}_s(k) \\ v_{dc}(k) \end{bmatrix}, \tag{3.10}$$

then the model (3.8) can be written in compact form via:

$$x(k+1) = A_{\mathbf{s}(k)}x(k) + B\mathbf{v}_s(k), \quad k \in \mathbb{N} \tag{3.11}$$

where:[2]

$$A_{\mathbf{s}(k)} \triangleq \begin{bmatrix} \Big(1 - \frac{r_s h}{L_s}\Big)I_2 & -\frac{h}{L_s}\mathbf{M}\mathbf{s}(k) \\ \frac{h}{C_{dc}}(\mathbf{s}(k))^T\mathbf{F} & 1 - \frac{h}{C_{dc}R_{dc}} \end{bmatrix}, \quad B \triangleq \begin{bmatrix} \frac{h}{L_s}I_2 \\ 0_{1\times 2} \end{bmatrix}. \tag{3.12}$$

[1] Since the switch combinations are held constant between updates, the AFE is linear time-varying where the system matrices are held constant between updates. Due to the simplicity of the model, and since the time constants are much larger than the sampling interval chosen, se Section 3.5, using an Euler approximation gives good results.

[2] I_2 denotes the 2×2 identity matrix, whereas $0_{1\times 2} = [0 \;\; 0]$ and the superscript ^{T} refers to transposition.

Remark 3.2.1 (Finite-set constraints) *It is worth noting that, each switch variable at time k, namely $\mathbf{s}(k)$, only takes values in the finite set*

$$\mathcal{S} \triangleq \left\{ \begin{bmatrix} 0 \\ 0 \\ 0 \end{bmatrix}, \begin{bmatrix} 0 \\ 0 \\ 1 \end{bmatrix}, \begin{bmatrix} 0 \\ 1 \\ 0 \end{bmatrix}, \begin{bmatrix} 0 \\ 1 \\ 1 \end{bmatrix}, \begin{bmatrix} 1 \\ 0 \\ 0 \end{bmatrix}, \begin{bmatrix} 1 \\ 0 \\ 1 \end{bmatrix}, \begin{bmatrix} 1 \\ 1 \\ 0 \end{bmatrix}, \begin{bmatrix} 1 \\ 1 \\ 1 \end{bmatrix} \right\}. \tag{3.13}$$

Expression (3.12) *then shows that the system matrix $A_{\mathbf{s}(k)}$ is also finite-set constrained, i.e., we have that $A_{\mathbf{s}(k)} \in \mathcal{A}$ for a given set $\mathcal{A}$ having eight elements. Discrete-time control design then amounts to choosing the sequence of switch values $\mathbf{s}(k) \in \mathcal{S}$, $k \in \mathbb{N}$ or, equivalently, selecting the sequence of system matrices $A_{\mathbf{s}(k)} \in \mathcal{A}$ for all $k \in \mathbb{N}$.* ■

In the following section, we will present a model predictive control strategy for the AFE rectifier, based on the model given in (3.11).

3.3 Model Predictive Control of the AFE

Model predictive control is based upon online optimization of a performance index for current system state and future reference trajectories; see, e.g., [12, 76, 77]. To obtain a practical method which does not require excessive computation times, in the present work we adopt a cost function which only evaluates the effect of the switch decisions to be made at current time instant. This is computationally attractive and, as will become apparent in Section 3.5, gives good performance. The cost function presented next quantifies a quadratic norm of the tracking error of the three components of the state vector at the next time-instant.[3]

From an electrical viewpoint, the main purpose of the AFE is to provide a dc-voltage to the load, whilst at the same time managing a desired balance between active and reactive power. According to the state-space model introduced in Section 3.2.2, for a given system state $x(k)$, the system state, which would result if at time k, the switches s_a, s_b and s_c

[3]Most applications of MPC in power electronics and drives use such *horizon-one* cost functions [10]. Interestingly, in some situations, the use of horizon one also gives the *optimal* solution to a formulation with a larger horizon, see [78, 79].

were set to $\mathbf{s}(k) \in \mathcal{S}$ is given by:

$$x'(k+1) = A_{\mathbf{s}(k)}x(k) + B\mathbf{v}_s(k). \tag{3.14}$$

By approximating $\mathbf{v}_s(k+1) = \mathbf{v}_s(k)$, we obtain that the associated predicted *active power* satisfies:

$$P'_s(k+1) = \mathbf{v}_s^T(k)\begin{bmatrix} 2 & 1 \\ 1 & 2 \end{bmatrix}\mathbf{i}'_s(k+1) = \mathbf{v}_s^T(k)\begin{bmatrix} 2 & 1 & 0 \\ 1 & 2 & 0 \end{bmatrix}x'(k+1), \tag{3.15}$$

whereas

$$Q'_s(k+1) = \mathbf{v}_s^T(k)\sqrt{3}\begin{bmatrix} 0 & 1 \\ -1 & 0 \end{bmatrix}\mathbf{i}'_s(k+1) = \mathbf{v}_s^T(k)\begin{bmatrix} 0 & \sqrt{3} & 0 \\ -\sqrt{3} & 0 & 0 \end{bmatrix}x'(k+1) \tag{3.16}$$

is the predicted *reactive power*, and

$$v'_{dc}(k+1) = \begin{bmatrix} 0 & 0 & 1 \end{bmatrix}x'(k+1), \tag{3.17}$$

the predicted dc-voltage.

The main control objective in an AFE rectifier is to transfer active power from the source, P_s, to the dc-load. To do this, in modulation-based strategies where the modulation index is the control input, it is common to equalize the average active power source $P_s(t)$ with the average rectifier power, $P_r(t)$. This procedure then leads to a relationship between $P_s(t)$ and the dc-voltage, $v_{dc}(t)$, see [75]. However, it is in general not possible to set $P_s(t) = P_r(t)$ at all instants. For example, when the power switches take the same value, say, $S_a(t) = S_b(t) = S_c(t)$, then the input and output side are decoupled. In this case, as shown in (3.7), the rectifier power is clearly null, $P_r(t) = 0$, while the source power presented in (3.4) may present a different value $P_s(t) \neq 0$. This motivates us to introduce a so-called *filtered* dc-voltage reference $\tilde{v}^\star_{dc}(t)$, which allows us to establish a relationship between an average value of these two variables.

The controller proposed in the present work uses the above prediction model for current

state $x(k)$ to choose the switching values $\mathbf{s}(k)$ which minimize a cost function of the form:[4]

$$\begin{aligned} J(\mathbf{s}(k)) =& \frac{1}{\overline{v_{dc}}^2}(\tilde{v}^{\star}_{dc}(k+1) - v'_{dc}(k+1))^2 \\ &+ \frac{k_p}{\overline{P}^2}(P^{\star}_s(k+1) - P'_s(k+1))^2 \\ &+ \frac{k_q}{\overline{P}^2}(Q^{\star}_s(k+1) - Q'_s(k+1))^2. \end{aligned} \tag{3.18}$$

In (3.18), the superscript * refers to reference values; k_p and k_q are tuning parameters, which allow the designer to trade capacitor voltage reference deviations for deviations in active and reactive power. It is important to have in mind that in the cost function, the three system states are normalized by the factors $\overline{v_{dc}}$ and $\overline{P}$, thus, providing comparable deviation errors. For our results, see Section 3.5, we chose $k_p = k_q = 1$ in which case the controller gives equal weight to all the deviation components.

The cost function in (3.18) uses $Q^{\star}_s(k+1)$, $P^{\star}_s(k+1)$, and also a *filtered* dc-voltage reference $\tilde{v}^{\star}_{dc}(k+1)$. In our formulation, we assume that the reference value $Q^{\star}_s(k+1)$ and also a reference for the dc-voltage, say $v^{\star}_{dc}(k+1)$, are given. In the following section, we will show how to obtain $P^{\star}_s(k+1)$ and $\tilde{v}^{\star}_{dc}(k+1)$ from $v^{\star}_{dc}(k+1)$ and $Q^{\star}_s(k+1)$. The aim is to design references which are *consistent* from an electrical viewpoint and when used in (3.18) allow the controller to give good performance, despite system constraints.

It is worth recalling that in standard control formulations for AFEs, it is common to only control the average reactive power, $Q_s(t)$, and the dc-voltage, $v_{dc}(t)$ due to the fact that, as seen above, the latter is coupled to the average active source power $P_s(t)$. In contrast, in the present formulation, we are interested in tracking a dynamic filtered reference from the instantaneous values of the system state variables. For that purpose we include the active power source, $P_s(k)$, in the cost function (3.18). This also allows us to incorporate a safety constraint for the power source, $P_s(k) \leq P^{\max}$, in order to avoid over currents in the ac-side.

[4] In our formulation, we assume that computation times are negligible when compared to the sampling period. This reflects the fact that, in our experimental platform, computations take $3[\mu s]$, whereas the sampling period is taken as $h = 20[\mu s]$.

Remark 3.3.1 (Plant State Weighting) *The choice made in* (3.18) *amounts to weighting a quadratic form of the tracking error of the predicted state vector. Many theoretical results on MPC algorithms for systems without finite-set constraints suggest that such a formulation will often lead to closed loops having favorable stability and performance features; see, e.g., [12, 13, 76, 77, 80]. The case of systems with finite* input *constraints was studied in [37, 81]. How to extend these results to the present situation where the system matrix is finite-set constrained, see Remark 3.2.1, remains an open, and certainly non-trivial, problem.* ■

3.4 Reference Design

As noted in the introduction, a key difficulty when controlling an AFE lies in that successful tracking of power and voltage references cannot be achieved for arbitrarily chosen and time-varying reference signals. In fact, active power $P_s(k)$ and dc-voltage $v_{dc}(k)$ are unavoidably coupled. This relationship is difficult to characterize exactly in closed form, since it depends not only upon electrical parameters of the system, but also upon the switching law used.

One way to find compatible reference values has been explored recently in [34], where the use of an additional PI-control loop was examined. It turns out that PI-control gives perfect tracking of constant references in steady state. However, tuning the external controller becomes a difficult task, since the AFE is a discrete-time switching system.

We will next present an alternative method to provide suitable references for the source power and the rectified voltage. Our formulation uses directly predictive control concepts and does not require an additional control loop.[5] Furthermore, the method proposed allows one to incorporate restrictions on maximum power levels, without any integrator windup problems.

[5] To some extent, our approach is related to ideas underlying so-called *reference governors* for model predictive control formulations; see, e.g., [82].

3.4.1 Design of Compatible References

Given references $v_{dc}^{\star}(k)$ and $Q_s^{\star}(k)$ and the current system state $x(k)$, the reference design problem considered consists in finding a compatible reference for $P_s(k+1)$ and an associated filtered reference value $\tilde{v}_{dc}^{\star}(k+1)$ as used in the cost function (3.18). For that purpose, it is convenient to examine some electrical properties inherent to the AFE topology.

We first note that the capacitor voltage v_{dc} can only be adjusted by the capacitor current i_c. Since the latter quantity cannot be made arbitrarily large, we will introduce a *reference prediction horizon*, say $N^{\star}$. This horizon value constitutes a design parameter which determines the filtered reference $\tilde{v}_{dc}^{\star}(k+1)$. More specifically, $\tilde{v}_{dc}^{\star}(k+1)$ is obtained from $v_{dc}^{\star}(k)$ and $v_{dc}(k)$ via

$$\tilde{v}_{dc}^{\star}(k+1) = v_{dc}(k) + \frac{1}{N^{\star}}\big(v_{dc}^{\star}(k) - v_{dc}(k)\big), \tag{3.19}$$

which amounts to allowing the converter to reach $v_{dc}^{\star}(k)$ linearly in $N^{\star}$ steps, see Fig. 3.2.

Having calculated $\tilde{v}_{dc}^{\star}(k+1)$, we next seek to find a compatible reference for the active input power. Here, it is important to recall that the capacitor current i_c needs to ultimately be provided by the ac-source and thereby affects the active input power P_s. To be more

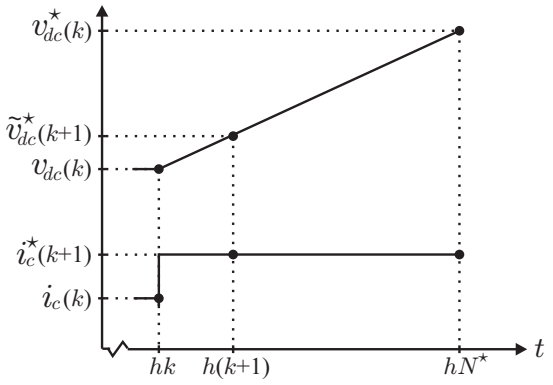

Figure 3.2: Dynamic reference design: Capacitor current $i_c^{\star}$ needed to increase the capacitor voltage v_{dc} in order to reach the reference $v_{dc}^{\star}$ in $N^{\star}$ time steps.

precise, the filtered reference $\tilde{v}_{dc}^{\star}(k+1)$ in (3.19) requires a capacitor current value of

$$i_c^{\star}(k+1) = \frac{C_{dc}}{h}\big(\tilde{v}_{dc}^{\star}(k+1) - v_{dc}(k)\big), \tag{3.20}$$

$$= \frac{1}{N^{\star}}\left(\frac{C_{dc}}{h}\big(v_{dc}^{\star}(k+1) - v_{dc}(k)\big)\right). \tag{3.21}$$

Thus, the capacitor current, i_c, is limited to a $(100/N^{\star})\%$ of the total current required to lead the dc-voltage, v_{dc}, to its desired reference $v_{dc}^{\star}$. This reduced capacitor current, in turn, necessitates a converter current, say $i_r^{\star}(k+1)$, given by:

$$i_r^{\star}(k+1) = i_c^{\star}(k+1) + \frac{1}{2R_{dc}}\big(v_{dc}(k) + \tilde{v}_{dc}^{\star}(k+1)\big). \tag{3.22}$$

Therefore, the overall rectifier power needed to track $\tilde{v}_{dc}^{\star}(k+1)$ satisfies:

$$\begin{aligned} P_r^{\star}(k+1) &= \tilde{v}_{dc}^{\star}(k+1) i_r^{\star}(k+1) \\ &= \Big(\frac{1}{2R_{dc}} + \frac{C_{dc}}{h}\Big)(\tilde{v}_{dc}^{\star}(k+1))^2 + \Big(\frac{1}{2R_{dc}} - \frac{C_{dc}}{h}\Big)\tilde{v}_{dc}^{\star}(k+1) v_{dc}(k), \end{aligned} \tag{3.23}$$

where we have used (3.20) and (3.22).

As noted before, the overall rectifier power needs to be provided by the ac-source. To obtain a value for the corresponding active input power reference, namely $P_s^{\star}(k+1)$, we will consider only the fundamental component of the alternating source currents. By taking into account the power losses which occur in the inductor resistances r_s, we obtain that compatible power references are (approximately) related by:

$$P_s^{\star}(k+1) = \frac{2r_s}{3\hat{V}_s^2}(P_s^{\star}(k+1))^2 + P_r^{\star}(k+1), \tag{3.24}$$

where $\hat{V}_s$ is the source voltage amplitude. The solution to (3.24) gives the desired reference for $P_s(k+1)$, namely:

$$P_s^{\star}(k+1) = \frac{3\hat{V}_s^2}{4r_s}\left(1 - \sqrt{1 - \frac{8r_s}{3\hat{V}_s^2}P_r^{\star}(k+1)}\right), \tag{3.25}$$

where $P_r^{\star}(k+1)$ is as in (3.23).

To summarise, the references used in the cost function (3.18) are obtained though expressions (3.19) and (3.25). It is worth emphasizing that the reference values $P_s^{\star}(k+1)$ and $\tilde{v}_{dc}^{\star}(k+1)$ are calculated at each time instant k for a given plant state $x(k)$ and references

$v_{dc}^{\star}(k)$ and $Q_s^{\star}(k)$. This allows the controller to track dynamic references. In Fig, 3.3 a block diagram of the proposed predictive methodology is presented. The reference prediction horizon $N^{\star}$ used in (3.19) serves to trade-off response times versus control effort by limiting the total increment in the capacitor current, i_c, as presented in (3.21). In fact, if a faster tracking response is desired, then $N^{\star}$ should be chosen small. However, this will, in general, lead to large converter currents. To incorporate current limitations, one can adopt the embellishments of the basic control algorithm presented in Section 3.4.2 below.

Remark 3.4.1 *The reference prediction horizon $N^{\star}$ slides forward in time in a moving horizon manner. Viewed from this perspective, the proposed control algorithm can be regarded as having a unit* switching horizon*, but an overall* prediction horizon *equal to $N^{\star}$, compare to ideas expressed in [73]. As will be apparent by the experimental results included in Section 3.5, our formulation gives good performance, but requires only a moderate computational effort.* ■

3.4.2 Incorporation of current limits

To avoid providing reference values which are associated with large converter currents, one can limit $P_s^{\star}(k+1)$ in (3.25) according to:

$$|P_s^{\star}(k+1)| \leq P^{\max}(k+1), \tag{3.26}$$

where

$$P^{\max}(k+1) \triangleq \sqrt{\left(3\hat{V}_s\hat{I}_s^{\max}/2\right)^2 - \left(Q_s^{\star}(k+1)\right)^2} \tag{3.27}$$

and $\hat{I}_s^{\max}$ is a limit for the components of $\mathbf{i}_s(k)$.

In addition, one can also restrict the possible switch combinations $\mathbf{s}(k)$ when minimizing the cost function $J(\mathbf{s}(k))$ in (3.18) to those $\mathbf{s}(k) \in \mathcal{S}$, which provide current predictions $\mathbf{i}_s'(k+1)$ satisfying the limit. The proposed modifications can be expected to lead to control loops which are not affected by windup problems typical of PI-control loops, see [83] for related discussions on the use of MPC for linear-time invariant systems with *convex* constraints.

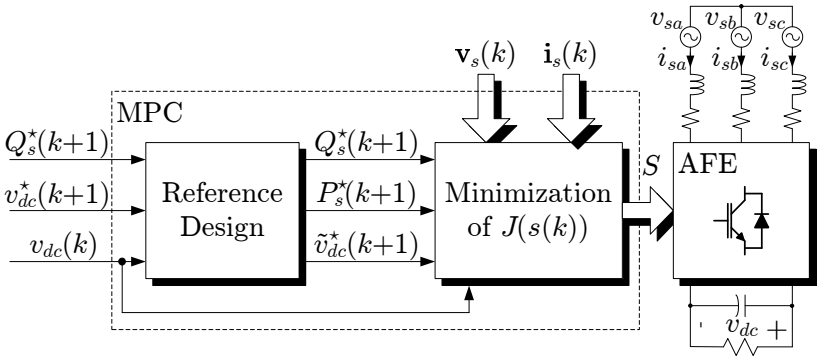

Figure 3.3: MPC with Dynamic Reference Design

3.5 Results

To verify the performance of the predictive control strategy proposed in the present work, simulation studies and experiments were carried out. Simulations were performed using Matlab/Simulink software. The lab prototype of the AFE rectifier, presented in Fig. 3.1, is comprised of a 6-pack IGBT module. The electrical parameters of the system are given by $r_s = 0.4\ \Omega$, $L_s = 15\ H$, $C_{dc} = 1500\ \mu F$ and $R_{dc} = 60\ \Omega$. To protect the power device, the source current is limited to a maximum of $\hat{I}_s^{\max} = 8\ A$. In addition, the source voltage is chosen to be $\hat{V}_s = 62\ V$, whereas its frequency is $f_o = 50\ Hz$. This voltage is obtained from the grid (220 V rms) and adapted by using an auto-transformer. It is important to emphasize that the grid voltage, v_s, contains 4.5% of fifth harmonic and a total harmonic distortion of 5%. This amount of fifth harmonic is taken into account in the simulation tests, which thereby exhibit a similar system behaviour to that observed in the experiments.

The algorithm of Sections 3.3 and 3.4 (including the modification presented in Section 3.4.2), was implemented in a digital platform using a Xilinx Spartan 3 FPGA considering a sampling period of $h = 20\ \mu s$. The weighting factors in the cost function $J(\mathbf{s}(k))$ were chosen as $k_p = k_q = 1$ and the reference prediction horizon was set as $N^\star = 320$. This allows the controller to limit the capacitor current increment to about 3% of the total current needed to lead the dc-voltage to its desired reference. To capture the required data, an Agilent

DSO5014A oscilloscope was used. It is important to emphasize that control calculations performed in the digital platform require less than 3 μs. Therefore, the optimal switch combination is applied to the converter with this delay, and before the following sampling instant.

3.5.1 DC-Voltage Tracking

We first investigate dc-voltage tracking. The performance of the proposed predictive strategy when a change in the dc-voltage reference $v_{dc}^{\star}$ is produced is depicted in Figs. 3.4 and 3.5. The initial dc-voltage is taken as $v_{dc} = 110\ V$, corresponding to a source power of the order of $P_s = 180\ W$. A unity power factor is desired, which results in null reactive power, i.e., $Q_s^{\star} = 0$ VAr. As can be clearly appreciated in the figures, the predictive controller accommodates this requirement, by making the source current i_{sa} be in phase with the source voltage v_{sa}.

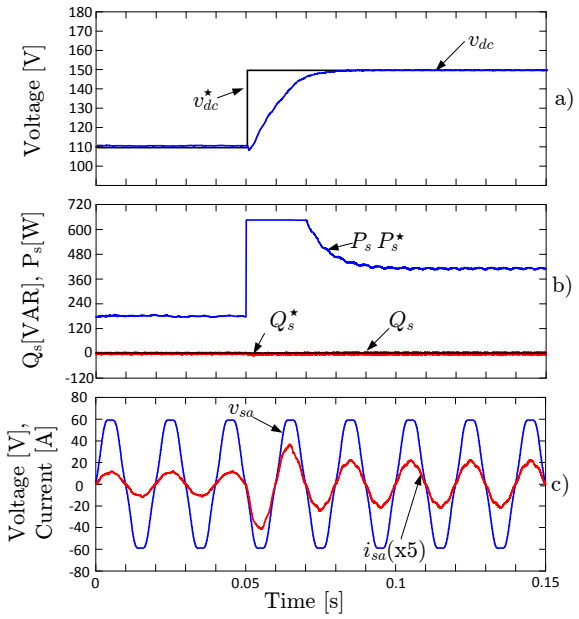

Figure 3.4: Performance of the MPC algorithm presented – Simulation: step in the (unfiltered) dc-voltage reference $v_{dc}^{\star}$.

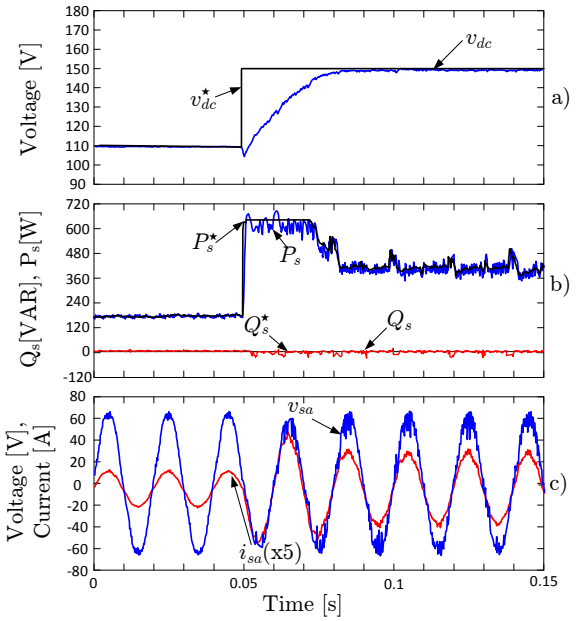

Figure 3.5: Performance of the MPC algorithm presented – Experiment: step in the (unfiltered) dc-voltage reference $v^{\star}_{dc}$.

To examine the effect of the tuning parameters on the AFE behaviour, we performed the same test but considering a smaller weighting factor for the reactive power, namely, $k_q = 0.01$. This result is shown in Fig. 3.6. Here, it can be appreciated that the reactive power exhibits a higher ripple during steady state when compared to the previous case. Additionally, it can be noticed that during the transient the increment in the reactive power error is considerable higher than in the previous case. Henceforth, due to the good performance obtained, in the remaining tests the tuning factors will be kept at their original values, namely, $k_p = k_q = 1$.

At time instant $t = 0.05[s]$, the dc-voltage reference is increased to $v^{\star}_{dc} = 150[V]$. This voltage increment requires active power from the source. However, the latter power is limited to $P_{\max} = 650[W]$ due to the fact that, as mentioned above, the current that the AFE prototype can manage is limited to $I_{\max} = \hat{I}^{\max}_s = 8[A]$. It can be noticed that both simulated and practical results illustrate a similar system behavior, despite the presence of the measurement noise. In particular, in both cases the system takes about $20[ms]$ to

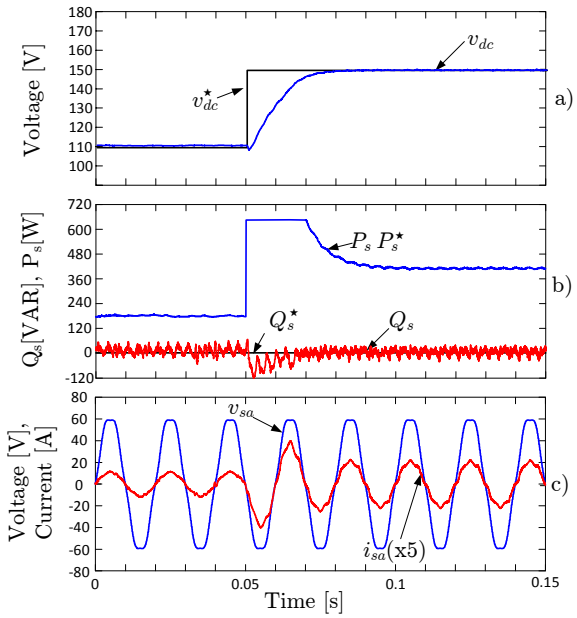

Figure 3.6: Performance of the MPC algorithm presented – Simulation: step in the (unfiltered) dc-voltage reference $v^{\star}_{dc}$. ($k_q = 0.01$).

reach the new dc-voltage reference. It can also be appreciated in Figs. 3.4 and 3.5 that the proposed controller gives good tracking performance, with no overshoot. It is remarkable that throughout the transient where saturations occur, the reactive power Q_s has been held approximately equal to zero by the controller, keeping the source current in phase with its associated voltage. The total harmonic distortion in the source current for the initial condition, $v_{dc} = 110[V]$, is $\text{THD}_i = 5\%$. For a dc-voltage of $v_{dc} = 150[V]$ the obtained distortion is $\text{THD}_i = 5\%$. It is important to emphasize that the current distortion is also affected by the distortion in the voltage source which is given by $\text{THD}_v = 5\%$.

3.5.2 Tracking of Dynamic Reactive Power References

One of the main uses of AFE converters is to compensate for the lack of reactive power of the electrical grid. Therefore, it is important to verify that the proposed controller can maintain the rectified dc-voltage even when different power factors are demanded of the system. Figs. 3.7 and 3.8 illustrate the achieved performance when facing this situation.

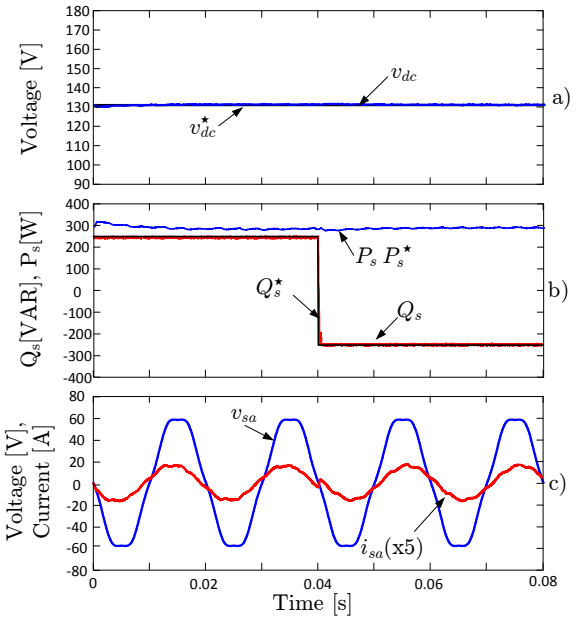

Figure 3.7: Performance of the MPC algorithm presented – Simulation: step in the reactive power reference $Q_s^{\star}$.

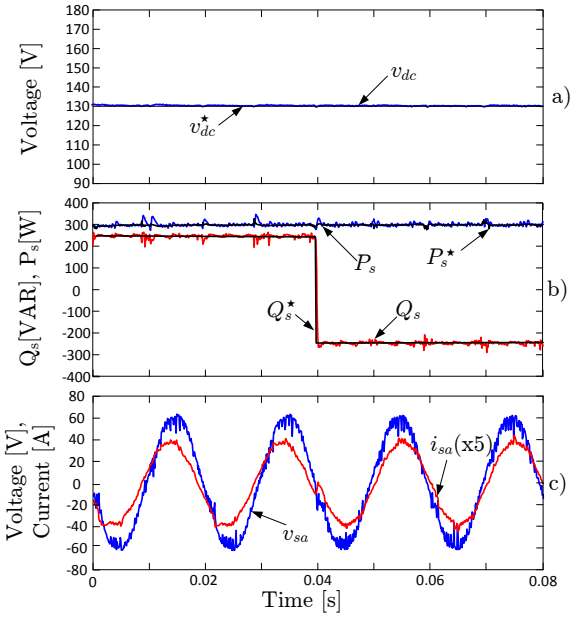

Figure 3.8: Performance of the MPC algorithm presented – Experiment: step in the reactive power reference $Q_s^{\star}$.

Similar to the test documented in Section 3.5.1, the initial condition of the system considers a dc-voltage of $v_{dc} = 130[V]$ and an active power in the order of $P_s = 300[W]$. However, reactive power $Q_s = 250$[VAr] is provided from the rectifier to the source, amounting to a positive power factor of PF $= 0.769$. Consequently, and as can be seen in the figures, the source current lags the source voltage by about 39.7^o.

To examine the tracking capabilities of the system, at approximately $t = 0.04[s]$, a step down change in the reactive power reference is introduced, from $Q_s = +250$[VAr] to $Q_s = -250$[VAr]. It can be appreciated in Figs. 3.7 and 3.8 that the controller makes the AFE track this step change quickly, barely affecting the active power P_s or the capacitor voltage v_{dc}. In steady state, the power factor is negative (PF $= -0.769$), the source current leading the source voltage by 39.7^o.

3.5.3 Load Changes

In practical applications, loads may be time-varying and, thus, R_{dc} needs to be estimated. Since estimators will unavoidably be affected by errors, another important aspect to be analyzed is robustness to unknown load changes. Experimental results are depicted in Fig. 3.9. Here we chose the same initial condition as in Section 3.5.1, namely, $Q_s = 0$[VAr], and $v_{dc} = 130[V]$, which amounts to an active power of about $P_s = 300[W]$.

At the instant $t = 0.1[s]$, a resistance load change of 50% is produced from $R_{dc} = 60[\Omega]$ to $R_{dc} = 30[\Omega]$. It can be observed in Fig. 3.9 that the predictive controller proposed was capable to keep the dc-voltage, v_{dc}, near its reference value $v_{dc}^{\star} = 130[V]$, despite the load disturbance. It is worth noting that the controller has no knowledge of the load disturbance. The system model used to predict the future behaviour simply assumes $R_{dc} = 60[\Omega]$ at all times. Consequently, a slight increment in the dc-voltage ripple occurs.

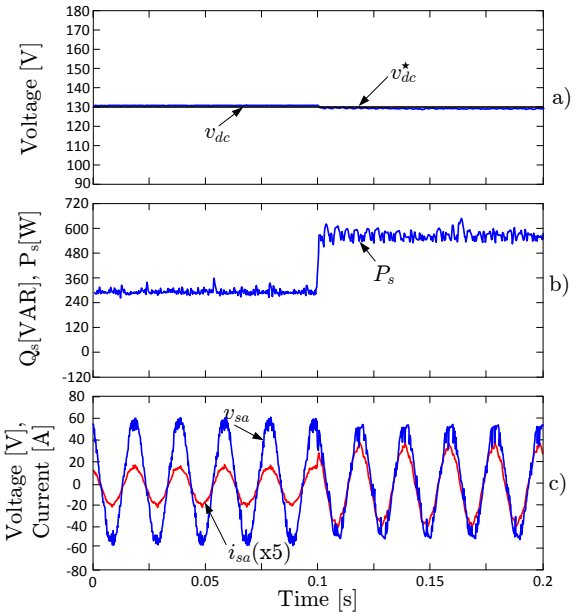

Figure 3.9: Performance of the MPC algorithm presented – Experiment: step in the load resistance R_{dc}.

3.5.4 Supply Voltage Variations

The robustness of the proposed control system to supply voltage variations is also analyzed. Results in Fig. 3.10 show the response of the system when the supply voltage is reduced in 40%. The reference values are $Q_s = 0$[VAr] and $v_{dc} = 130[V]$. Here, a soft decrement of the voltage source from $v_s = 55[V]$ to $v_s = 30$ is introduced. The active power presents an increment from $P_s = 300[W]$ to $P_s = 330[W]$ to compensate the variation and keep the dc-voltage fixed at it reference. The input current is increased accordingly from $I_s = 3,5[A]$ rms to $I_s = 7[A]$ rms.

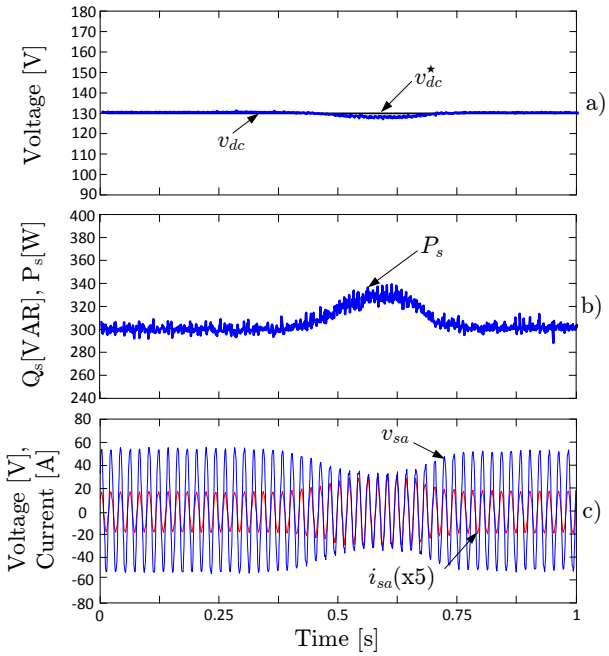

Figure 3.10: Performance of the MPC algorithm presented – Experiment: supply voltage variation.

3.6 Conclusions

We have presented a model predictive control formulation for AFE rectifiers. The proposed control algorithm operates in discrete-time and does not require any additional modulators to drive the switches. The switching horizon is chosen equal to one. Thus, the search set for on-line optimizations has only eight elements, making the switching signals easy to calculate in practice.

The key novelty of our approach lies in the way dynamic references are handled. To be more specific, careful examination of electrical properties of the rectifier topology has allowed us to elucidate the issue of finding compatible references for active source power and dc-voltage.

Our method is capable of providing suitable references for the source active power and the rectified voltage, without use of additional control loops. The control architecture proposed also incorporates possible saturations of source currents directly in its formulation. This

allows one to ensure safe operation of the device. Here the introduction of a *reference prediction horizon*, which may differ from the *switching horizon*, has proven useful, allowing the system designer to trade-off tracking bandwidth for control effort.

Simulations and experimental results on a lab-prototype show that fast and accurate tracking of dynamic dc-voltage and reactive power references can be achieved. Interestingly, due to the way that constraints on maximum power levels of the rectifier are treated, good transient performance can be observed even when saturation limits are reached. It is important to emphasize that, during transients where saturations occur, overshoots are avoided.

Future work may include studying robustness of the approach, adapting the formulation to non-resistive loads, deriving tuning guidelines, and also investigating closed loop stability issues. The latter have been examined for related, but simpler, systems in [37, 81].

4

FCS-MPC with Improved Steady-State Performance

4.1 Introduction

As shown in previous chapters, the control target of FCS-MPC is to minimise the system tracking error produced at each sampling instant. Consequently, the predictive controller will optimise the *at sample response* of the converter. However, since the system states are continuous, e.g., output current, the converter may achieve a poor continuous-time performance. Therefore, it is important to analyse the continuous-time response of the controlled converter when using the discrete-time control law provided by FCS-MPC. In [84], extensive simulations were carried out, showing that existing FCS-MPC algorithms give, in general, a non-zero steady-state error. Moreover, this error is more relevant when lower switching frequency and/or lower magnitude references are used. In this work, we extend the study presented in [84] by performing a mathematical analysis to determine the steady-state error. To mitigate this problem, two different approaches are proposed in this work. The first one is based on the idea of using different sampling and actuation instants, resembling classical PWM techniques. The second one takes into account the tracking errors not only at the sampling instant, but also during the inter-sampling.

To facilitate the understanding of the problem and the proposed solutions, we apply our proposals to control the output current of a simple four-quadrant chopper converter.

4.2 Finite Control Set Model Predictive Control

In this section, a brief review of FCS-MPC is presented. Further theoretical analysis can be found in [37,81,85]. For some examples of applications in power electronics see [10,14,25].

4.2.1 Basic Principles

FCS-MPC operates in discrete time with fixed sampling frequency $f_s = h^{-1}$. Therefore, it is necessary to obtain a discrete-time model of the plant

$$x^{k+1} = F(x^k, S^k), \tag{4.1}$$

where x represents the system states and S stands for the control inputs. In this case, FCS-MPC directly considers the converter power switches as the control input of the system. Thus, each control input can adopt only two values, remaining constant during the sampling period, h, i.e. $S_i(t) \in \{0, 1\}$, for all $t \in [kh, (k+1)h]$. Consequently, the input belongs to a finite control set of switch combinations $S \in \mathbb{S} = \{S_1, \ldots, S_n\}$.

To forecast the future system behaviour, FCS-MPC uses a cost function, namely $g(k, \vec{S})$, where $\vec{S} = \{S^k, \ldots, S^{k+N-1}\}$ is a *feasible* input sequence. Thus, the optimal switching sequence is obtained by minimizing this cost function

$$\vec{S}_{op} = \left\{ S^k_{op}, \ldots, S^{k+N-1}_{op} \right\} \triangleq \arg \left\{ \min_{\vec{S} \in \mathbb{S}^N} g(k, S^k) \right\}.$$

Since the input belongs to a finite set, the minimization process is carried out by evaluating all the possible switch combinations. Finally, the optimal switching input to be applied is the first element of the optimal switching sequence

$$\mathbf{S^k} = S^k_{op}.$$

Thus, this predictive strategy directly provides the optimal switching actions to be applied to the converter. Consequently, no intermediate modulation stages are required [14].

4.2.2 Implementation

In practical implementations of FCS-MPC with prediction horizon $N = 1$, there exist three main processes: Measurement, Estimation and Prediction. A temporal scheme of these stages is depicted in Fig. 4.1.

Measurement: Since this predictive strategy works in discrete time, it is necessary to take measurements of the state variables, $\mathbf{x^k}$, at each sampling instant k. (in some cases, some of these variables can be observed [86]). These current state values are used by the controller to decide upon the optimal switching action to be applied.

Estimation: To account for computational delaying, in standard formulations, the optimal switching action is applied at time $k+1$, $\mathbf{S^{k+1}}$. Thus, the effect of this action will be observed only at the instant $k+2$. This delay of one sampling period results in the need to predict not only the value of the variables to be controlled at the instant $k+2$, but also to know their values at the instant $k+1$. To do this, we take advantage of the fact that the previous optimal switching action, $\mathbf{S^k}$, remains constant until the next sampling instant $k+1$. Thus, considering the system model presented in (4.1), the system state, at the instant $k+1$, can be estimated by:

$$\widetilde{x}^{k+1} = F(\mathbf{x^k}, \mathbf{S^k}). \tag{4.2}$$

Prediction: In order to obtain the optimal input, FCS-MPC forecasts the system state behaviour at the instant $k+2$ by evaluating all the possible switch combinations. This is expressed via:

$$x^{k+2} = F(\widetilde{x}^{k+1}, S^{k+1}), \tag{4.3}$$

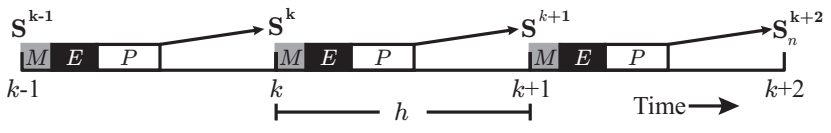

Figure 4.1: Temporal scheme of Finite-Control-Set MPC.

where $S^{k+1} \in \mathbb{S}$. These predictions are compared to the reference by evaluating a cost function, $g^k(S_i)$, i.e.,

$$g^k = \left(\overset{*}{x}^{k+2} - x^{k+2}\right)^T W \left(\overset{*}{x}^{k+2} - x^{k+2}\right),$$

where W is a positive definite matrix (weighting matrix). Thus, the optimal switching input $\mathbf{S^{k+1}}$ is that one which produces the minimum value in the cost function.

4.3 Steady-State Issues

In this section we investigate the steady-state performance of FCS-MPC in terms of the average value.

4.3.1 Theoretical Background

As presented in Section 4.2, it is clear that FCS-MPC seeks to minimise the tracking error produced at each sampling instant k. Hence, this predictive strategy provides a discrete-time control law. Nevertheless, in most of the cases this control paradigm is used to control continuous-time variables, e.g., converter output current. Therefore, it is important to analyse the continuous-time system response of the converter when governed by FCS-MPC.

To quantify the continuous-time performance, we propose to consider the *deviation from the average* of the controlled variable during the intersampling. This is expressed via:

$$\delta_{av}^k = \left|\overset{*}{x}^k - \bar{x}^k\right| \tag{4.4}$$

where $\bar{x}^k$ is the average value of the controlled variable:

$$\bar{x}^k = \frac{1}{h}\int_{kh}^{(k+1)h} x(t) \cdot dt$$

As will be shown latter, with standard FCS-MPC the average value of the controlled variable, $\bar{x}^k$, will not always be the same as the desired reference, $\overset{*}{x}^k$. This issue constitutes the main motivation of the present work.

4.3.2 Study Case: H-Bridge

As an illustrative example, we analyse the continuous-time performance of a four-quadrant chopper converter under FCS-MPC. This topology is very popular in audio applications [87, 88] as well as power drives [89].

This converter is comprised of two pairs of complementary power switches (S_1, $\overline{S}_1$, and $S_2, \overline{S}_2$) and a dc-voltage source V_{dc}, as depicted in Fig 4.2.

The load voltage can be easily obtained from:

$$v_l(t) = V_{dc} S(t),$$

where $S(t) = S_1(t) - S_2(t)$. Thus, the continuous-time dynamic model for the load current is given by:

$$\frac{d\, i_l(t)}{dt} = -\frac{R}{L} i_l(t) + \frac{V_{dc}}{L} S(t). \tag{4.5}$$

Since $S_1, S_2 \in \{0, 1\}$, the control input, $S(t)$, belongs to the finite set

$$S(t) \in \mathbb{S} = \{-1, 0, 1\}.$$

Therefore, v_l can take only one of three different values, namely V_{dc}, 0 and $-V_{dc}$.

Due to the fact that with FCS-MPC the power switches remain constant during the intersampling, the output current in (4.5) can be exactly represented, in continuous-time, via:

$$\begin{aligned} i_l(t) &= F\left(\mathbf{x}^{\mathbf{k}}, \mathbf{S}^{\mathbf{k}}, t\right), \\ &= \mathbf{i}_{\mathbf{l}}^{\mathbf{k}} e^{-t/\tau} + \frac{V_{dc}}{R}\left(1 - e^{-t/\tau}\right) \mathbf{S}^{\mathbf{k}}, \end{aligned} \tag{4.6}$$

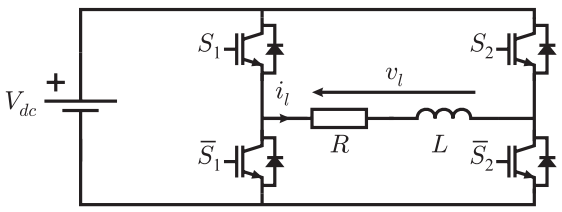

Figure 4.2: Four-quadrant chopper converter.

for all $t \in [kh, (k+1)h]$, where $\tau = L/R$.

Consequently, the value of the load current at the next sampling instant is:

$$\begin{aligned} i_l^{k+1} &= F(\mathbf{x^k}, \mathbf{S^k}, h), \\ &= \mathbf{i_l^k} e^{-h/\tau} + \frac{V_{dc}}{R}\left(1 - e^{-h/\tau}\right)\mathbf{S^k}. \end{aligned} \tag{4.7}$$

To analyse the steady-state performance of this converter when governed by FCS-MPC, we focus on the particular periodical input sequence $\vec{S} = \{1, 0, 1, 0, \ldots\}$. Under this situation, the system will reach a steady-state behaviour as depicted in Fig. 4.3. To properly describe this pattern, it is necessary to obtain the steady-state bounds, I_L and I_H, of the state trajectory. From Fig. 4.3, we can notice that the lower bound satisfies that $I_L = i_l^k = i_l^{k+2}$. Thus, from (4.7) we have that:

$$I_L = \frac{V_{dc}}{R}\left(\frac{e^{-h/\tau}}{1 + e^{-h/\tau}}\right), \tag{4.8}$$

while the upper bound, I_H, can be obtained via:

$$I_H = \frac{I_L}{e^{-h/\tau}} = \frac{V_{dc}}{R}\left(\frac{1}{1 + e^{-h/\tau}}\right). \tag{4.9}$$

Consequently, the average value, $\bar{i}_l$, produced by this pattern can be determined as follows:

$$\begin{aligned} \bar{i}_l =& \frac{1}{2h}\int_0^h \left(I_L e^{-t/\tau} + \frac{V_{dc}}{R}\left(1 - e^{-t/\tau}\right)\right) \cdot dt + \frac{1}{2h}\int_h^{2h} I_H e^{-t/\tau} \cdot dt \\ =& \frac{V_{dc}}{2R}. \end{aligned} \tag{4.10}$$

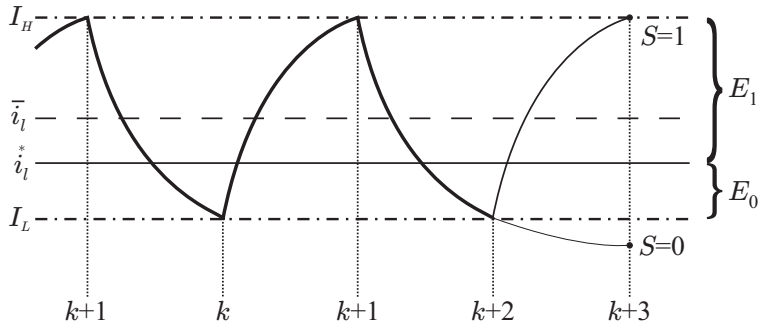

Figure 4.3: Steady-state pattern for an input sequence $\vec{S} = \{1, 0, 1, 0, \ldots\}$.

We next analyse under which conditions FCS-MPC will provide the sequence $\vec{S} = \{1, 0, 1, 0, \ldots\}$. To obtain the optimal input to be applied at the instant $k+2$, i.e., $\mathbf{S^{k+2}}$ (see Fig. 4.3), the predictive controller will compare the forecast error at the next sampling instant, $k+3$, produced by the different possible inputs, i.e. $e^{k+3} = \overset{*}{i}_l - i^{k+3}$. Considering that $\overset{*}{i}_l < \bar{i}$, the input $S^{k+2} = 0$ will generate the tracking error E_0 represented via:

$$E_0 = \overset{*}{i}_l - I_{P0} = \bar{i}_l - \delta_{av} - I_L e^{-h/\tau},$$

while the input $S^{k+2} = 1$ will produce the tracking error E_1 expressed by:

$$E_1 = I_{P1} - \overset{*}{i}_l = I_H - \bar{i}_l + \delta_{av},$$

where, from (4.4), $\delta_{av} = \bar{i}_l - \overset{*}{i}$.

To maintain this periodical pattern, at the instant $k+2$ an input $S^{k+1} = 1$ should be applied to the converter. Due to the optimization carried out by FCS-MPC, this will occur whenever $E_0 > E_1$. Thus, a critical average error, δ_{cr}, can be obtained by equalizing both predicted errors $E_0 = E_1$. We thus have:

$$\begin{aligned} \delta_{cr} &= \bar{i}_l - \frac{1}{2}\left(I_H + I_L e^{-h/\tau},\right), \\ &= \frac{I_L}{2}\left(1 - e^{-h/\tau}\right). \end{aligned} \tag{4.11}$$

Therefore, if $\delta_{av} < \delta_{cr}$, then the minimum forecast error will be E_1. Consequently, $\mathbf{S^{k+2}} = 1$ will be applied.

It is important to emphasize that the input sequence pattern, $\vec{S} = \{1, 0, 1, 0, \ldots\}$, will prevail provided $\bar{i}_l > \overset{*}{i}_l > \bar{i}_l - \delta_{cr}$. This lower limit can be determined via:

$$\begin{aligned} \overset{*}{i}_{cr} &= \bar{i}_l - \delta_{max}, \\ &= \frac{V_{dc}}{2R}\left(\frac{e^{h/\tau} + e^{-h/\tau}}{1 + e^{-h/\tau}}\right) e^{-h/\tau}. \end{aligned} \tag{4.12}$$

Assuming that $h < \tau/2$, it is possible to approximate $e^{h/\tau} + e^{-h/\tau} \approx 2$. Then, from (4.12), the critical reference can be approximated as:

$$\overset{*}{i}_{cr} \approx \frac{V_{dc}}{R}\left(\frac{e^{-h/\tau}}{1 + e^{-h/\tau}}\right) = I_L. \tag{4.13}$$

A similar result can be obtained for the case when $\overset{*}{i}_l > \bar{i}$, then the critical limit becomes i_H.

The preceding analysis shows that for any reference which belongs to the range

$$\overset{*}{i}_l \in (I_L, I_H),$$

FCS-MPC will produce *the same average value*

$$\bar{i}_L = \frac{V_{dc}}{2R}.$$

This steady-state analysis can be extended for different steady-state patterns.

In the following sections we will propose two modifications of FCS-MPC which are aimed at reducing the steady-state error.

4.4 Intermediate Sampling (IS-MPC)

4.4.1 Basic Principle

The use of synchronous current sampling with PWM schemes is wide-spread. By sampling either at the maximum or minimum of the triangular carrier. Thus, a good approximation of the average value of the controlled variable can be obtained, as shown in Fig. 4.4.

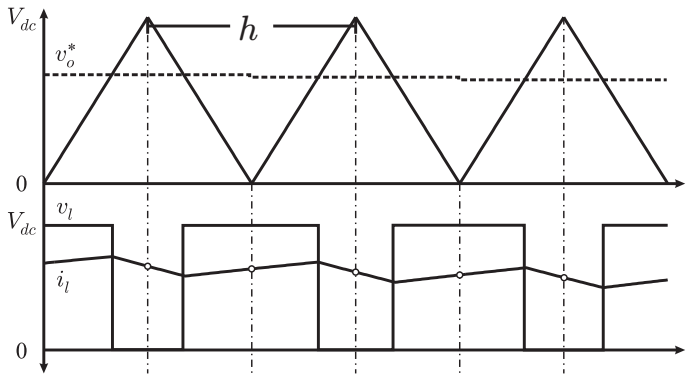

Figure 4.4: Synchronous current sampling with PWM.

This idea can be easily adapted to be used in the FCS-MPC strategy in order to approximate the average value of $x(t)$. As previously stated, FCS-MPC can only change the value of the converter switches at the beginning of each sampling period, $t = kT$. Then, the measurement of $x(t)$ is taken at each instant $t = kh + h/2$, which will be denoted by $\mathbf{x^{k+\frac{1}{2}}}$. Due to this temporal shift of $h/2$, the final estimate of system state can be calculated as:

$$\widetilde{x}^{k+1} = F(\mathbf{x^{k+\frac{1}{2}}}, \mathbf{S^k}, h/2)$$

Then, similar to the standard FCS-MPC algorithm, predictions are calculated by considering the measurement $\mathbf{x^{k+\frac{1}{2}}}$ and the system state estimation, $\widetilde{x}^{k+1}$. For IS-MPC, however, predictions are obtained for the instant $t = (k+1)h + h/2$. This gives a better approximation to the average value of the system state, $\bar{x}(t)$, which then gets closer to the reference. Thus, the proper expression for the prediction is:

$$x^{(k+1)+\frac{1}{2}} = F(\widetilde{x}^{k+1}, S^{k+1}, T/2).$$

This expression is used to evaluate the IS-MPC cost function:

$$g^k = \left(\overset{*}{x}^{k+2} - x^{(k+1)+\frac{1}{2}}\right)^T W \left(\overset{*}{x}^{k+2} - x^{(k+1)+\frac{1}{2}}\right) \tag{4.14}$$

for all possible combinations of $S^{k+1} \in \mathbb{S}$. The optimal switching action, $\mathbf{S^{k+1}}$, which minimises (4.14) is then chosen. The temporal scheme of the IS-MPC algorithm is shown in Fig.4.5.

Remark 4.4.1 *Notice that, since the measurements are taken in the middle of the sampling period, the obtained samples are less affected by commutation noises. Additionally, IS-MPC obtains predictions of the system state for one sampling period ahead after mea-*

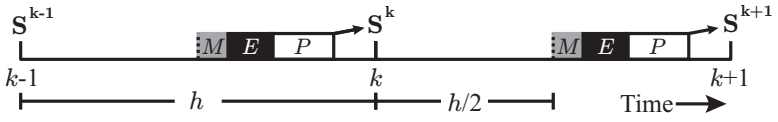

Figure 4.5: Temporal scheme of Intermediate Sampling MPC

surements are taken (see Fig. 4.5) while standard FCS-MPC carries out the state predictions for two sampling periods ahead, as described in Section 4.2. This decreases the estimation and prediction errors.

4.4.2 Application to H-Bridge

Here, we apply the proposed IS-MPC algorithm to the four-quadrant chopper presented in Section 4.3.2. At the middle of each sampling period, $k + 1/2$, a measurement of the load current is taken, $\mathbf{i_l^{k+\frac{1}{2}}}$. Then, from (4.7), the load current, at the instant $k + 1$, is estimated by:

$$\widetilde{i}_l^{k+1} = \mathbf{i_l^{k+\frac{1}{2}}} e^{-h/2\tau} + \frac{V_{dc}}{R}\left(1 - e^{-h/2\tau}\right)\mathbf{S^k} \tag{4.15}$$

Afterwards, the predictions are obtained considering $\widetilde{i}_l^{k+1}$, from (4.15), as the initial state. Thus, the prediction horizon is considered to be $N = h/2$:

$$i_l^{(k+1)+\frac{1}{2}} = \widetilde{i}_l^{k+1} e^{-h/2\tau} + \frac{V_{dc}}{R}\left(1 - e^{-h/2\tau}\right) S^{k+1} \tag{4.16}$$

Finally, the load current prediction obtained by (4.16) is compared with the desired reference given at the beginning of the next sampling period, $\overset{*}{i}_l^{k+1}$. Thus, the cost function for the four-quadrant chopper under IS-MPC is expressed via:

$$g^k = \left(\overset{*}{i}_l^{k+1} - i_l^{(k+1)+\frac{1}{2}}\right)^2 \tag{4.17}$$

4.5 Integral Error Term (IE-MPC)

4.5.1 Basic Principle

As mentioned in Section 4.3.1, FCS-MPC optimises the at sample response of the system. However, since the system states are normally continuous, a poor intersample response can be obtained in some cases. To overcome this situation, we propose to take into account the intersample performance by adding an extra term in the cost function, g^k. This term will be chosen as the integral of the error between the reference, $\overset{*}{x}(t)$, and the predicted continuous behaviour of the controlled variable within a sampling period h,

$x(t) = F(\widetilde{x}^{k+1}, S^{k+1}, t)$. Taking into account the one-sampling-period delay, this integral error is represented via:

$$I^{k+1} = \frac{1}{h}\int_{k(h+1)}^{k(h+2)} \left(\overset{*}{x}(t) - F(\widetilde{x}^{k+1}, S^{k+1}, t)\right) d\,t \tag{4.18}$$

This integral term gives us information about the average error generated by each switch combination, $S^{k+1} \in \mathbb{S}$. In addition, we propose to include previous integral error to improve the continuous performance of the predictive controller. Thus, the proposed cost function, for the IE-MPC strategy, is given by:

$$g^k = \left(\overset{*}{x}^{k+2} - x^{k+2}\right)^T W \left(\overset{*}{x}^{k+2} - x^{k+2}\right) + K_i \left(I^{k+1} + \sum_{j=1}^{m} \mathbf{I^{k+1-j}}\right)^2 \tag{4.19}$$

where K_i is a weighting factor which gives us a higher/lower importance to the integral term, while $\mathbf{I^{k+1-j}}$ represents previous integral errors. The temporal scheme of the IE-MPC algorithm is depicted in Fig.4.6.

Remark 4.5.1 *Notice that this cost function can be associated with a discrete Proportional-Integral (PI) controller, which is comprised of two parts. A proportional part, which acts over the instantaneous error, δ^k, and provides a fast response, and an integral part, which is related with the accumulated error. In this case, the accumulated error considers the intersample behaviour of the system state in order to achieve a better continuous performance. Therefore, the factor K_i can be adjusted in a similar fashion than in a PI design.*

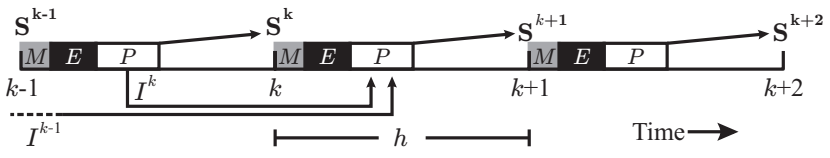

Figure 4.6: Temporal scheme of Finite-Control-Set MPC with integral minimisation.

4.5.2 H-Bridge

The integral term, I^{k+1}, for the four-quadrant chopper is obtained by replacing (4.6) in (4.18):

$$I^{k+1} = \overset{*}{i}{}^{k+1} - \frac{\tau}{h}\left(1 - e^{-h/\tau}\right)\mathbf{i^k} + \left(\frac{\tau}{h}\left(1 - e^{-h/\tau}\right) - 1\right)\frac{V_{dc}}{R}S^{k+1} \tag{4.20}$$

Finally, according to (4.19) and considering m previous integral errors, the final cost function to be evaluated for this particular case, becomes:

$$g^k = \left(\overset{*}{i}{}_l^{k+2} - i_l^{k+2}\right)^2 + K_i\left(I^{k+1} + \sum_{j=1}^{m}\mathbf{I^{k+1-j}}\right)^2 \tag{4.21}$$

Remark 4.5.2 *It is important to emphasise that only the last term of* (4.20) *depends on the switching input. The term* $\sum_{j=1}^{m}\mathbf{I^{k+1-j}}$ *depends on previous calculated errors. Thus, most of this expression does not need to be recalculated when predictions are carried out. Consequently, the on-line implementation of this cost function does not represent a high increment in the process time when compared to standard FCS-MPC.*

4.6 Results

To verify the performance of the prosed solutions, simulation and experimental studies were carried out on an H-Bridge converter depicted in Fig. 4.2. A main dc-link voltage source of $V_{dc} = 150\ V$ was considered. The electrical load parameters are $R = 15\ \Omega$ and $L = 10\ mH$. The proposed solutions as well as the standard FCS-MPC strategy were implemented using a sampling period of $h = 200\ \mu s$. In this case, the load current, $i_l(t)$, is the variable to be controlled and the control target is to maintain its average value near to the reference.

Since we are interested in controlling only one variable, standard FCS-MPC and IS-MPC, as shown in previous sections, do not require any tuning. On the other hand, as previously stated in Section 4.5, and according to (4.21), IE-MPC strategy requires to select the weight factor K_i and the number of previous integral errors m. In this case, these tuning parameters where chosen as $K_i = 1.5$ and $m = 2$.

4.6.1 Average Error

The steady-state average errors, for different current reference, produced by the standard FCS-MPC and the proposed solutions, IS-MPC and IE-MPC, are presented in Fig. 4.7. Here, only positive values of the load current, i_l, are considered due to the fact that the average error pattern is symmetric with respect to zero.

It can be observed that standard FCS-MPC generates higher errors when the current reference is near to zero and when it is near to the maximum current. This is due to the fact that this predictive strategy applies a null voltage, $v_l = 0$, whenever the current reference is $\overset{*}{i}_l \in (0,\, 0.8)\, A$ and a maximum voltage, $v_l = V_{dc}$, whenever the current reference is $\overset{*}{i}_l \in (9.2,\, 10)\, A$. For these particular references, it can be noticed that the proposed solutions, IS-MPC and IE-MPC, reduce these average errors.

Another interesting case is related to the error produced around 5 A (half of the maxim load current). This error is generated by the particular input sequence, $\vec{S} = \{1, 0, 1, 0, \ldots\}$, analysed in Section 4.3.2. Therefore, FCS-MPC applies this input sequence whenever the

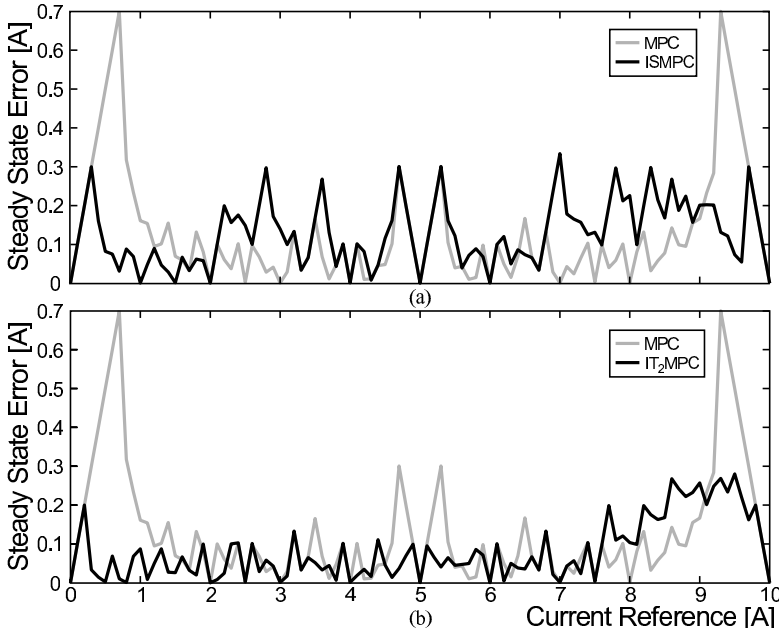

Figure 4.7: Average error as a function of the current reference.

current reference is $\overset{*}{i_l} \in (4.7, 5.3)\ A$. Regarding the proposed solution, for this reference range, IS-MPC presents a similar average error than standard FCS-MPC while IE-MPC reduces this error considerably.

Fig. 4.8 shows a normalised average error as a function of the current reference value. In this way a better sense of the importance of the average error can be observed. From this viewpoint, the main problem of the predictive techniques are around zero, in this zone the benefits of the use of IE-MPC, and even IS-MPC, are clear.

4.6.2 Experimental Results

In this section, experimental results of standard FCS-MPC and our proposals, IS-MPC and IE-MPC, are presented. The predictive strategies were implemented in a standard TMS320C6713 DSP. Then, the optimal input was applied to the converter by using an XC3S400 field-programmable gate array (FPGA). Table 4.1 summarises the execution times taken by the predictive algorithms. Here, it is possible to see that IS-MPC takes the same time than standard FCS-MPC to obtain the optimal input, due to the fact that no extras calculation are needed. On the other hand, IS-MPC takes about double of the time more to obtain the optimal input when compared to the standard FCS-MPC.

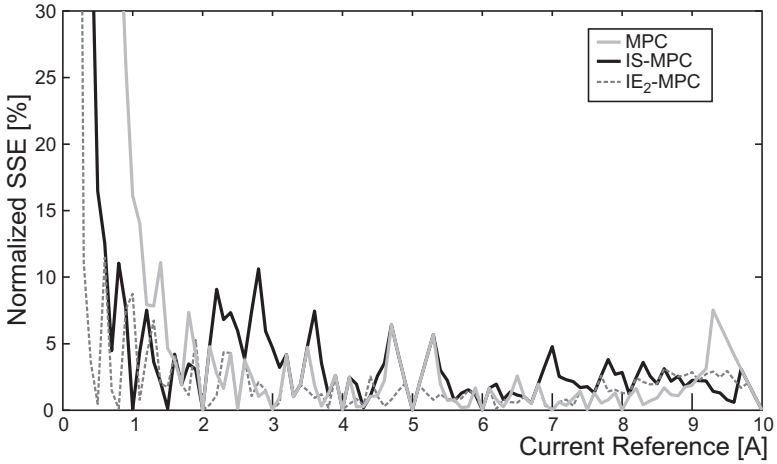

Figure 4.8: Normalized average error.

Table 4.1: Execution Time of each Predictive Algorithm.

Predictive Strategy	FCS-MPC	IS-MPC	IE-MPC
Execution Time (μs)	2.14	2.14	4.1

Fig. 4.9 shows the steady-state performance achieved by the different predictive strategies for a load current of $\overset{*}{i}_l = 0.6\,A$. Here, it is possible to observe that the converter applies a null voltage, $v_l = 0\,V$, to the load when governed by standard FCS-MPC. This behaviour

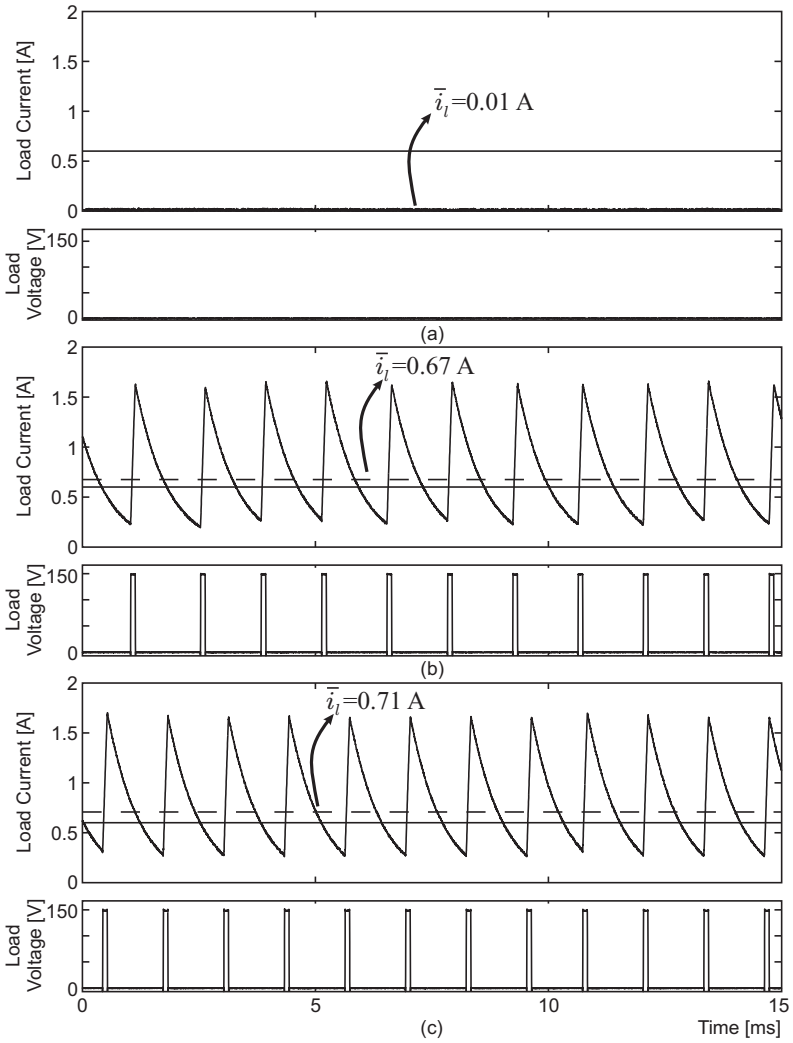

Figure 4.9: Steady-state performance: $\overset{*}{i}_l = 0.6\,A$. (a) FCS-MPC; (b) IS-MPC; (c) IE-MPC.

is improved when IS-MPC and IE-MPC are implemented. An average value of $\bar{i}_l = 0.67\,A$ is obtained when IS-MPC is used while $\bar{i}_l = 0.71\,A$ is achieved with IE-MPC.

A different situation occurs when a reference of $\overset{*}{i}_l = 4.8\,A$ is desired. Here, FCS-MPC generates the optimal sequence, $\vec{S} = \{1, 0, 1, 0, \ldots\}$, previously analyzed in Section 4.3.2. This situation is depicted in Fig. 4.10. Thus, an average reference of $\bar{i}_l = 4.99\,A$ is obtained. For the same reference, IS-MPC produce the same optimal pattern than standard FCS-MPC. Therefore, the same average value, for the load current, is achieved. On the

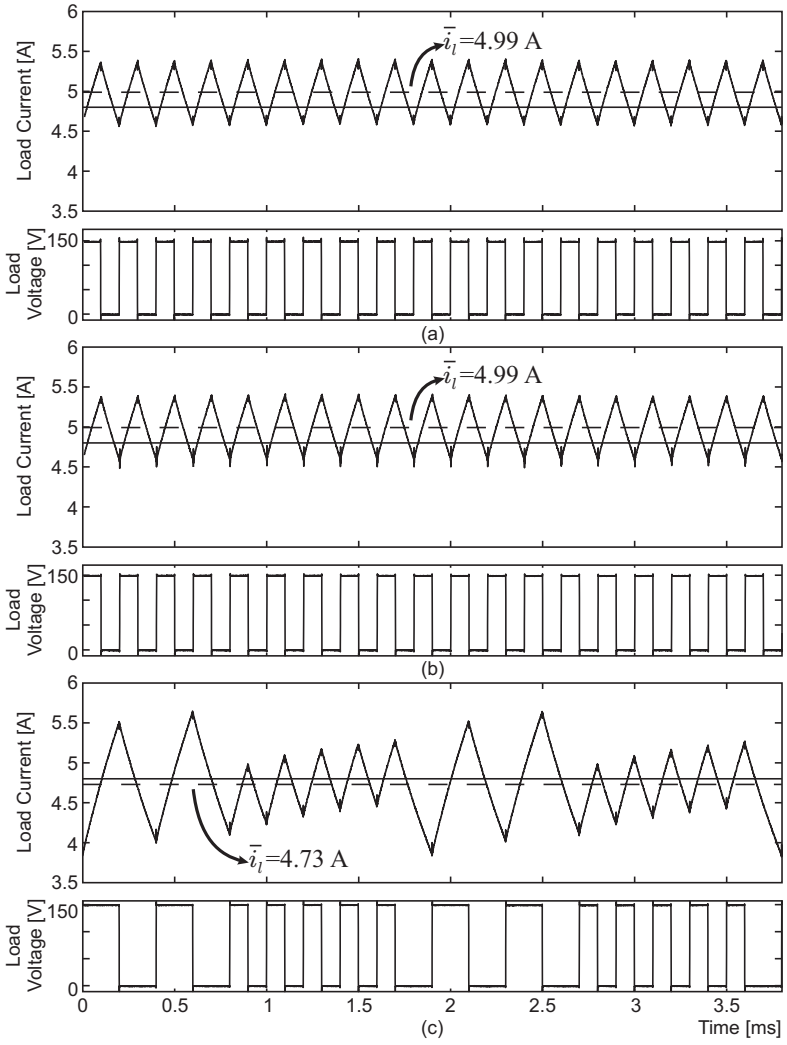

Figure 4.10: Steady-state performance: $\overset{*}{i}_l = 4.8\,A$. (a) FCS-MPC; (b) IS-MPC; (c) IE-MPC.

other hand, when the converter is governed by IE-MPC, a different pattern is obtained. This results in a decrease in the average error, achieving an average value for the load current of $\bar{i}_l = 4.73\,A$. Nevertheless, as a side effect, an increment in the load current ripple is obtained. Therefore, there is a trade-off between the average steady-state error and the ripple achieved in the load current.

In Fig. 4.11, the steady-state behaviour for a load current reference of $\overset{*}{i}_l = 7.4\,A$ is presented. For this reference, the three predictive strategies produce a similar average

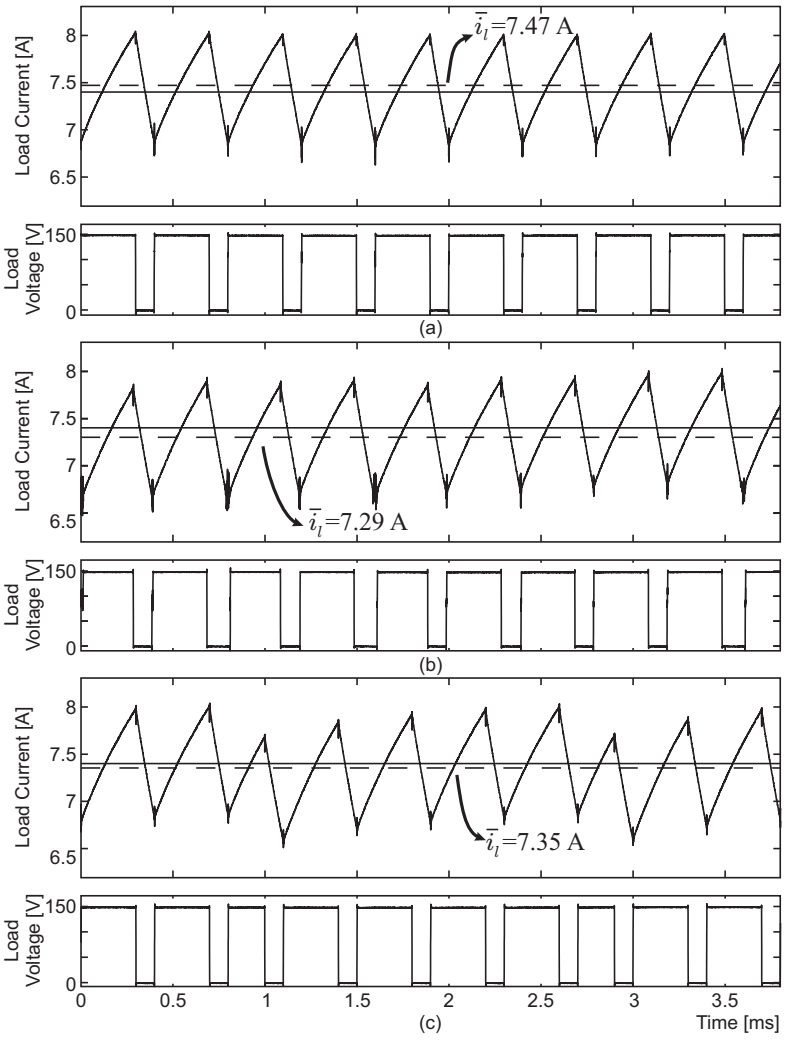

Figure 4.11: Steady-state performance: $\overset{*}{i}_l = 7.4\,A$. (a) FCS-MPC; (b) IS-MPC; (c) IE-MPC.

value, as anticipated in Fig. 4.7.

One of the most important benefits of FCS-MPC is the high dynamic response achieved with this strategy [14]. Fig. 4.12 shows the step response for a load current reference from $\overset{*}{i}_l = 2\,A$ to $\overset{*}{i}_l = 7\,A$. Here, it is possible to observe that the proposed modifications to standard FCS-MPC do not affect the dynamic performance of this control methodology. Thus, these modifications only improve the steady-state performance of this predictive strategy.

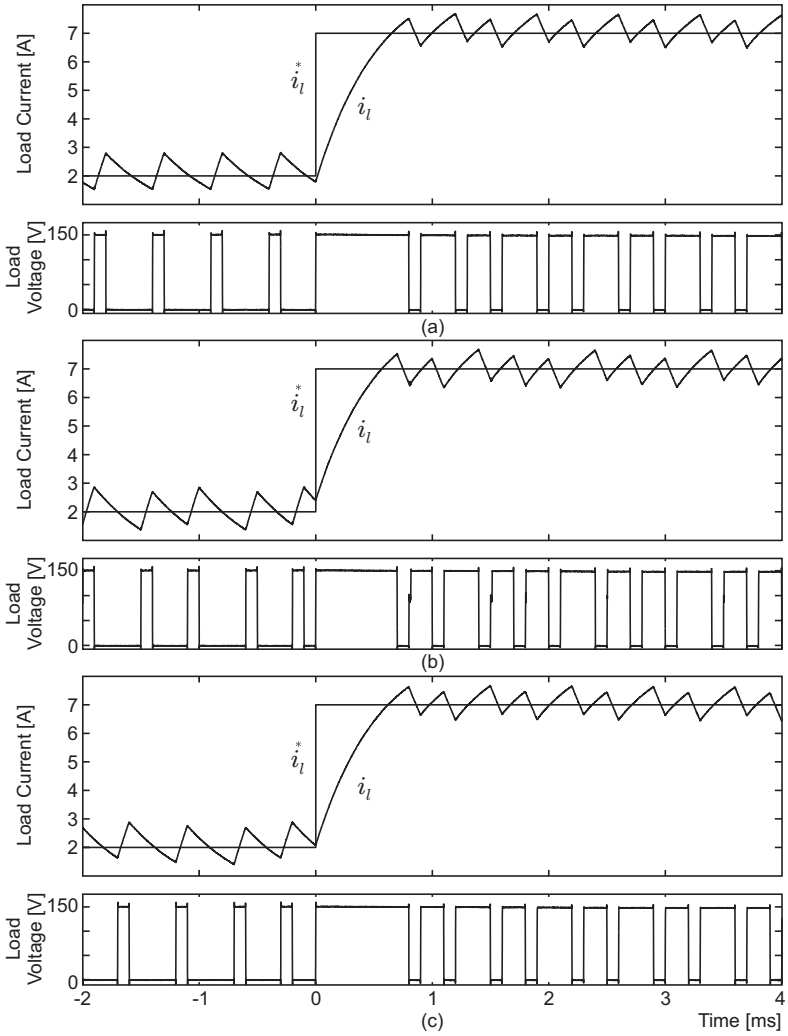

Figure 4.12: Step response (a) FCS-MPC; (b) IS-MPC; (c) IE-MPC.

4.7 Conclusions

In this work, we have studied the steady-state performance of power converters when governed by FCS-MPC. We have shown, analytically and experimentally, that existing FCS-MPC gives, in general, a non-zero steady-state error, even when models and parameter values are exactly known. To deal with this issue, two different modifications to the existing FCS-MPC strategy have been proposed. In the first one, IS-MPC, the measurements and the optimal switch implementation are temporarily shifted by half of the sampling period. This allows one to approximate the average value of the variable to be controlled by the sample value. On the oder hand, the second modification, IE-MPC, reduces the average tracking error, by using an analytical expression of the intersampling integral error. Thus, the continuous-time trajectory of the variable to be controlled is considered. Moreover past integral errors can be also included to improve the continuos-time response of the average tracking.

An important characteristic of our proposals, as shown in Section 4.6.2, is that they do not affect the dynamic response achieved with standard FCS-MPC. The approaches only improve, as was required, the steady-state performance.

According to the presented results, IS-MPC reaches a low average steady-state error only for low reference values, while IE-MPC algorithm, considering two previous integral errors, gives in general the best steady-state performance. However, a higher ripple in the load current is obtained. Consequently, there is a trade-off between the ripple in the variable to be controlled and its average steady-state error.

5

MPC Algorithm Robustness for Achieving Fault Tolerance in FCCs

5.1 Introduction

Multilevel converters (MCs) have emerged as an important technology in many industrial applications. The main reason for this is that MCs are able to operate at far higher power levels and also provide output voltages and currents with lower distortion than their two level counterparts [38]. However, a major disadvantage of MCs is the increased probability of failure due to the larger number of devices required [35, 90].

In particular, flying capacitor converters (FCCs) have attracted significant attention [91]. As depicted in Fig. 5.1, FCCs are composed of multiple interconnected cells. Each cell contains a capacitor C_x and a pair of switches S_{xi} and $\overline{S}_{xi}$, which work in a complementary fashion. In an FCC, an internal short circuit occurs whenever these complementary switches conduct at the same time, then the adjacent capacitors are forced to change its voltage, generating an increase of the current through it. Fortunately this fault currents decay quickly, since the associated capacitors seek voltage balance [90]. These characteristics open the possibility to reconfigure the converter and continue its operation, albeit in general, at reduced performance level, as seen by the loads connected. To achieve ro-

bustness to failures, faults need to be isolated correctly and appropriate remedial actions must be taken quickly. Otherwise, additional faults will be triggered, leading to damages in the entire converter and, possibly, the load.

In [90], a fault detection strategy for FCCs with switching patterns provided by open-loop PWM was proposed. Faults are detected in the frequency spectrum of the output voltage. As a remedial action, the switching patterns are changed via shifting of the PWM carrier phases. Thus, under fault conditions, the resultant output voltage waveform is synthesised with less levels. We can see that, whilst the method proposed in [90] gives some degree of robustness with respect to cell faults, performance is sacrificed significantly, when compared to normal operating conditions.

This work presents a novel fault detection strategy for flying capacitor multilevel converters, which is based on predictive control. To allow the controller to detect internal short circuits and to determine which cell has failed, switch sequences are constrained to a reduced set. Whenever faults are detected, the prosed controller isolates the faulty cell and changes capacitor voltage references in order to keep the number of available levels in the output voltage. This reconfiguration method allows the converter to produce an output voltage characteristic, which closely resemble those obtained under normal operating conditions.

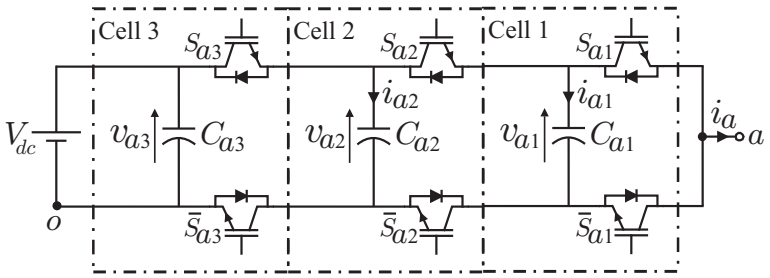

Figure 5.1: Three-cell FC converter (phase a).

5.2 Flying Capacitor Converter

In this section we describe the flying capacitor topology in more detail and develop a model for the system.

5.2.1 Converter Model

In the present work, we will focus on an electrical system consisting of a three-phase FCC connected to a coupled inductive load, as depicted in Fig. 5.2. The way in which the cells are connected, together with the capacitor voltages of each cell, determines the waveform of the synthesised output voltage.

Figure 5.1 shows a schematic of a single phase leg of a three-cell flying capacitor converter. As mentioned above, each cell consists of a capacitor and two switching elements which, at the same instant, cannot present the same state. To characterize the output voltages of the three phase converter, we first note that, for phase a, we have:

$$v_{ao}(t) = v_{a1}(t)S_{a1}(t) + (v_{a2}(t) - v_{a1}(t))S_{a2}(t) + (V_{dc} - v_{a2}(t))S_{a3}(t), \tag{5.1}$$

The associated capacitor currents are

$$i_{a1}(t) = i_a(t)(S_{a2}(t) - S_{a1}(t)), \tag{5.2}$$

$$i_{a2}(t) = i_a(t)(S_{a3}(t) - S_{a2}(t)). \tag{5.3}$$

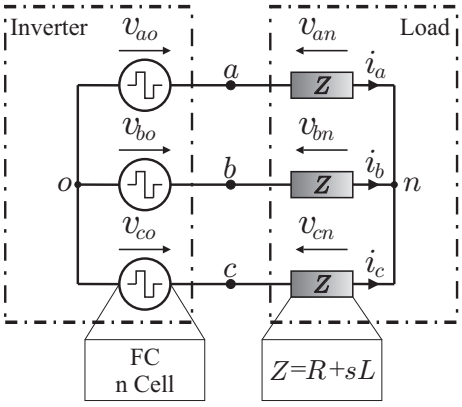

Figure 5.2: Three phase FCC and load connection.

Table 5.1 shows the output voltages and currents for phase a, as a function of switch states.

The load voltages of the three phase converter are, thus, described via

$$\begin{bmatrix} v_{an}(t) \\ v_{bn}(t) \\ v_{cn}(t) \end{bmatrix} = \begin{bmatrix} 2/3 & -1/3 & -1/3 \\ -1/3 & 2/3 & -1/3 \\ -1/3 & -1/3 & 2/3 \end{bmatrix} \begin{bmatrix} v_{ao}(t) \\ v_{bo}(t) \\ v_{co}(t) \end{bmatrix} \tag{5.4}$$

A simple dynamic model of the system can be developed by noting this for one phase (in this case, the phase a) we have:

$$v_{a1}(t) = \frac{1}{C_{a1}} \int_{-\infty}^{t} i_{a1}(\tau)\, d\tau \tag{5.5}$$

$$v_{a2}(t) = \frac{1}{C_{a2}} \int_{-\infty}^{t} i_{a2}(\tau)\, d\tau \tag{5.6}$$

$$L\frac{di_a(t)}{dt} + Ri_a(t) = v_{an}(t), \tag{5.7}$$

$$v_{an}(t) = \frac{2}{3}v_{ao}(t) - \frac{1}{3}v_{bo}(t) - \frac{1}{3}v_{co}(t). \tag{5.8}$$

Similar equations are obtained for phases b and c.

Table 5.1: Switch states and output voltages of an FCC (phase a)

$S_a(S_{a3}, S_{a2}, S_{a1})$	$v_{ao}(t)$	$i_{a1}(t)$	$i_{a2}(t)$
$S_a(0,0,0) = 0$	0	0	0
$S_a(0,0,1) = 1$	$v_{a1}(t)$	$-i_a$	0
$S_a(0,1,0) = 2$	$v_{a2}(t) - v_{a1}(t)$	i_a	$-i_a(t)$
$S_a(0,1,1) = 3$	$v_{a2}(t)$	0	$-i_a(t)$
$S_a(1,0,0) = 4$	$V_{dc} - v_{a2}(t)$	0	$i_a(t)$
$S_a(1,0,1) = 5$	$V_{dc} - v_{a2}(t) + v_{a1}(t)$	$-i_a(t)$	$i_a(t)$
$S_a(1,1,0) = 6$	$V_{dc} - v_{a1}(t)$	$i_a(t)$	0
$S_a(0,0,0) = 7$	V_{dc}	0	0

5.3 Fault Analysis in Flying Capacitor Converters

There are several kinds of failures that can occur in an FCC and many reasons causing them. Due to the large number of semiconductors which make up an FCC and the stresses to which they are exposed, switching failures in these converters are more likely than in their two-level counterparts.

The most common switch used in power converters is the Isolated Gate Bipolar Transistor (IGBT). Although, these elements can fail either short-circuit or open-circuit, open-circuit faults can be avoided by using an appropriated IGBT gate drive [90, 92]. Therefore, in the sequel we will concentrate on short-circuit faults.

5.3.1 Effects of a switch fault in a Flying Capacitor

In an FCC, a short circuited IGBT does not affect to the rest of the converter by itself. The fault only manifests itself once the complementary IGBT switches from OFF to ON. We call this a *cell fault*. Thus, a key observation is that a cell fault can only be produced at a switching instant.

Depending on which cell has failed, three different situations may arise in a three-cell FCC. To elucidate this issue, in Fig. 5.3-a) a fault in the cell 3 is shown (phase a). As a result of this fault, capacitor voltage v_{a2} increases its value until reaching a value equal to the dc-link voltage V_{dc}. If the fault is produced in an internal cell (in this case cell 2), then the capacitor voltages from each side of the faulty IGBT become equal to each other, adopting an average value between their previous value under normal operating conditions. In the case of a 3-cell converter this would give v_{a2}=v_{a1}=$V_{dc}/2$, as shown in Fig. 5.3-b). Finally, Fig. 5.3-c) shows that a fault produced in the first cell of the converter forces this cell's capacitor to discharge completely, i.e. v_{a1}=$0[V]$. The time taken to reach these capacitor voltages depend on the capacitance values and the IGBT impedances and will be, in general, faster than a standard sampling period [90]. If the fault is not detected on time, a train of internal short circuits can be produced, which can destroy the IGBT's [93].

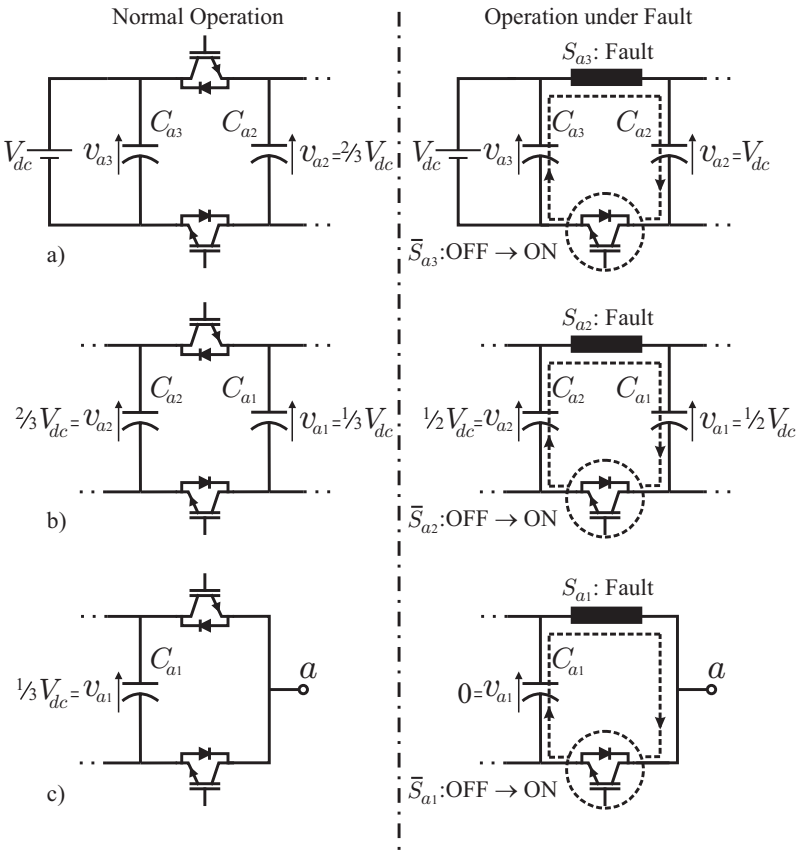

Figure 5.3: Short circuits in an FCC. a) Fault in Cell 3; b) Fault in Cell 2; c) Fault in Cell 1.

5.3.2 Output Voltage Under a Fault Condition

As mentioned above, a cell fault can only be produced when a commutation is realised, i.e., at a switching instant. This causes changes in one or two internal capacitor voltages, e.g. v_{aj}, but not necessarily in the output voltage, v_{ao}. Table 5.2 shows how a cell fault will manifest itself in the output voltage, v_{ao}, for a three-cell FCC.

Whether internal faults can be observed in the converter output voltages depends on which cell has failed and its switches state. For example, if the switch combination S_a=3 is applied, then the expected output voltage will be $v_{ao} = v_{a2}$, see Table 5.1. Thus, if a fault has occurred in cells 2 or 3, then the output voltage will not be the expected one, i.e., $v_{a0} \neq v_{a2}$, as shown in Table 5.2. Therefore, these two internal faults can be observed in

Table 5.2: Output voltages of an FCC Under a Fault Condition (phase a)

$S_a = (S_{a3}, S_{a2}, S_{a1})$	$v_{ao}(t)$ in a Normal Condition	Failed Cell	$v_{ao}(t)$ in a Fault Condition
$S_a = (0,0,0) = 0$	0	Cell 1	0
		Cell 2	0
		Cell 3	0
$S_a = (0,0,1) = 1$	$v_{a1}(t)$	Cell 1	0
		Cell 2	$(v_{a2}(t) + v_{a1}(t))/2$
		Cell 3	$v_{a1}(t)$
$S_a = (0,1,0) = 2$	$v_{a2}(t) - v_{a1}(t)$	Cell 1	$v_{a2}(t)$
		Cell 2	0
		Cell 3	$V_{dc} - v_{a1}(t)$
$S_a = (0,1,1) = 3$	$v_{a2}(t)$	Cell 1	$v_{a2}(t)$
		Cell 2	$(v_{a2}(t) + v_{a1}(t))/2$
		Cell 3	V_{dc}
$S_a = (1,0,0) = 4$	$V_{dc} - v_{a2}(t)$	Cell 1	$V_{dc} - v_{a2}(t)$
		Cell 2	$V_{dc} - (v_{a2}(t) + v_{a1}(t))/2$
		Cell 3	0
$S_a = (1,0,1) = 5$	$V_{dc} - v_{a2}(t) + v_{a1}(t)$	Cell 1	$V_{dc} - v_{a2}(t)$
		Cell 2	V_{dc}
		Cell 3	$v_{a1}(t)$
$S_a = (1,1,0) = 6$	$V_{dc} - v_{a1}(t)$	Cell 1	V_{dc}
		Cell 2	$V_{dc} - (v_{a2}(t) + v_{a1}(t))/2$
		Cell 3	$V_{dc} - v_{a1}(t)$
$S_a = (1,1,1) = 7$	V_{dc}	Cell 1	V_{dc}
		Cell 2	V_{dc}
		Cell 3	V_{dc}

the output voltage, v_{ao}, whenever the switch combination $S_a = 3$ is applied. Nevertheless, if a fault has been produced in the cell 1, the output voltage will still be the same than the expected one, i.e., $v_{ao} = v_{a2}$, see Table 5.2. Consequently, an internal fault produced in the cell 1 can not be observed in the output voltage, v_{ao}, when the switch combination $S_a = 3$ is applied.

To make faults easily detectable from output voltage measurements, switching states sequences should be chosen as in Table 5.3 (the states for the other two phases are similar). These sets, namely $\mathcal{S}_a$, allow one to ensure that when a fault occurs, it will manifest itself in the output voltage, once a commutation is realised.

The only cases where an internal fault cannot be detected are when the switch combinations S_a=0 or S_a=7 are selected. However, in this situation a fault will always be detected at the next commutation instant. Consequently, we can always use the measurement of the output voltages v_{ao}, v_{bo}, v_{co} to identify a failed cell in one or, at most, two commutation instants.

Table 5.3: Set of Switching States Depending on the Previous State (phase a)

$S_a(k-1)$	$S_a(k)$
0	$\{0, 1, 2, 4\}$
1	$\{0, 1, 2, 3, 5\}$
2	$\{0, 1, 2, 4, 7\}$
3	$\{1, 2, 3, 5, 7\}$
4	$\{0, 2, 4, 5, 6\}$
5	$\{0, 3, 5, 6, 7\}$
6	$\{2, 4, 5, 6, 7\}$
7	$\{3, 5, 6, 7\}$

5.4 Fault Tolerant Predictive Control Strategy

We can distinguish the following control objectives:

i. Tracking of three-phase output current references.

ii. Tracking of capacitors voltage references.

To achieve these objectives, even if a fault occurs, we will next present a predictive controller which minimizes a suitably defined cost function and where switching state sequences are restricted according to Table 5.3 (and similar sequences in the other two phases).

5.4.1 Basic Principles

The predictive control strategy is implemented in discrete time with sampling frequency $f_s = h^{-1}$. To obtain a discrete time model of the converter, we use a forward Euler approximation. Expression (5.1)-(5.8), then yields:

$$v_{ao}[k] = v_{a1}[k]S_{a1}[k] + (v_{a2}[k] - v_{a1}[k])S_{a2}[k] + (V_{dc} - v_{a2}[k])S_{a3}[k], \tag{5.9}$$

$$v_{a1}[k+1] = v_{a1}[k] + \frac{h}{C_{a1}}\left(S_{a2}[k] - S_{a1}[k]\right) i_a[k], \tag{5.10}$$

$$v_{a2}[k+1] = v_{a2}[k] + \frac{h}{C_{a2}}\left(S_{a3}[k] - S_{a2}[k]\right) i_a[k], \tag{5.11}$$

$$i_a[k+1] = \left(1 - \frac{hR}{L}\right) i_a[k] + \frac{h}{L} v_{an}[k], \tag{5.12}$$

$$v_{an}[k] = \frac{2}{3} v_{ao}[k] - \frac{1}{3} v_{bo}[k] - \frac{1}{3} v_{co}[k]. \tag{5.13}$$

where $x[k] \triangleq x(kh)$.

To incorporate the tracking objectives (i.) and (ii.), we define the error signals per phase via:

$$e_y[k] \triangleq \begin{bmatrix} v_{y1}[k] - v^*_{y1}[k] \\ v_{y2}[k] - v^*_{y2}[k] \\ i_y[k] - i^*_y[k] \end{bmatrix}, \quad y \in \{a, b, c\} \tag{5.14}$$

where $i_y^*[k]$ are the desired three phase sinusoidal current references.

Under normal fault-free operating conditions, the so-called "balanced" capacitor voltage references are chosen [94],

$$v_{y1}^*[k] = \frac{V_{dc}}{3}$$
$$v_{y2}^*[k] = \frac{2V_{dc}}{3}$$

As a remedial action, if a *cell fault* is detected, then the capacitor voltage references of the associated phase are changed to maintain the output voltage levels, despite the fault conditions [48].[1]

At each sampling instant k, a measurement of the capacitor voltages and load currents is used for the minimisation of the following cost function:

$$J(S_a, S_b, S_c)[k] = \sum_{y \in \{a,b,c\}} e_y[l]^T P e_y[l] \tag{5.15}$$

where

$$P = diag\{\lambda_1, \lambda_2, 1\} \tag{5.16}$$

Here, λ_1 and λ_2 are design parameters, which allow one to trade current tracking errors versus capacitor voltage tracking errors and, thus, achieve the proposed goals (i) and (ii). The decision variables are S_a, S_b and S_c, which are restricted to belong to the finite sets defined in Table 5.3, to allow the fastest fault detection.

The optimal switching action to be applied at time $k+1$, namely $S_{opt}[k]$, is obtained by minimising $J(S_a, S_b, S_c)[k]$. Then, at the next sampling instant, $k+1$, the cost function $J(S_a, S_b, S_c)[k+1]$ is minimized using fresh state measurements. This gives $S_{opt}[k+1]$, and so on.

As will be apparent in Section 5.5, this control method gives robust performance of the

[1] The use of non-conventional capacitor voltage references was also investigated in this thesis as can be seen in Chapter 2.

converter, as seen by the load. Consequently, the FCC does not need to be shut down immediately, but can be repaired when convenient.

5.4.2 Estimation of Capacitor Voltages using Output Voltage Feedback

The predictive controller proposed in the previous section, in principle requires 3 sensors per phase when applied to a 3-cell FCC [50]. They are 2 measurements of the capacitor voltages and one of the output current. In addition, we also require measuring the output voltages v_{ao}, v_{bo}, v_{co} to identify a possible cell fault. More generally, in a three-phase n-cell FCC the number of sensors would be $3(n+1)$. To reduce the number of sensors needed, we estimate the capacitor voltages from (5.5)-(5.6), which in discrete time can be rewritten via:

$$\begin{aligned} v_{y1}[k] =& v_{y1}[k-1] + \frac{h}{C_{y1}}(S_{y2}[k-1] - S_{y1}[k-1])i_y[k] \\ v_{y2}[k] =& v_{y1}[k-1] + \frac{h}{C_{y2}}(S_{y3}[k-1] - S_{y2}[k-1])i_y[k] \end{aligned}$$

where $i_y[k]$, $y \in \{a, b, c\}$ refers to the current values.

In a real implementation, this rather simple approach can produce an incremental error due to inaccuracy of the model used, e.g., dead times, saturations, voltage drops, and capacitors tolerance. To improve this situation, estimates can be corrected by measuring, at some instants the capacitor voltages. For that propose, one can simply utilise the output voltage measurement whenever the applied state is $S_a(t)$=1 or $S_a(t)$=3. The output voltage will be $v_{ao}(t)$=$v_{a1}(t)$ or $v_{ao}(t)$=$v_{a2}(t)$, respectively. The above method allows one to reduce the number of sensors, using only one measurement of voltage per phase to determine the internal values of the capacitor voltages and to detect a fault condition. This is especially useful for a large number of cells.[2]

[2]Recently, we have also investigated the us of a Discrete-Kalman Filter to improve the capacitor voltage estimations, see [86].

5.5 Results

To verify the performance of the proposed strategy, simulation studies were carried out on a three-phase with three cells per phase. A main dc-link voltage of $V_{dc} = 300\ V$ was used. The electrical parameters were: $C_{yj} = 470\ \mu F$, $R = 2.5\ \Omega$ and $L = 1\ mH$. The three-phase current references i_y^* have an amplitude of 50 A and a frequency of $f_o = 50\ Hz$.

These simulations consisted of exposing the converter to an internal fault. The performance of the converter operating with the proposed method is compared with the standard predictive control applied under the same conditions. Additionally, the proposed scheme was compared to standard PWM reconfiguration.

5.5.1 Standard Predictive Control

Standard predictive control was applied using a sampling frequency of f_s=25[kHz]. Furthermore, the controller is adjusted using weight factors λ_1=λ_2=0.1. In this case, the switch combination $S_y[k]$ does not depend on his previous value $S_y[k-1]$. The results of this simulation are presented in Fig. 5.4. It is possible to see from the figure that the controller achieved good performance in the three phase currents and the capacitor voltages. At the instant $t = 51.48\ ms$ switch S_{a2} is kept in a permanent ON state in order to simulate a short circuit failure of the switch. Thus, a *cell fault* occurs every time that switch $\bar{S}_{a2}$ commutates to an ON state, therefore, the *cell fault* is not always present. In this case the capacitor voltages v_{a1} and v_{a2} are equalised, reaching a value of $V_{dc}/2$. This causes a reduction in the number of levels in the output voltage $v_{ao}(t)$. Since the controller does not know that cell 2 has failed, it still tries to control the capacitor voltages v_{a1} and v_{a2}. This reduces the performance in the output voltage $v_{ao}(t)$ and in the line to line voltage $v_{ab}(t)$. This behaviour could be detrimental to the converter causing a succession of faults and eventually a catastrophic failure [93].

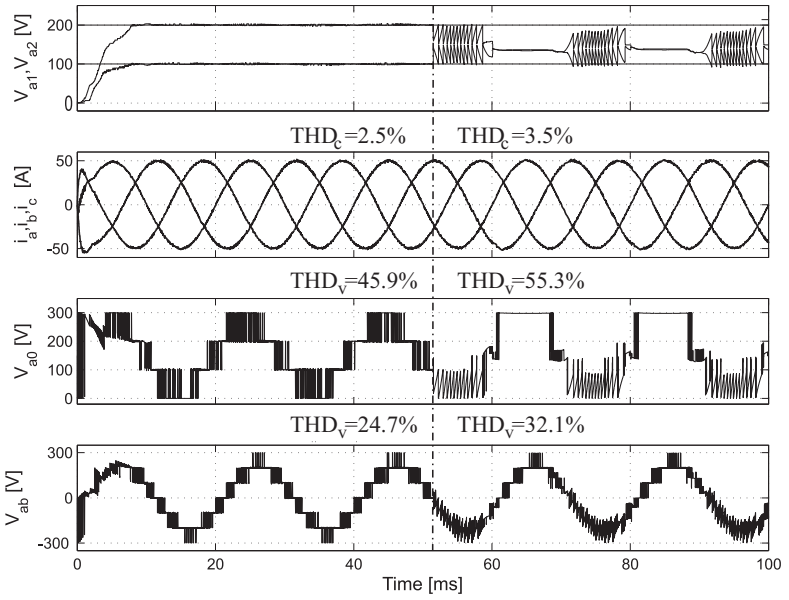

Figure 5.4: Standard predictive control strategy, λ_1=λ_2=0.1: capacitor voltages v_{a1},v_{a2}; load currents i_a, i_b, i_c; output voltage v_{ao}; line to line voltage v_{ab}.

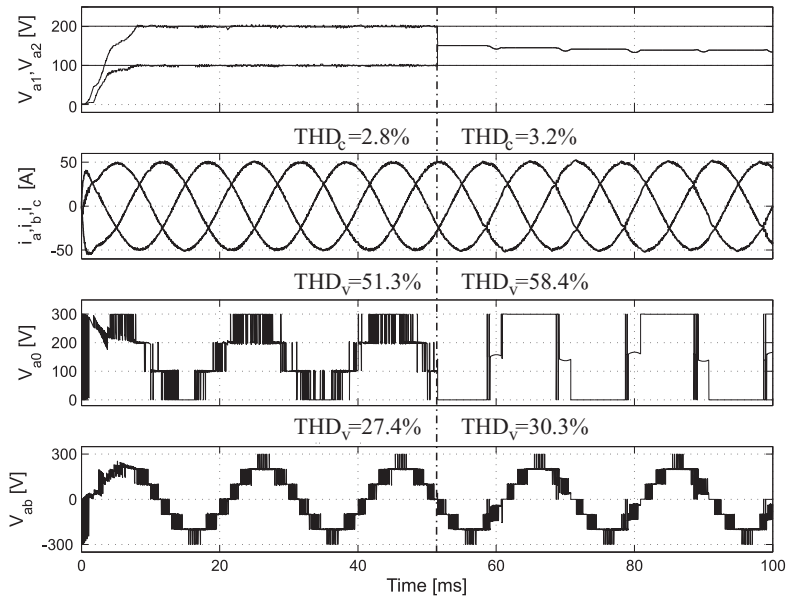

Figure 5.5: Predictive control robustness to fault, λ_1=λ_2=0.1: capacitor voltages v_{a1},v_{a2}; load currents i_a, i_b, i_c; output voltage v_{ao}; line to line voltage v_{ab}.

5.5.2 Fault Tolerant Strategy

We next examine the algorithm proposed in Sec. 5.4. In this case, the capacitor voltages are estimated using output voltage feedback and switching states are restricted according Table 5.3. As can be seen in Fig. 5.5, the startup is similar to the *standard predictive control*. It is possible to see that, in a fault free condition, the electrical variables have a distortion slightly higher than the standard method. This is because of the reduced set of permitted switch state sequences. When the fault is produced, the capacitor voltages are equalised, but in this case the fault is detected and then the faulty cell is isolated. Thus, voltage v_{a2} is not include ahead in the optimization. Therefore, the line to line voltage, v_{ab}, presents a better behaviour (THDv=30.3%) than in the standard predictive control (THDv=32.1%).

5.5.3 Standard phase shifted PWM with Fault Reconfiguration

To analyze the reconfiguration performance, we next study the method proposed in [90], which uses phase shifted PWM modulation. This method achieves reconfiguration by changing the phase of the carrier in order to obtain a three level output voltage.

In the simulation, the carrier frequency selected per cell is $f_{cc} = 1.5\ kHz$, obtaining a switching output voltage of $f_c = 4.5\ kHz$. In Fig. 5.6, the result of the same fault case as considered previously is shown. (Note, that startup performance was not included in this simulation due to the fact that it takes a long time using PWM [50] and it is not the focus of this work). This strategy improves the output voltage of the phase that has failed but does not achieve good performance with respect to the line to line voltage.

5.5.4 Predictive Control Robustness to Faults with Reconfiguration

In this case, a change in the reference of the capacitor voltages is proposed as a reconfiguration method. Figure 5.7 shows the results of the fault case considered in the previous

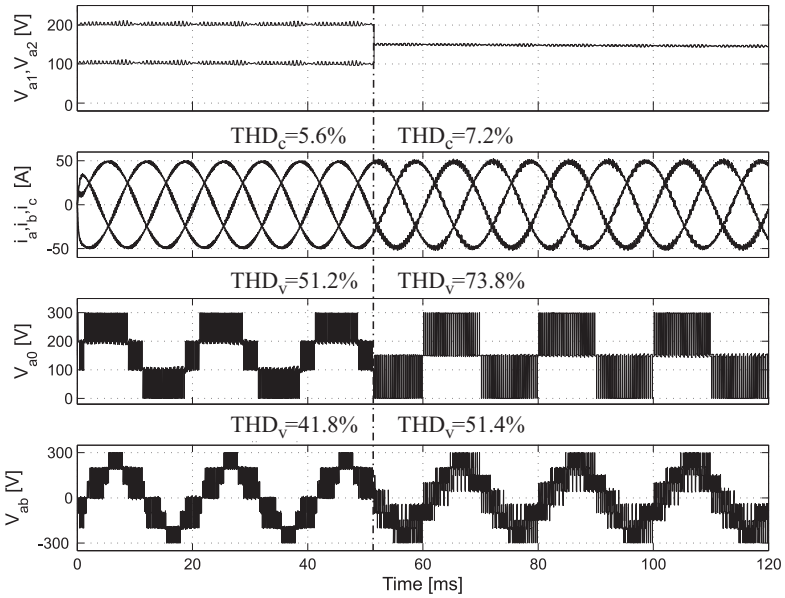

Figure 5.6: Standard phase-shift PWM with reconfiguration: capacitor voltages v_{a1},v_{a2}; load currents i_a, i_b, i_c; output voltage v_{ao}; line to line voltage v_{ab}.

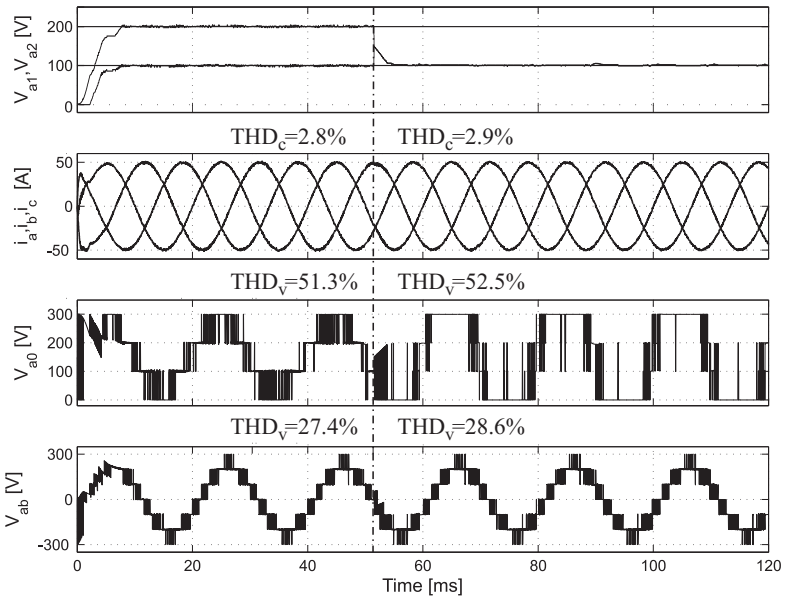

Figure 5.7: Predictive control robustness to fault with reconfiguration: capacitor voltages v_{a1},v_{a2}; load currents i_a, i_b, i_c; output voltage v_{ao}; line to line voltage v_{ab}.

three simulation studies. When the fault occurs (at $t \approx 51.48\ ms$), the phase output voltage loses one level. Under this fault conditions, v_{a1} and v_{a2} works as a unique capacitor, then phase a operates as a 2-cell FCC. So, as proposed in [48], the number of levels can be increased by changing the capacitors voltage ratio. Thus, as a remedial method, the equivalent capacitor between C_{a1} y C_{a2} is forced to take a voltage of $V_{dc}/3$, restoring the fourth level in the output voltage v_{ao}. Moreover, the distortion increment in the electrical variables, under a fault condition, is clearly less than in the other cases studied, achieving a good performance in both situations.

Finally, a zoom of the fault instant is presented in Fig. 5.8. In this figure it is possible to see how the switch combination S_a follows a permitted sequence according to Table. 5.3. In addition, the reader should note that the fault occurs when the state S_a changes from $S_a(0,0,1) = 1$ to $S_a(0,1,1) = 3$. Under normal operating conditions the expected value of the output voltage is $v_{ao} = v_{a2}$=200 V (see Table 5.1), but the measured output voltage is $v_{ao} = 150\ V$. Inspection of Table 5.2 tells us that a fault in cell 2 has occurred.

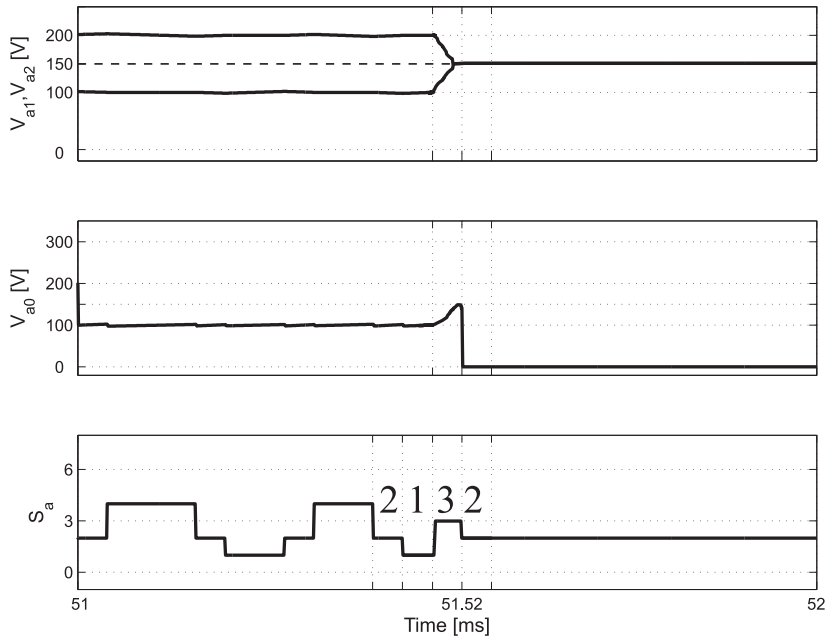

Figure 5.8: Predictive control robustness to fault with reconfiguration: capacitor voltages v_{a1},v_{a2}; output voltage v_{ao}; switch sequence applied S_a.

5.6 Conclusion

A Predictive Control strategy to achieve robustness to faults has been proposed. This methodology is applied to a three-phase three-cell FCC. The most important benefits of this method is the good performance achieved in the tracking of the capacitor voltages and the three-phase currents even when a fault occurs. The fault is identified using the measurement of the output voltages. To ensure the fault be detected quickly, switching sequences are restricted to a reduced set. We also showed how to estimate the capacitors voltages from output voltage measurements, thus reducing the number of sensors needed for implementation. We consider that the proposed strategy expands the possibilities of the predictive control in industrial application not only to achieve good performance in the tracking errors but also to accelerate fault tolerant operation of power converters.

6

Stability Analysis of MPC with a Discrete Input Alphabet

6.1 Introduction

In a variety of applications, system inputs are restricted to belong to a discrete alphabet of allowed values [79, 95–100]. There are several works related to stabilization of this kind of systems, mainly focusing on uniform quantization [101, 102], and logarithmic quantization [103, 104]. However, in many applications, the control set is given. One of the most studied cases is related to on-off systems, e.g. power converters [105], and audio applications [87], where each input is restricted to take only two values. This motivates the study of systems with arbitrary discrete control alphabets.

Model predictive control (MPC) [12] is especially suited for constrained systems. Control actions are calculated by solving, at each sampling instant, an optimal control problem which forecasts, over a finite horizon, the future system behaviour from the current system state. This generates an optimal control sequence. The control action to be applied to the plant is the first element of this sequence.

Whilst stability of convex MPC formulations is relatively well understood, less is known in the discrete alphabet case. In [36], stability analysis of a receding-horizon formulation for LTI systems with quantized inputs has been presented. The focus of [36] is on characterizing the region of attraction of the predictive controller. The stability analysis in [37]

is based on designing a *final state weighting* term using an algebraic Lyapunov equation. The main drawback of the stability analysis in [37] is its limitation to open-loop stable systems. Moreover, the origin is required to belong to the control alphabet. Another way to study closed-loop stability of MPC with finite alphabet constraints is by using robust control concepts [85]. To do this, one can regard the finite set as a quantization of a bounded nominal input set and solve a nominal optimization yielding a so-called nominal input. Afterwards, a quantization process is performed in order to apply an available input from the original finite set. This situation can be interpreted as the nominal input being affected by a disturbance: the quantization error. Consequently, robustness analysis of MPC under bounded disturbances can be carried out to establish sufficient conditions for practical stability based on the nominal solution, see e.g. [106–109]. Unfortunately, as was shown in [85], stability analysis based on this approach becomes unnecessary conservative due to the fact that the quantization error is propagated ahead over all state predictions to account for a worst case scenario.

To overcome the limitations of stability analyses outlined above, it is necessary to carefully take into account the nature of the input. A key observation is that when system inputs are restricted to belong to a discrete set, in general, the best one can hope for is to obtain bounded state trajectories [102]. Therefore, in the present work we will focus on practical stability (ultimate boundedness) [110]. To establish practical stability of LTI systems governed by MPC with a discrete control set, we consider the (quadratic) MPC cost function as a candidate practical-Lyapunov function and design the terminal cost by using an algebraic Riccati equation. The associated terminal region, $\mathbb{X}_f$, is designed based on a convex control set. The original discrete input alphabet set becomes a quantization of this convex set. The *local controller* is chosen to be the one-step optimal solution, as presented in [37]. Thus, we can characterize a ultimately bounded invariant set, $\mathcal{D}_\delta$, by regarding the quantization error generated by the proposed local controller, as a bounded disturbance. Moreover, we establish sufficient conditions to guarantee that this ultimately bounded invariant set is a subset of the terminal region, $\mathcal{D}_\delta \subseteq \mathbb{X}_f$. This along with a careful design of the terminal cost, allows us to establish asymptotic practical stability of the predictive strategy.

Notation and Basic Definitions

Let $\mathbb{R}$ and $\mathbb{R}_{\geq 0}$ denote the real and non-negative real number sets. The difference between two given sets $\mathcal{A} \subseteq \mathbb{R}^n$ and $\mathcal{B} \subseteq \mathbb{R}^n$ is denoted by $\mathcal{A} \backslash \mathcal{B} = \{x \in \mathbb{R}^n : x \in \mathcal{A}, x \notin \mathcal{B}\}$. We represent the transpose of a given matrix A and a vector x via $(Ax)' = x'A'$. The Euclidean norm is denoted via $|\cdot|$ while the weighted Euclidean norm is denoted by $|x|_P^2 = x'Px$. Additionally, the induced norm of a given matrix A is its largest singular value. The maximum and minimum eigenvalues of a given matrix A are represented via $\lambda_{\max}(A)$ and $\lambda_{\min}(A)$ respectively.

Definition 6.1.1 *[$\mathcal{K}$-Functions [111]] A function σ: $\mathbb{R}_{\geq 0} \to \mathbb{R}_{\geq 0}$ is said to be a $\mathcal{K}$-function if it is continuous, strictly increasing and $\sigma(0) = 0$; σ is a $\mathcal{K}_\infty$ function if it is a $\mathcal{K}$-function and unbounded ($\sigma(s) \to \infty$ as $s \to \infty$); a function β: $\mathbb{R}_{\geq 0} \times \mathbb{R}_{\geq 0} \to \mathbb{R}_{\geq 0}$ is a $\mathcal{KL}$-function if it is continuous and if, for each $t \geq 0$, the function $\beta(\cdot, t)$ is a $\mathcal{K}$-function and for each $s \geq 0$ the function $\beta(s, \cdot)$ is non-increasing and satisfies that $\beta(s, t) \to 0$ as $t \to \infty$.*

6.2 Practical Stability

In this section we revise some basic aspects on practical stability for discrete-time systems based on the regional input-to-state practical stability framework presented in [112, 113]. Here, the term *regional* is related to the fact that stability properties hold only in a specific region, which is often the case when system constraints are present, see [114, 115]. The term *practical* is used to emphasize that only stability of a neighbourhood of the origin is studied. The latter property is, at times, also referred to as ultimate boundedness [110]. For further details on input-to-state stability see [111, 116].

Consider a discrete-time system described by:

$$x_{k+1} = f(x_k), \quad f(0) = 0, \tag{6.1}$$

where $x_k \in \mathbb{R}^n$ is the system state.

Definition 6.2.1 (Positively Invariant Set) *A set $\mathcal{A} \subseteq \mathbb{R}^n$ is said to be a* positively invariant set *(PIS) for the system* (6.1) *if $f(x) \in \mathcal{A}$, for all $x \in \mathcal{A}$.*

Definition 6.2.2 (UpAS) *The system* (6.1) *is said to be* Uniformly practically Asymptotically Stable *(UpAS) in $\mathcal{A} \subseteq \mathbb{R}^n$ if $\mathcal{A}$ is a PSI for* (6.1) *and if there exist a $\mathcal{KL}$-function β, and a nonnegative constant $\delta \geq 0$ such that*

$$|x_k| \leq \beta(|x_0|, k) + \delta, \quad \forall x_0 \in \mathcal{A}$$

If $\mathcal{A} \triangleq \mathbb{R}^n$ then, the system (6.1) *is said to be globally UpAS.*

Definition 6.2.3 (Practical-Lyapunov function) *A (not necessarily continuous) function $V : \mathbb{R}^n \to \mathbb{R}_{\geq 0}$ is said to be a* practical-Lyapunov function *in $\mathcal{A}$ for the system* (6.1) *if $\mathcal{A}$ is a PIS and if there exist a compact set $\Omega \subseteq \mathcal{A}$, $\mathcal{K}_\infty$-functions α_1, α_2, and α_3, and some constants $d_1, d_2 \geq 0$, such that*

$$V(|x|) \geq \alpha_1(|x|), \qquad \forall x \in \mathcal{A}, \tag{6.2}$$

$$V(|x|) \leq \alpha_2(|x|) + d_1, \qquad \forall x \in \Omega, \tag{6.3}$$

$$V(f(x)) - V(x) \leq -\alpha_3(|x|) + d_2, \quad \forall x \in \mathcal{A}. \tag{6.4}$$

If $\mathcal{A} \triangleq \mathbb{R}^n$ then, the function, V, is said to be a global practical-Lyapunov function.

Theorem 6.2.1 ([113]) *If* (6.1) *admits a practical-Lyapunov function in $\mathcal{A}$, then it is UpAS in $\mathcal{A}$.* ■

In the sequel, we will use the above tools to study practical stability of MPC with finite input set constraints.

6.3 Finite-Control-Set MPC

Consider the following LTI system

$$x_{k+1} = Ax_k + Bu_k, \tag{6.5}$$

where $x_k \in \mathbb{R}^n$ is the system state (assumed known to the controller), $u_K \in \mathbb{U}$ is the control input vector, and the matrix A is not necessarily Schur stable. The distinguishing issue of the situation at hand is that the input constraint set has a finite number of elements[1]:

$$u_k \in \mathbb{U} = \{u_1, u_2, \ldots, u_p\} \subset \mathbb{R}^m. \tag{6.6}$$

6.3.1 Quadratic MPC with a finite input alphabet

The MPC optimization of interest for the current state, $x_k = x$, is given as

$$\mathbb{P}_N(x): \quad V_N^{op}(x) = \min_{\vec{u}} \{V_N(x, \vec{u}) \mid \vec{u} \in \mathcal{U}(x)\}, \tag{6.7}$$

where $\mathcal{U}(x) \in \mathbb{U}^N$ contains the constrained input predictions $\vec{u} = \left[\hat{u}_0', \ldots, \hat{u}_{N-1}'\right]'$. The associated predicted state trajectories

$$\vec{x} = \left[\hat{x}_0', \ldots, \hat{x}_N'\right]', \tag{6.8}$$

are generated using the following prediction model:

$$\hat{x}_{j+1} = A\hat{x}_j + B\hat{u}_j. \tag{6.9}$$

where $\hat{x}_0 = x_k$ is the current plant state. The optimization problem (6.7) is constrained as per:

$$\hat{u}_j \in \mathbb{U}, \ \forall j \in \{0, \ldots, N-1\}, \tag{6.10}$$

$$\hat{x}_N \in \mathbb{X}_f. \tag{6.11}$$

Here, (6.10) encompasses the finite control set constraint along the prediction horizon, while (6.11) is a terminal constraint, with terminal region $\mathbb{X}_f \subseteq \mathbb{R}^n$. The cost function is chosen as

$$V_N(x, \vec{u}) = \sum_{j=0}^{N-1} \ell(\hat{x}_j, \hat{u}_j) + V_f(\hat{x}_N), \tag{6.12}$$

where N is the prediction horizon, and where $\ell(\hat{x}, \hat{u}) = |\hat{x}|_Q^2 + |\hat{u}|_R^2$ is the stage cost with Q and R positive definite matrices. The term $V_f(\hat{x}) = |\hat{x}|_P^2$, in which P is positive definite,

[1] In Section 6.4, we illustrate the use of our results when $\mathbb{U}$ is countably infinite, see Corollary 6.4.1.

represents the terminal cost. As in convex MPC formulations, the terminal region $\mathbb{X}_f$ and terminal cost $V_f(\cdot)$ can be used to guarantee stability of the resulting control loop [12]. Their design will be considered in the stability analysis of Section 6.4.

Consequently, the optimal input sequence, $\vec{u}^{op}(x)$, is that one which minimizes the cost function,

$$\vec{u}^{op}(x) \triangleq \arg\left\{\min_{\vec{u}\in\mathcal{U}(x)} V_N(x,\vec{u})\right\}. \tag{6.13}$$

For future reference, we denote its components via

$$\vec{u}^{op}(x) = \left[(\hat{u}_0^{op})', \ldots, (\hat{u}_{N-1}^{op})'\right]', \tag{6.14}$$

while the resulting optimal state sequence is $\vec{x}^{op}(x) = \left[x', (\hat{x}_1^{op})', \ldots, (\hat{x}_N^{op})'\right]'$. We also denote the domain of the cost function V_N, via $X_N \triangleq \{x \in \mathbb{R}^n : \mathcal{U}(x) \neq \emptyset\}$. Therefore, X_N contains all $x \in \mathbb{R}^n$ such that there exists a sequence $\vec{u} \in \mathcal{U}(x)$ satisfying the constraints (6.10)-(6.11).

Only the first element of $\vec{u}^{op}(x)$ is applied to the system at each sampling instant. The solution of the optimal problem, $\mathbb{P}_N(x)$ in (6.7), yields the MPC control law, $\kappa_N(\cdot) : X_N \to \mathbb{U}$,

$$\kappa_N(x) \triangleq \hat{u}_0^{op}. \tag{6.15}$$

Thus, the resulting finite alphabet MPC loop can be represented via

$$x_{k+1} = Ax_k + B\kappa_N(x_k). \tag{6.16}$$

In Section 6.4.2 we will also investigate a related Dual-Mode controller.

6.3.2 Optimal Solution without Terminal Constraints

Here we present a closed form expression for the solution of the finite alphabet MPC problem without terminal constraint (6.11), as established in [37]. Firstly, we define the predicted state sequence as, see (6.8), $\vec{x}_{[1:N]} = [\hat{x}_1', \ldots, \hat{x}_N']'$. Considering an initial system

state $\hat{x}_0 = x$, from (6.9), we obtain $\vec{x}_{[1:N]} = \Phi\vec{u} + \Lambda x$, where

$$\Phi \triangleq \begin{bmatrix} B & 0 & \cdots & 0 & 0 \\ AB & B & \cdots & 0 & 0 \\ \vdots & \vdots & \ddots & \vdots & \vdots \\ A^{N-1}B & A^{N-2} & \cdots & AB & B \end{bmatrix}, \quad \Lambda \triangleq \begin{bmatrix} A \\ A^2 \\ \vdots \\ A^N \end{bmatrix}.$$

Thus, the cost function (6.12) can be re-written as

$$V_N(x, \vec{u}) = \nu(x) + \vec{u}'W\vec{u} + 2\vec{u}'Fx,$$

where the term $\nu(x)$ is independent of $\vec{u}$ and

$$W \triangleq \Phi'\mathcal{Q}\Phi + \mathcal{R} \in \mathbb{R}^{Nm\times Nm},$$
$$F \triangleq \Phi'\mathcal{Q}\Lambda \in \mathbb{R}^{Nm\times m},$$

with

$$\mathcal{Q} \triangleq diag\{Q, \ldots, Q, P\} \in \mathbb{R}^{Nn\times Nn},$$
$$\mathcal{R} \triangleq diag\{R, \ldots, R\} \in \mathbb{R}^{Nm\times Nm}.$$

Notice that, since Q and R are positive definite, so is W.

Remark 6.3.1 (Unconstrained Solution) *If in $\mathbb{P}_N(x)$ presented in* (6.7) *the control and terminal constrains* (6.10)-(6.11) *are not taken into account, i.e. $\mathbb{U} = \mathbb{R}^m$ and $\mathbb{X}_f = \mathbb{R}^n$, then $V_N(x, \vec{u})$ is minimized when*

$$\vec{u}^{op}_{uc}(x) \triangleq \arg\left\{\min_{\vec{u}\in\mathbb{R}^{Nm}} V_N(x, \vec{u})\right\} \triangleq -W^{-1}Fx. \tag{6.17}$$

Definition 6.3.1 (Vector Quantizer (see e.g. [100])) *Consider a set $\mathcal{A} \subseteq \mathbb{R}^n$ a finite set $\mathcal{B} \triangleq \{b_1, \ldots, b_p\} \subset \mathbb{R}^n$. A function $q_{\mathcal{B}}(\cdot) : \mathcal{A} \to \mathcal{B}$ is an Euclidean vector quantizer if $q_{\mathcal{B}}(a) = b_i \in \mathcal{B}$ if and only if b_i satisfies that $\mid a - b_i \mid \leq \mid a - b_j \mid$, for all $b_j \neq b_i$, where $b_j \in \mathcal{B}$. The associated quantization error is defined as $\eta_{\mathcal{B}}(a) \triangleq q_{\mathcal{B}}(a) - a$.* ■

The following result was established in [37].

Theorem 6.3.1 *Consider* $\mathbb{P}_N(x)$ *in* (6.7)*, and suppose that there is no terminal constraint* (6.11)*, i.e.,* $\mathbb{X}_f = \mathbb{R}^n$*. Denote the elements of* $\mathbb{U}^N \triangleq \mathbb{U} \times \cdots \times \mathbb{U}$ *via* $\{\mu_1, \ldots, \mu_r\}$*. Then, the optimal minimizing solution in* (6.13) *is given by*

$$\vec{u}^{op}(x) = W^{-1/2} q_\nu \left(W^{1/2} \vec{u}^{op}_{uc}(x) \right) = W^{-1/2} q_\nu \left(-W^{-1/2} F x \right), \tag{6.18}$$

where the vector quantizer q_ν *maps* $\mathbb{R}^{Nm}$ *to* $\mathcal{V}$*, represented via* $\mathcal{V} \triangleq \{\nu_1, \ldots, \nu_r\} \subset \mathbb{R}^{Nm}$*, in which* $\nu_i = W^{1/2}\mu_i$ *for all* $\mu_i \in \mathbb{U}^N$*.*

6.4 Practical Stability of FCS-MPC

Stability of LTI systems with a discrete input alphabet under quadratic MPC has been studied in [37]. However, the analysis in those works is limited to open-loop stable plants ($\lambda_{\max}(A) < 1$) and the origin belongs to the control alphabet $\mathbb{U}$. Whilst [37] gives some insights stability issues for open-loop unstable plants, it fails to treat this case in a satisfying manner, providing only a computational method. In the present section, we will establish sufficient conditions for practical stability of the MPC formulation of Section 6.3. We also give results for a related Dual-Mode approach.

6.4.1 Finding a Suitable Quantized Local Control Law

A widely-used idea to establishing stability of MPC is based on finding a known controller, $\kappa_f(x)$, which can stabilize the system within the terminal region $\mathbb{X}_f$, see [12] and compare to [117]. It is well known that for a disturbance-free LTI system with convex constraints, say $x_{k+1} = Ax_k + B\bar{u}_k$, under quadratic MPC, one can use a fixed state feedback gain as a stabilizing controller for the terminal region $\mathbb{X}_f$ (see Section 2.5 in [12]). To adapt this idea to systems with discrete alphabet control inputs, we first introduce an associated convex set via:

$$\bar{\mathbb{U}} \triangleq \{\bar{u} \in \mathbb{R}^m : |\bar{u}| \leq \bar{u}_{\max}\},$$

where $\bar{u}_{\max} \in (0, \infty)$ is a design parameter. Since $\bar{\mathbb{U}}$ is bounded, so is the quantization error, thus

$$\Delta_q \triangleq \max_{\bar{u} \in \bar{\mathbb{U}}} |q_{\mathbb{U}}(\bar{u}) - \bar{u}| < \infty. \tag{6.19}$$

Note that Δ_q depends upon $\bar{u}_{\max}$.

Taking this ideas, we propose to prove stability of discrete alphabet MPC by examining properties of a local controller, namely, the optimal solution presented in (6.18) with prediction horizon $N = 1$, in which case

$$\bar{u}_{uc}^{op}(x) = \bar{u}_f(x) = Kx, \tag{6.20}$$

with $K = -W^{-1}F$, where $F = B'PA$ and

$$W = B'PB + R. \tag{6.21}$$

Thus, the proposed local controller can be expressed via (see (6.17)):

$$\kappa_f(x) = W^{-1/2} q_\nu \left(W^{1/2} \bar{u}_f(x) \right) = Kx + W^{-1/2} \eta_\nu(x), \quad \forall x \in \mathbb{X}_f. \tag{6.22}$$

Clearly,

$$\begin{aligned} |\eta_\nu(x)| &\leq |q_\nu \left(W^{1/2} \bar{u}_f(x) \right) - W^{1/2} \bar{u}_f(x)| && (6.23) \\ &\leq |W^{1/2} q_{\mathbb{U}} \left(\bar{u}_f(x) \right) - W^{1/2} \bar{u}_f(x)| \\ &\leq |W|^{1/2} |q_{\mathbb{U}} \left(\bar{u}_f(x) \right) - \bar{u}_f(x)| && (6.24) \\ &\leq |W|^{1/2} \Delta_q, && (6.25) \end{aligned}$$

where we have used (6.19). The above motivates us to define the terminal region in (6.11) as:

$$\mathbb{X}_f \triangleq \left\{ x \in \mathbb{R}^n : |x| \leq b \triangleq \frac{\bar{u}_{\max}}{|K|} \right\}. \tag{6.26}$$

providing $|\eta_\nu(x)| \leq |W|^{1/2} \Delta_q$ for all $x \in \mathbb{X}_f$.

Consequently, system (6.5) with the finite alphabet controller $\kappa_f(x)$ in (6.22), can be expressed via:

$$x_{k+1} = A_K x_k + w_f(x_k), \quad A_K = A + BK, \quad \forall x_k \in \mathbb{X}_f, \tag{6.27}$$

where $w_f(x_k) = BW^{-1/2} \eta_\nu(x_k)$ represents the effect if the quantization on the "nominal system", $x_{k+1} = A_K x_k$.

Notice that in (6.27) $w_f(x_k)$ is not an external disturbance but a known discontinuity, produced by the quantization, which makes (6.27) a nonlinear system. The key point here is that $w_f(x)$ is bounded for all $x \in \mathbb{X}_f$. This motivates us to analyze the closed-loop dynamics by regarding $w_f(x_k)$ as a bounded disturbance; cf. [118].

The following preliminary result uses this approach:

Lemma 6.4.1 *Consider the following positive constants:* $a_1 = \lambda_{\min}(P)$, $a_2 = \lambda_{\max}(P)$, $a_3 = \lambda_{\min}(Q)$, $a_4 = |B'PB + R|$, *and* $\rho = 1 - \frac{a_3}{a_2} \in (0,1)$. *Let* $\mathcal{D}_{\delta_f} \triangleq \{x \in \mathbb{X}_f : |x| \leq \delta_f\}$ *be a neighborhood of the origin, where*

$$\delta_f^2 \triangleq \gamma \Delta_q^2, \quad \gamma \triangleq \frac{a_4}{a_1(1-\rho)}. \tag{6.28}$$

Suppose that the matrix P *in the terminal cost,* $V_f(x)$, *is chosen to be the solution to the algebraic Riccati equation*

$$A_K' P A_K + Q^* - P = 0, \quad Q^* = Q + K'RK, \tag{6.29}$$

where K *is as in* (6.20). *If* Δ_q *in* (6.19) *is bounded by*

$$\Delta_q^2 < \left(\frac{a_1 - a_2\rho}{a_4} \right) b^2, \tag{6.30}$$

where b *is as in* (6.26), *then* $\kappa_f(x)$ *in* (6.22) *is a practically stabilizing controller in* $\mathbb{X}_f$ *for system* (6.5) *with* $\mathcal{D}_{\delta_f} \subset \mathbb{X}_f$ *as an ultimately bounded set.*

Proof. We apply Theorem 6.2.1 with $\alpha_1(s) = a_1 s^2$, $\alpha_2(s) = a_2 s^2$, and $d_1 = 0$. Direct calculations give that:

$$\begin{aligned} &V_f(Ax + B\kappa_f(x)) + \ell(x, \kappa_f(x)) - V_f(x) \\ &\quad = |A_K x + BW^{-\frac{1}{2}} \eta_v(x)|_P^2 + |x|_Q^2 + |Kx + W^{-\frac{1}{2}} \eta_\nu(x)|_R^2 - |x|_P^2, \\ &\quad = x'\big(A_K' P A_K + Q^* - P\big)x + 2x'(A_K' PB + K'R)\eta_\nu(x) + |\eta_\nu(x)|^2, \end{aligned}$$

where W is as in (6.21). Since matrix P is chosen according to (6.29), we have that $A_K' PB + K'R = A'PB + K'(B'PB + R) = 0$. Considering that in $\mathbb{X}_f$ the quantization error $\eta_\nu(x)$ is bounded as in (6.30), it follows that

$$V_f(Ax + B\kappa_f(x)) + \ell(x, \kappa_f(x)) - V_f(x) \leq |W| \Delta_q^2, \quad \forall x \in \mathbb{X}_f. \tag{6.31}$$

Thus, property (6.4) holds with $\alpha_3(s) = a_3 s^2$ and $d_2 = a_4\Delta_q^2$. Consequently, it follows that $\Delta V_f(x) = V_f(x_{k+1}) - V_f(x) \leq -a_3|x|^2 + a_4\Delta_q^2$, for all $x \in \mathbb{X}_f$.

This allows us to establish the following relationship

$$V_f(x_{k+1}) \leq \rho V_f(x_k) + a_4\Delta_q^2, \quad \forall x_k \in \mathbb{X}_f,$$

which implies that

$$|x_{k+1}|^2 \leq \frac{a_2}{a_1}\rho|x_k|^2 + \frac{a_4}{a_1}\Delta_q^2, \quad \forall x_k \in \mathbb{X}_f. \tag{6.32}$$

Suppose that $x_k \in \mathbb{X}_f$, i.e. $|x_k| \leq b$, and that the quantization error is bounded as in (6.30), thus we obtain that

$$|x_{k+1}|^2 \leq \frac{a_2}{a_1}\rho b^2 + \frac{a_4}{a_1}\frac{(a_1 - a_2\rho)}{a_4}b^2 \leq b^2,$$

thus $x_{k+1} \in \mathbb{X}_f$ and $\mathbb{X}_f$ is a PIS for (6.27). Therefore, by iterating (6.32), it is posible to exponentially bound the system state evolution via:

$$|x_k|^2 \leq \frac{a_2}{a_1}\rho^k|x_0|^2 + \left(\frac{1-\rho^k}{1-\rho}\right)\frac{a_4}{a_1}\Delta_q^2, \quad \forall k > 0, x_0 \in \mathbb{X}_f.$$

Thus, $\limsup_{k\to\infty}|x_k| \leq \delta_f$ provided $x_0 \in \mathbb{X}_f$. Consequently, by Theorem 6.2.1, the proposed local controller, $\kappa_f(x)$ in (6.22), is a practically stabilizing controller for the system (6.5) for all $x \in \mathbb{X}_f$. ■

The above result establishes that provided the set $\mathbb{U}$ is such that (6.30) is satisfied and the cost function is appropriated chosen , the one-step solution (6.22) is locally stabilizing in $\mathbb{X}_f$. This fact is used in the sequel to derive conditions for the practical stability the multi-step controller in (6.15).

6.4.2 MPC with a finite Alphabet

For the finite alphabet controller in (6.15), we can establish sufficient conditions for the practical stability based on the proposed local controller, $\kappa_f(k)$.

Theorem 6.4.1, given bellow, establishes that for all $x_0 \in X_N$, the system will be steered by the multi-step predictive controller towards the terminal region $\mathbb{X}_f \subseteq X_N$ and then (with the same controller) into an ultimately bounded set $\mathcal{D}_{\delta_N} \subset \mathbb{X}_f$.

Theorem 6.4.1 *Let $\mathcal{D}_{\delta_N} \triangleq \{x \in \mathbb{X}_f : |x| \leq \delta_N\}$ be a neighborhood of the origin, where*

$$\delta_N^2 \triangleq \gamma_N \Delta_q^2, \quad \gamma_N \triangleq \left(\frac{1+(1-\rho)N}{\lambda_{\min}(Q)(1-\rho)}\right)|W|. \tag{6.33}$$

Suppose that the matrix P in $V_f(x)$ satisfies (6.29)*. If Δ_q in* (6.19) *is bounded by*

$$\Delta_q^2 < \frac{b^2}{\gamma_N}, \tag{6.34}$$

then system (6.16) *is UpAS, i.e.,* $\limsup_{k\to\infty} |x_k| \leq \delta_N$ *for all $x_0 \in X_N$. Furthermore, there exists a finite instant $t > 0$, such that x_k converges at an exponential rate, i.e., there exists $c > 0$, such that*

$$|x_k|^2 \leq c\rho^{k-t}|x_t|^2 + \gamma_N \Delta_q^2, \forall k \geq t. \tag{6.35}$$

Proof. To prove this theorem we verify the conditions given in Definition 6.2.3. Clearly (6.2) holds with $\alpha_1(s) = c_1 s^2$ for all $x \in X_N$, where $c_1 = \lambda_{\min}(Q)$.

Using $\kappa_f(x)$ in (6.22), we can obtain the following feasible input sequence

$$\tilde{u}(x) = [\kappa_f(x)', \kappa_f(\hat{x}_1)', \ldots, \kappa_f(\hat{x}_{N-1})']',$$

see also [79]. Taking into account Lemma 6.4.1, it follows that

$$|\hat{x}_{N-1}|_Q^2 + |\kappa_f(\hat{x}_{N-1})|_R^2 + |\hat{x}_N|_P^2 = |\hat{x}_{N-1}|_P^2 + |\eta_\nu(\hat{x}_{N-1})|^2.$$

By iterating this procedure and using optimality, we obtain the bound

$$V_N(x, \vec{u}^{op}(x)) \leq V_N(x, \tilde{u}(x)) = |x|_P^2 + \sum_{j=0}^{N-1} |\eta_\nu(\hat{x}_j)|^2, \quad \forall x \in \mathbb{X}_f.$$

Therefore, (6.3) holds with $\alpha_2(s) = c_2 s^2 + d_1$, where $c_2 = \lambda_{\max}(P)$, and $d_1 = N|W|\Delta_q^2$ for all $x \in \mathbb{X}_f$.

Considering the optimizing sequence $\vec{u}^{op}(x)$ in (6.14) we obtain that the optimal value of the cost function is given by

$$V_N^{op}(x) = V_N(x, \vec{u}^{op}(x)). \tag{6.36}$$

Taking into account the proposed stabilizing local controller, $\kappa_f(x)$, we can adopt the shifted sequence approach [12] and use the following feasible input sequence

$$\tilde{u} = [(\hat{u}_1^{op})', \ldots, (\hat{u}_{N-1}^{op})', \kappa_f(\hat{x}_N)']',$$

where, by constraint (6.11), $\hat{x}_N \in \mathbb{X}_f$. By optimality, we obtain the bound

$$V_N^{op}(x_{k+1}) \leq V_N(x_{k+1}, \tilde{u}). \tag{6.37}$$

Comparing (6.36) with (6.37), and taking into account (6.12), we obtain that (with $x_k = x$)

$$\begin{aligned}\Delta V_N(x) =& V_N^{op}(x_{k+1}) - V_N^{op}(x) \leq V_N(x_{k+1}, \tilde{u}) - V_N^{op}(x) \\ =& -\ell(x, \kappa_N(x)) + V_f\left(A\hat{x}_N + B\kappa_f(\hat{x}_N)\right) + \ell(\hat{x}_N, \kappa_f(\hat{x}_N)) - V_f(\hat{x}_N).\end{aligned}$$

Therefore, considering (6.31), it follows that

$$\Delta V_N(x) \leq -c_3|x|^2 + a_4\Delta_q^2, \ \forall x \in X_N. \tag{6.38}$$

Finally, from (6.38), property (6.4) holds with $\alpha_3(s) = c_3 s^2$ and $d_2 = a_4\Delta_q^2$ where $c_3 = \lambda_{\min}(Q)$ for all $x \in X_N$.

Suppose that for an instant $t > 0$, $x \in \mathbb{X}_f$. Then, using (6.38) we can derive

$$V_N(x_{k+1}) \leq \rho V_N(x) + (1 + (1-\rho)N)\,|W|\Delta_q^2, \quad \forall x \in \mathbb{X}_f.$$

Thus, by iterating this procedure, it is possible to exponentially bound the system state evolution via:

$$|x_k|^2 \leq \frac{c_2}{c_1}\rho^{k-t}|x_t|^2 + \gamma_N\Delta_q^2, \quad \forall x_t \in \mathbb{X}_f, k \geq t.$$

Since $\rho \in (0,1)$, it is clear that $\limsup_{k\to\infty} |x_k| \leq \delta_N$ for all $x_t \in \mathbb{X}_f$. Therefore, considering (6.34), we have that $\mathcal{D}_{\delta_N} \subset \mathbb{X}_f$.

Now, for our analysis, it is convenient to introduce the following constant:

$$\epsilon \triangleq \left(\frac{1 + (1-\rho)(N-1)}{1-\rho}\right) a_4\Delta_q^2$$

Since $N \geq 1$ and $\rho \in (0,1)$, then $\epsilon > 0$. Thus, from (6.38) and considering (6.33), it follows that

$$\Delta V(x) \leq -c_3\delta_N^2 + a_4\Delta_q^2 = -\epsilon, \quad \forall x \in X_N \backslash \mathcal{D}_{\delta_N}.$$

Therefore, for any initial state $x_0 \in X_N$, there exists a finite instant $t > 0$, such that $x_k \in \mathbb{X}_f$ for all $k > t$ and, thus, (6.35) holds. Consequently, by Theorem 6.2.1, the finite alphabet MPC loop (6.16) is UpAS for all $x_0 \in X_N \backslash \mathbb{X}_f$ and practically exponentially stable for $k > t$. ■

Dual-Mode MPC Formulation

By using the local controller in (6.22), it is possible to define a dual-mode finite alphabet MPC strategy as follows:

$$\kappa_{DM}(x) = \begin{cases} \kappa_N(x), & x \in X_N \backslash \mathbb{X}_f \\ \kappa_f(x), & x \in \mathbb{X}_f \end{cases}$$

Thus, the resulting dual-mode finite alphabet MPC loop can be represented via:

$$x_{k+1} = Ax_k + B\kappa_{DM}(x_k), \quad \forall x_k \in X_N. \tag{6.39}$$

Theorem 6.4.2 (Stability of Dual-Mode MPC) *Suppose that the matrix P in the terminal cost, $V_f(x)$, satisfies* (6.29)*, and the quantization error is bounded as in* (6.30)*, then* (6.39) *is UpAS, i.e.,* $\limsup_{k\to\infty} |x_k| \leq \delta_f$ *for all* $x_0 \in X_N$.

The proof of Theorem 6.4.2 can be derived based on the proof of Lemma 6.4.1 and Theorem 6.4.1.

MPC with a Discrete Alphabet

We conclude our analysis by considering infinitely countable alphabets. The following result can now be easily derived.

Corollary 6.4.1 *Suppose that the control set, $\mathbb{U}$, is infinitely countable and that there exists $\Delta_{\max} < \infty$, such that for all $u_j \in \mathbb{U}$:*

$$\min_{u_i \in \mathbb{U}} |u_j - u_i| \leq \Delta_{\max}.$$

If the quadratic cost function, $V_N(x, \vec{u})$, is designed according to (6.29)*, then both, the MPC loop* (6.16) *and the dual-mode loop* (6.39) *are globally UpAS.*

Proof. Since $\mathbb{U}$ is an infinitely countable set, we can chose $\bar{\mathbb{U}} \triangleq \mathbb{R}^m$, i.e., $\bar{u}_{\max} = \infty$. From (6.26), we have that the terminal region is $\mathbb{X}_f \triangleq \mathbb{R}^n$. Thus, Δ_q in (6.19) satisfies that $\Delta_q \leq \frac{\Delta_{\max}}{2}$ for all $\bar{u} \in \mathbb{R}^m$. Therefore, from Lemma 6.4.1, $V_f(x)$ is a practical-Lyapunov function for the system (6.5), with respect to the associated quantization error, for all $x \in \mathbb{R}^n$. Consequently, the region of attraction of the discrete alphabet MPC loop (6.16) is $X_N \triangleq \mathbb{R}^n$ and the result follows from Theorem 6.4.1. The dual-mode formulation can be treated in a similar manner. ■

An important case where Corollary 6.4.1 establishes UpAS (which was not treated in previous works) is for open-loop unstable systems (6.5) and where the input set $\mathbb{U}$ is a lattice [98, 100, 119].

6.5 Illustrative Example

Consider a finte-set constrained system (6.5), (6.6), where

$$A = \begin{bmatrix} 0.3 & 0 \\ 0.3 & 1.1 \end{bmatrix}, \; B = -\begin{bmatrix} 0.2 \\ 0.8 \end{bmatrix}. \tag{6.40}$$

The input is restricted to belong to the nonuniform finite set:

$$\mathbb{U} \triangleq \{-0.7, -0.4, \; 0.2, \; 0.5, \; 1\}, \tag{6.41}$$

In this case we choose $\bar{u}_{\max} = 1$. Therefore, the associated convex control set can be characterized by $\bar{\mathbb{U}} \triangleq [-1, \; 1]$, obtaining $\Delta_q = 0.3$. The MPC strategy (6.16) was implemented

with parameters $N = 4$, $Q = I_2$ and $R = 0.01$. The terminal cost, $V_f = |x|_P^2$, is chosen in order to satisfy the first condition in Theorem 6.4.1, see (6.29), yielding:

$$P = \begin{bmatrix} 1.0532 & -0.0573 \\ -0.0573 & 1.0938 \end{bmatrix}, \quad K = [0.4204 \quad 1.2945].$$

The terminal region is characterized by:

$$\mathbb{X}_f \triangleq \left\{ x \in \mathbb{R}^2 : |x| \leq b \triangleq \frac{\bar{u}_{\max}}{|K|} = 0.7347 \right\}.$$

It is important to emphasize that the predictive controller directly provides a valid input to steer the system towards the ultimately bounded set, i.e., only elements of the finite set (6.41) are considered in the minimization of the quadratic cost function.

To guarantee stability of the predictive closed-loop, we verify the condition (6.34) presented in Theorem 6.4.1, where

$$\Delta_q^2 = 0.09 < \frac{b^2}{\gamma_N} = 0.1185,$$

with $\gamma_N = 4.5562$. Thus, the ultimately bounded set can be expressed by:

$$\mathcal{D}_{\delta_N} \triangleq \{ x \in \mathbb{X}_f : |x| \leq \delta_N = 0.6404 \}.$$

Figure 6.1 depicts the system state evolution of the finite set constrained MPC loop (6.16), starting from different initial conditions until reaching the ultimately bounded set, $\mathcal{D}_{\delta_N}$. In addition, Fig. 6.1 also shows the ultimately bounded set $\mathcal{D}_{\delta_f}$ for the dual-mode formulation (6.39). It is worth emphasizing that the trajectories obtained by using $\kappa_N(x)$ and $\kappa_{DM}(x)$, in general, differ.

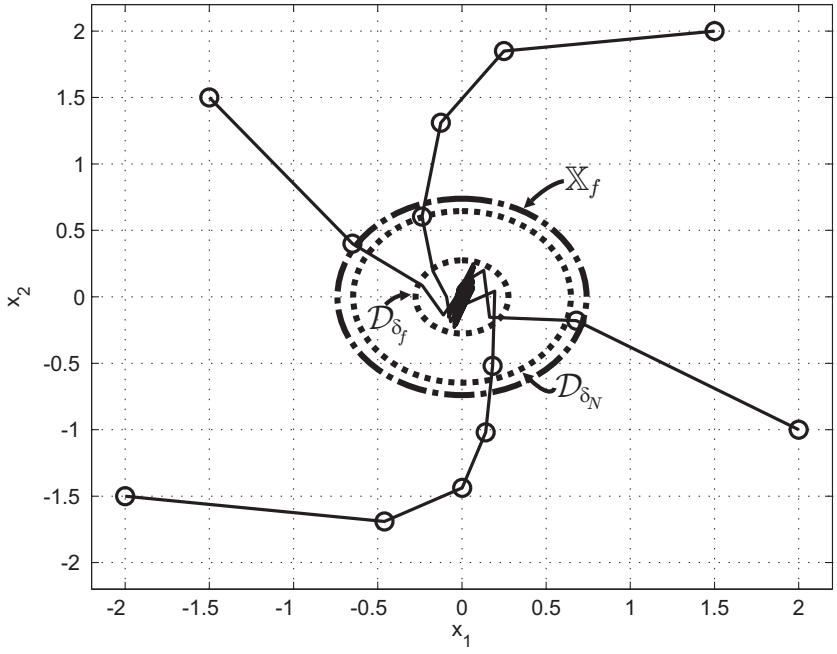

Figure 6.1: Evolution of the system state under quadratic MPC with a finite control set (6.15).

6.6 Conclusions

In this work, sufficient conditions to ensure practical stability of LTI systems with a discrete input alphabet have been presented. It is shown that stabilization of a neighbourhood of the origin when using the finite alphabet MPC loop is possible if the cost function is designed as per our results. Further work includes tracking of time-varying references and the design of a robust MPC strategies with a discrete input alphabet for systems with external disturbances.

7

FCS-MPC of Power Converters: Stability and Performance

7.1 Introduction

Based on the results presented in Chapter 6, a stability and performance analysis of FCS-MPC for power converters is presented is this section.

To emphasize the importance of the lack of stability guarantees, one can analyze the problem from a different viewpoint. It can be noticed that the available switch combinations generate a finite set of subsystems, i.e., $x(k+1) = A_i x(k) + B_i u(k)$ for given matrix pairs (A_i, B_i). Thus, a power converter can be modeled as a switched linear system. Consequently, obtaining an optimal switching input is equivalent to choosing an optimal subsystem, (A_i^{op}, B_i^{op}), at each sampling instat. Thus, the control goal is achieved by commuting among these subsystems. However, even when each subsystem is open-loop stable, i.e., $\lambda_{\max}(A_i) < 1$ for all i, the resulting closed-loop system generated by the control law may be unstable, i.e. become unbounded. Further details related to stability of switched systems can be found in [120].

A practical case when stability problems arise in power electronics is when FCS-MPC is applied to active front end rectifiers (AFEs). In general, FCS-MPC is applied to control the active and reactive power in the ac-side of the converter while, to regulate the dc-link voltage, a second control loop, based on a PI controller, is used [33, 34]. Recently,

a predictive formulation for AFEs which considers both the ac and dc sides has been proposed in our recent work [121]. Here, it has been shown that an AFE can be modeled as a switched linear system. Nonetheless, stabilizing this converter when FCS-MPC is applied, without using a second control loop, can be a complex task. To overcome this problem, in [121] we have proposed to derive compatible dynamic references for the dc-voltage and the active power in order to smoothly achieve the control goals in a larger horizon, without requiring additional control loops.

Another important issue related to FCS-MPC comes from the fact that this MPC strategy, in general, does not provide an explicit solution. This makes characterizing the resulting closed-loop performance a non-trivial task.

The above issues motive us to focus on the stability analysis of FCS-MPC for power converters. A remarkable tool to address this problem is Lyapunov stability theory [110]. More precisely, for convex MPC formulations it has been shown that stability can be established, by considering the cost function of the optimal problem as a candidate Lyapunov function [12, 13].

In the present work we present a stability analysis of FCS-MPC for power converters. The key idea of our approach is based on representing power converters as linear systems with quantized inputs. This allows us to establish practical stability of the power converter to a neighbourhood of a set point (desired system reference). The present work shows, in a semi-tutorial manner, how the ideas of our recent submission [122] can be applied to the analysis and design of FCS-MPC for power electronics and drives. From a technical viewpoint, the current work extends the framework of [122] to encompass, not only constant, but also sinusoidal references. As illustrative examples, our results are applied to FCS-MPC for a buck dc-dc converter and a 2-level dc-ac inverter.

Notation

Let $\mathbb{R}$ and $\mathbb{R}_{\geq 0}$ denote the real and non-negative real numbers. The difference between two given sets $\mathcal{A} \subseteq \mathbb{R}^n$ and $\mathcal{B} \subseteq \mathbb{R}^n$ is denoted by $\mathcal{A} \backslash \mathcal{B} = \{x \in \mathbb{R}^n : x \in \mathcal{A}, x \notin \mathcal{B}\}$. We represent the transpose of a given matrix A and a vector x via $(Ax)^T = x^T A^T$. The maximum and minimum eigenvalues of a given matrix A are represented by $\lambda_{\max}(A)$ and $\lambda_{\min}(A)$ respectively. $|\cdot|$ stands for the Euclidean norm. For any positive definite matrix P, $|x|_P^2 = x^T P x$ represents the square weighted Euclidean norm. We denote by $I_{n\times n}$ the identity matrix of size $n \times n$.

7.2 Preliminaries on Practical Stability

As foreshadowed in the introduction, a key observation when studying power converters is that since system inputs (switch combinations) are restricted to belong to a finite set, in general, the best one can hope for, is that state trajectories be bounded near the desired system reference. Therefore, in the present work we will focus on *practical stability* or *ultimate boundedness*. The term *practical* is used to emphasize that only stability of a neighbourhood of the system reference can be guaranteed. To understand this concept, some useful definitions are provided below. Further background on practical stability can be found in Chapter 5.2 of [110].

7.2.1 Coordinate Transformation

Consider that the power converter to be controlled can be modeld as a discrete-time LTI system via

$$\hat{x}(k+1) = f(\hat{x}(k), \hat{u}(k)) = A\hat{x}(k) + B\hat{u}(k), \tag{7.1}$$

where $\hat{x} \in \hat{\mathbb{X}} \subseteq \mathbb{R}^n$ is the system state (e.g. voltages and currents) and $\hat{u} \in \hat{\mathbb{U}} \subset \mathbb{R}^m$ is the control input (e.g. input voltages or power switches). The desired reference is represented by $x^\star \in \hat{\mathbb{X}}$. The control goal is represented by an equilibrium point via the

target $\hat{x}(k+1) = \hat{x}(k) = x^\star$. From this, it follows that

$$x^\star = Ax^\star + Bu^\star \Rightarrow x^\star = (I - A)^{-1}Bu^\star,$$

where $u^\star \in \hat{\mathbb{U}}$ is the required input to maintain $x^\star$. If we define the system deviation as $x = \hat{x} - x^\star$, then

$$\begin{aligned} x(k+1) &= \hat{x}(k+1) - x^\star \\ &= A(x(k) + x^\star) + B(u(k) + u^\star) - x^\star. \end{aligned}$$

Since $x^\star = Ax^\star + Bu^\star$, we obtain that

$$x(k+1) = f(x(k), u(k)) = Ax(k) + Bu(k), \tag{7.2}$$

In the sequel, we consider that $x \in \mathbb{X} \subseteq \mathbb{R}^n$ is the system state and $u \in \mathbb{U} \subset \mathbb{R}^m$ is the control input. Consequently, the control goal becomes one of leading the system (7.2) to the origin. Clearly, the origin is an equilibrium point, $f(0,0) = 0$, for (7.2). This is equivalent to leading the original system (7.1) to the desired reference, $x^\star$.

7.2.2 Practical Asymptotic Stability

Definition 7.2.1 *(Control positively invariant set). A set $\mathcal{A} \subseteq \mathbb{R}^n$ is said to be a control positively invariant set (PIS) for the system* (7.2) *if there exists an input $u \in \mathbb{U}$ such that $f(x,u) \in \mathcal{A}$, for all $x \in \mathcal{A}$.*

Definition 7.2.2 *(Practical Asymptotic Stability) The system* (7.2) *is said to be* practically *Asymptotically Stable (PAS) in $\mathcal{A} \subseteq \mathbb{R}^n$ if $\mathcal{A}$ is a PIS for* (7.2) *and if for an initial condition $x_0 \in \mathcal{A}$ there exists a positive constant δ, and a function $\beta(|x_0|, k)$, which is monotonically decreasing in k and monotonically increasing in $|x_0|$, such that*

$$|x(k)|^l \leq \beta(|x_0|, k) + \delta, \tag{7.3}$$

for all $k \geq 0$.

In the case that the function $\beta(|x_0|, k)$ is given by $\beta(|x_0|, k) = c|x_0|^l\rho^k$, where $c \geq 1$, $\rho \in (0,1)$ and $l > 0$, we will say that system (7.2) *is* practically *Exponentially Stable*

(PES) in $\mathcal{A}$. Thus, (7.3) *can be expressed by:*

$$|x(k)|^l \leq c|x_0|^l \cdot \rho^k + \delta, \tag{7.4}$$

for all $x_0 \in \mathcal{A}$ and $k \geq 0$.

Definition 7.2.3 *(Ultimately invariant set) Notice from* (7.3) *that, if system* (7.2) *is PAS, since the function $\beta(|x_0|, k)$ decreases over time, $\beta(|x_0|, k) \to 0$ as $k \to \infty$, the system state will ultimately be confined in*

$$\mathcal{D}_\delta = \{x \in \mathbb{R}^n : |x(k)| \leq \delta\}.$$

Accordingly, we will say that the set $\mathcal{D}_\delta$ is PAS for the system (7.2)*. This situation is depicted in Fig. 7.1.*

Remark 7.2.1 *If in* (7.3) *and* (7.4) *$\delta = 0$, then the system* (7.2) *is said to be asymptotically stable (AS) and exponentially stable (ES) respectively. Thus, since $\beta(|x_0|, k)$ decreases over time, i.e., $\beta(|x_0|, k) \to 0$ as $k \to \infty$, then the origin is AS for the system* (7.2)*.*

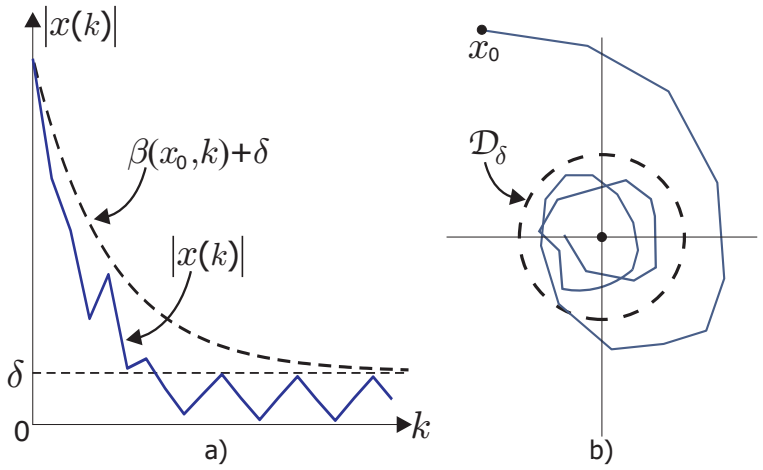

Figure 7.1: Practical stability representation: a) Practical asymptotic (exponential) stability. b) Ultimately invariant set $\mathcal{D}_\delta$.

7.2.3 The Role of Lyapunov Functions

To understand the Lyapunov function idea, it is convenient to recall the energy behaviour in a passive electrical system. For example, in an RLC circuit, the total stored energy is the sum of individual stored energy in the inductor, $E_L = \frac{1}{2}Li_L^2$, and in the capacitor, $E_C = \frac{1}{2}Cv_c^2$. This energy is dissipated in the resistance R as time proceeds. Thus, the total system energy, $E_T = E_L + E_C$, will decay to zero. Consequently, the system state, namely $(i_L,\ v_c)$, tends to a final equilibrium point, $i_L = v_c = 0$. Lyapunov stability methods follow a similar concept. If one can find a function for a given system which evolves over time similarly to the energy in a passive system, then the system state will converge to an equilibrium point. From this intuitive idea, we next give a simplified discussion of this theory. See [110] for a more thorough presentation.

Definition 7.2.4 *(Practical control-Lyapunov Function) A (not necessarily continuous) function $V : \mathbb{R}^n \to \mathbb{R}_{\geq 0}$ is said to be a practical control-Lyapunov function (CLF) in $\mathcal{A} \subseteq \mathbb{R}^n$ for the system* (7.2) *if $\mathcal{A}$ is a control PIS and if there exists a compact (i.e., closed and bounded) set $\Omega \subseteq \mathcal{A}$, some positive constants a_1, a_2, a_3, d, and σ such that, for all $x \in \mathcal{A}$, there exist $u \in \mathbb{U}$*

$$V(x) \geq a_1|x|^l, \qquad \forall x \in \mathcal{A}, \tag{7.5}$$

$$V(x) \leq a_2|x|^l + d, \qquad \forall x \in \Omega, \tag{7.6}$$

$$V(f(x,u)) - V(x) \leq -a_3|x|^l + \sigma, \tag{7.7}$$

for some $l \geq 1$.

Theorem 7.2.1 *(Converse theorem [113]) If the system* (7.2) *admits a practical control-Lyapunov function in $\mathcal{A}$, then it is PAS in $\mathcal{A}$.* ■

The above result tells us that, if we can find a CLF for the system to be controlled, then it is PAS (or PES) as presented in Definition 7.2.2. In other words, a practical CLF provides sufficient conditions for the existence of a controller $u(x) = \kappa(x)$ which ensures asymptotic (exponential) stability to a neighbourhood of the origin $\mathcal{D}_\delta$ for the controlled system $x(k+1) = f(x(k), \kappa(x(k)))$.

In the remainder of this work, we will build upon the above concepts to study stability and performance of power converters governed by FCS-MPC.

7.3 Examples

In this section we present two kinds of power converters which can be modeled as LTI systems with a quantized input.

7.3.1 Buck DC-DC Converter

This power converter, presented in Fig. 7.2, contains three power switches. Each of them can adopt only two values, i.e., $S_i = 0$ if the switch is open and $S_i = 1$ when it is closed. It means that $S_i \in \{0, 1\}$, for all $i \in \{1, 2, 3\}$. It is clear that, for avoiding internal faults, some of the switch combinations are forbidden.

Thus, if we define the switching input vector as: $s(t) = \begin{bmatrix} S_1(t) & S_2(t) & S_3(t) \end{bmatrix}^T$, then it will be restricted to belong to the following set:

$$s(t) \in \left\{ \begin{bmatrix} 0 \\ 0 \\ 1 \end{bmatrix}, \begin{bmatrix} 0 \\ 1 \\ 0 \end{bmatrix}, \begin{bmatrix} 1 \\ 0 \\ 0 \end{bmatrix} \right\}.$$

This is equivalent to consider the input voltage, $v_i(t)$, as control input, which is constrained according to:

$$v_i(t) \in \mathbb{V} \triangleq \left\{ 0, \frac{V_{dc}}{2}, V_{dc} \right\}. \tag{7.8}$$

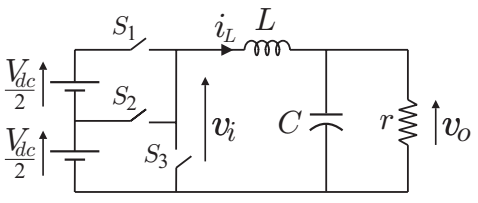

Figure 7.2: Three-level buck dc-dc converter.

The continuous-time model for the buck dc-dc converter is expressed via:

$$\begin{aligned}\frac{di_L(t)}{dt} &= -\frac{1}{L}v_o(t) + \frac{1}{L}v_i(t),\\ \frac{dv_o(t)}{dt} &= \frac{1}{C}i_L(t) - \frac{1}{rC}v_o(t).\end{aligned} \tag{7.9}$$

To facilitate the analysis, we next study the power converter in per-unit frame. To do this, we choose a base voltage, $V_{base} = V_{dc}$, and a base current, $I_{base} = V_{dc}/r$.

Afterwards, using a forward Euler approximation, we transform the continuous-time model in (7.9) into discrete-time form. Thus, the buck dc-dc converter in per-unit frame, can be expressed by:

$$\begin{aligned}i_{L,pu}(k+1) &= i_{L,pu}(k) - \frac{hr}{L}v_{o,pu}(k) + \frac{hr}{L}v_{i,pu}(k),\\ v_{o,pu}(k+1) &= \frac{h}{rC}i_{L,pu}(k) + \left(1 - \frac{h}{rC}\right)v_{o,pu}(k),\end{aligned}$$

where h stands for the sampling period.

Considering $\hat{x} = [i_{L,pu}\ v_{0,pu}]^T$, the buck dc-dc converter can be represented as a switched system via:

$$\hat{x}(k+1) = A_i\hat{x}(k) + B_i, \quad \forall i \in \{1,2,3\}, \tag{7.10}$$

where

$$\begin{aligned}&A_1 = A_2 = A_3 = A,\\ &B_1 = 0_{2\times 1}, \quad B_2 = \frac{1}{2}B, \quad B_3 = B,\end{aligned}$$

in which

$$A = \begin{bmatrix} 1 & -\frac{hr}{L} \\ \frac{h}{rC} & 1 - \frac{h}{rC} \end{bmatrix}, \quad B = \begin{bmatrix} \frac{hr}{L} \\ 0 \end{bmatrix}.$$

To represent this power converter as an LTI system with quantized input, we consider $\hat{u} = v_{i,pu}$, as the control input. Thus, the model presented in (7.10) becomes

$$\hat{x}(k+1) = A\hat{x}(k) + B\hat{u}(k). \tag{7.11}$$

Now, we assume that we seek to obtain an output voltage of $v_o^\star = \alpha V_{dc}$, with $\alpha \in (0,1)$. From the system model, one can see that this voltage reference will be reached when the

inductor current is $i_L^\star = v_o^\star/r = \alpha V_{dc}/r$. On the other hand, the required voltage input, $v_i^\star$, to keep this desired steady state is $v_i^\star = v_o^\star = \alpha V_{dc}$. Thus, the per-unit references become $i_{L,pu}^\star = v_{o,pu}^\star = \alpha$, yielding $x^\star = [\alpha\ \alpha]^T$.

Remark 7.3.1 *Notice that the desired output voltage reference, $v_o^\star = \alpha V_{dc}$, may not be an element of the finite set $\mathbb{V}$ in* (7.8)*. Therefore, it is not always possible to achieve an equilibrium point. Thus, the best one can hope for, is that state trajectories be bounded near the desired reference. It is for this reason we focus on practical stability as shown in Fig. 7.1.* ■

Finally, the system state representation of the buck dc-dc converter, in per-unit frame, is given by

$$x(k+1) = Ax(k) + Bu(k),$$

where $x = \hat{x} - x^\star$ and $u = v_{i,pu} - \alpha$. Consequently, since $v_i \in \mathbb{V}$, the control input, u, is restricted to belong to the finite set $\mathbb{U}$ expressed via:

$$u(k) \in \mathbb{U} \triangleq \left\{-\alpha, \quad \tfrac{1}{2} - \alpha, \quad 1 - \alpha\right\}.$$

7.3.2 2-Level Inverter

The topology of this dc-ac converter is presented in Fig. 7.3. The continuous-time dynamic model for each output current, i_y, is given by:

$$\frac{di_y(t)}{dt} = -\frac{r}{L} i_y(t) + \frac{1}{L}(V_{dc} s_y(t) - v_{no}(t)), \quad \forall y \in \{a, b, c\},$$

where v_{no} stands for the common mode voltage defined as $v_{no}(t) = \frac{1}{3}(v_{ia}(t) + v_{ib}(t) + v_{ic}(t))$.

In this case, the input, s_y, belongs to the following finite set

$$\mathbb{S} \triangleq \left\{ \begin{bmatrix} 0 \\ 0 \\ 0 \end{bmatrix}, \begin{bmatrix} 0 \\ 0 \\ 1 \end{bmatrix}, \begin{bmatrix} 0 \\ 1 \\ 0 \end{bmatrix}, \begin{bmatrix} 0 \\ 1 \\ 1 \end{bmatrix}, \begin{bmatrix} 1 \\ 0 \\ 0 \end{bmatrix} \begin{bmatrix} 1 \\ 0 \\ 1 \end{bmatrix}, \begin{bmatrix} 1 \\ 1 \\ 0 \end{bmatrix}, \begin{bmatrix} 1 \\ 1 \\ 1 \end{bmatrix} \right\}.$$

It is well known that, for sinusoidal references in a 3-phase system, we can apply the so-called abc-to-dq transformation. Firstly, we define a current vector in abc frame as: $i_{abc} =$

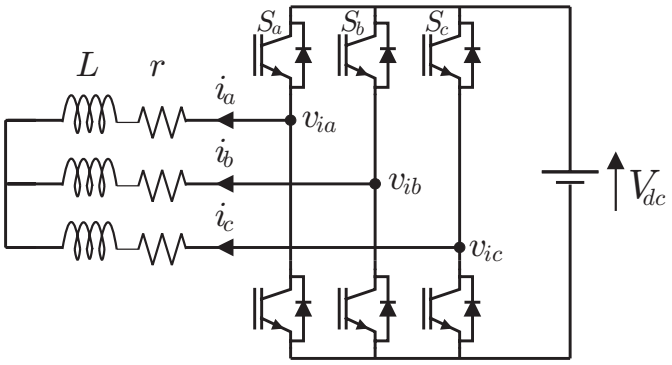

Figure 7.3: Two-Level inverter topology.

$[i_a\ i_b\ i_c]^T$. Then, it is transformed into dq frame by applying the following transformation:

$$i_{dq}(t) = \Gamma(t) i_{abc}(t),$$

where:

$$\Gamma(t) = \frac{2}{3}\begin{bmatrix} \sin(\omega t) & \sin(\omega t - \frac{2\pi}{3}) & \sin(\omega t + \frac{2\pi}{3}) \\ \cos(\omega t) & \cos(\omega t - \frac{2\pi}{3}) & \cos(\omega t + \frac{2\pi}{3}) \end{bmatrix}, \tag{7.12}$$

and $i_{dq}(t) = [i_d(t) \quad i_q(t)]^T$.

Thus, the continuous-time model of the 2-level inverter, in dq frame, is expressed by:

$$\frac{di_{dq}(t)}{dt} = \begin{bmatrix} -r/L & \omega \\ -\omega & -r/L \end{bmatrix} i_{dq}(t) + \begin{bmatrix} \frac{V_{dc}}{L} & 0 \\ 0 & \frac{V_{dc}}{L} \end{bmatrix} s_{dq}(t),$$

where, $s_{dq}(t) = [s_d(t) \quad s_q(t)]^T = \Gamma(t) s_{abc}(t)$, in which $s_{abc} = [s_a(t)\ s_b(t)\ s_c(t)]^T$ is the inverter switches vector.

Similar to the buck converter, we define the state and input deviations, x, for the 2-level inverter. In this case we seek a constant amplitud reference, $I^\star$, for the output currents i_{abc}. This is equivalent to setting $i^\star_{dq} = [I^\star\ 0]^T$. On the other had, the input required for maintaining this state value is $s^\star_{dq} = [rI^\star/V_{dc} \quad \omega L I^\star/V_{dc}]^T$. Thus, the system state deviation in dq frame is characterized via:

$$x = i_{dq} - i^\star_{dq}, \quad u = s_{dq} - s^\star_{dq}$$

Then, using forward Euler approximation, we obtain the discrete-time model

$$x(k+1) = Ax(k) + Bu(k),$$

where

$$A = \begin{bmatrix} 1 - h\frac{r}{L} & \omega h \\ -\omega h & 1 - h\frac{r}{L} \end{bmatrix}, \quad B = \begin{bmatrix} \frac{h}{L}V_{dc} & 0 \\ 0 & \frac{h}{L}V_{dc} \end{bmatrix},$$

in which

$$u(k) \in \mathbb{U}(k) = \Gamma(k)\mathbb{S} - s^{\star}_{dq}.$$

In Section 7.6.2 we will show that our results can also be applied when the input is restricted to belong to a bounded time-varying finite set of the form give above. For ease of presentation, however, we will first focus on the time-invariant case.

7.4 Finite-Control-Set MPC

In this section we formalize the predictive control problem for power converters in terms of a quadratic programme with finite set constraints. For further background of MPC with finite set constraints, see [37, 96].

As already mentioned, we focus on power converters which can be modeled, in a state space framework, via:

$$x(k+1) = f(x(k), u(k)) \triangleq Ax(k) + Bu(k), \tag{7.13}$$

where $x \in \mathbb{R}^n$ stands for the n-system state variables and $u \in \mathbb{U} \subset R^m$ represents the m-control inputs of the power converter, i.e., the switch positions. This model encompasses a variety of converter topologies, including those presented in Section 7.3. In this case, due to the nature of the system, we deal with a linear system wich presents a finite control set of p elements, such that

$$u(k) \in \mathbb{U} = \{u_1, u_2, \ldots, u_p\}. \tag{7.14}$$

In particular, FCS-MPC uses predictions of the future behaviour of the system, from the current state $x(k) = x$. We will consider the following quadratic cost function with a

prediction horizon $N \geq 1$,

$$V_N(x, \vec{u}) = V_f(x'(N)) + \sum_{j=0}^{N-1} \ell(x'(j), u'(j)), \tag{7.15}$$

where the term

$$\ell(x', u') = |x'|_Q^2 + |u'|_R^2 = (x')^T Q x' + (u')^T R u', \tag{7.16}$$

is called *stage cost*, in which Q and R are positive definite matrices, and the term

$$V_f(x') = |x'|_P^2 = (x')^T P x,$$

is the *final cost*, in which P is also positive definite. The predicted state trajectories, $x'(j)$, are generated by the following model

$$x'(j+1) = Ax'(j) + Bu'(j), \quad x'(0) = x(k) = x, \tag{7.17}$$

while

$$\vec{u} = [\ (u'(0))^T \quad (u'(1))^T \quad \dots \quad (u'(N-1))^T\ ]^T \in \mathbb{U}^N \tag{7.18}$$

contains the constrained input predictions.

Now, the FCS-MPC strategy can be stated as an optimal control problem, $\mathbb{P}_N(x)$, for the system (7.13), as:

$$\mathbb{P}_N(x): \quad V_N^{op}(x) = \min_{\vec{u}} \{V_N(x, \vec{u}) \mid \vec{u}(x) \in \mathcal{U}(x)\} \tag{7.19}$$

subject to:

$$x'(j) \in \mathbb{R}^n, \quad \forall j \in \{0, \cdots, N\}, \tag{7.20}$$

$$u'(j) \in \mathbb{U}, \quad \forall j \in \{0, \cdots, N-1\}, \tag{7.21}$$

$$x'(N) \in \mathbb{X}_f. \tag{7.22}$$

Here, (7.20) considers the system state constraints while (7.21) encompasses the finite control set constraint along the prediction horizon. Constraint (7.22) is the so-called *terminal constraint*, with a terminal region $\mathbb{X}_f \subset \mathbb{R}^n$. Therefore, $\mathcal{U}(x) \subseteq \mathbb{U}^N$ contains all the *feasible* input predictions which satisfy (7.20)-(7.22). Thus, we denote the domain of the cost function via

$$X_N = \{x \in \mathbb{X} : \mathcal{U}(x) \neq \emptyset\}.$$

Consequently, the optimal input sequence, $\vec{u}^{op}(x)$, is that one which minimizes the cost function,

$$\vec{u}_{op}(x) \triangleq \arg\left\{\min_{\vec{u}\in\mathcal{U}(x)} V_N(x,\vec{u})\right\}. \tag{7.23}$$

For future reference, we denote its components via

$$\vec{u}_{op}(x) = \left[\ (u'_{op}(0))^T \quad \dots \quad (u'_{op}(N-1))^T\right]^T, \tag{7.24}$$

while the resulting optimal state sequence is

$$\vec{x}_{op}(x) = \left[x^T \quad (x'_{op}(1))^T \quad \dots \quad (x'_{op}(N))^T\ \right]^T.$$

Following the receding horizon paradigm, only the first element of $\vec{u}^{op}(x)$ is applied to the converter at each sampling instant. The solution of the optimal problem, $\mathbb{P}_N(x)$ in (7.19), yields the MPC control law, $\kappa_N(\cdot) : X_N \to \mathbb{U}$,

$$\kappa_N(x) \triangleq u'_{op}(0). \tag{7.25}$$

Thus, the resulting FCS-MPC loop can be represented via

$$x(k+1) = Ax(k) + B\kappa_N(x(k)). \tag{7.26}$$

Remark 7.4.1 *It is important to notice that, in the cost function $V_N(x,\vec{u})$, Q and R are weighting matrices used to penalize predicted behaviour. Hence, these are given matrices. On the other hand, matrix P is used to penalize the final predicted state, $x'(N)$. This term is used to guarantee stability of the predictive strategy. The design of matrix P will be analyzed in Section 7.5.*

Remark 7.4.2 *Choosing lager prediction horizons $N \geq 1$, in general, gives better closed-loop performance than choosing short ones. It is for this reason that we consider prediction horizons $N \geq 1$ [12, 13]. Unfortunately, for FCS-MPC, obtaining the optimal input sequence, $\vec{u}^{op}(x)$, requires that one solve a combinatorial optimization problem. This limits the use of larger horizons in practical applications. Interestingly, recent research has shown that, in some situations, the use of horizon one also gives the optimal solution to a formulation with a larger horizon, see [79].*

7.5 Lyapunov-Based Stability and Performance Analysis of FCS-MPC

There exist several methodologies in the literature to study stability of MPC, which have some common ingredients that allow one to formalize this field (see [123]). The main common ingredient is the fact that these predictive strategies rely on a cost function to forecast the future behaviour of the system to be controlled. Hence, a key aspect to establish stability of MPC is based on considering this cost function as a candidate-Lyapunov function. To guarantee practical stability when FCS-MPC is applied to system (7.13), by Theorem 7.2.1, it is sufficient to design the cost function, $V_N(x, \vec{u})$ in (7.15), in order to satisfy the conditions (7.5)-(7.7) presented in Definition 7.2.4. Thus, the cost function can be considered as a practical CLF. Further background related to practical stability of MPC can be found in [113].

7.5.1 Practical Stability of MPC

A widely-used idea to guarantee that the cost function is a CLF is based on finding a known controller, $\kappa_f(x)$, which can stabilize the system within the terminal region $\mathbb{X}_f$, see [12].

To adapt this idea to systems with finite control sets, we first introduce the following definition:

Definition 7.5.1 (Vector Quantizer (see e.g. [100])) *Consider a set $\mathcal{A} \subseteq \mathbb{R}^n$ a finite set $\mathcal{B} \triangleq \{b_1, \ldots, b_p\} \subset \mathbb{R}^n$. A function $q_{\mathcal{B}}(\cdot) : \mathcal{A} \to \mathcal{B}$ is an Euclidean vector quantizer if $q_{\mathcal{B}}(a) = b_i \in \mathcal{B}$ if and only if b_i satisfies that $\mid a - b_i \mid \leq \mid a - b_j \mid$, for all $b_j \neq b_i$, where $b_j \in \mathcal{B}$. The associated quantization error is defined as $\eta_{\mathcal{B}}(a) \triangleq q_{\mathcal{B}}(a) - a$.* ■

This allows us to introduce an associated nominal set for the finite set $\mathbb{U}$ via

$$\bar{\mathbb{U}} \triangleq \{\bar{u} \in \mathbb{R}^m : |\bar{u}| \leq \bar{u}_{\max}\},$$

where $\bar{u}_{\max} \in (0, \infty)$ is a design parameter. Since $\bar{\mathbb{U}}$ is bounded, so is the quantization

error, thus

$$|\eta| \triangleq \Delta_q \triangleq \max_{\bar{u}\in\bar{\mathbb{U}}} |q_{\mathbb{U}}(\bar{u}) - \bar{u}| < \infty. \tag{7.27}$$

Note that Δ_q depends upon $\bar{u}_{\max}$.

Given the nature of our problem, and in view of results for unconstrained systems (see Chapter 2.5 of [12]) we choose $\kappa_f(x)$ as follows:

$$\kappa_f(x) = q_{\mathbb{U}}(Kx) = Kx + \eta(x), \tag{7.28}$$

where

$$K = -W^{-1}B^T PA, \quad W = B^T PB + R. \tag{7.29}$$

Thus, system (7.13), in the terminal region, $\mathbb{X}_f$, can be modeled by:

$$x(k+1) = A_K x(k) + w_f(x(k)), \quad \forall x_k \in \mathbb{X}_f, \tag{7.30}$$

where $A_K \triangleq A + BK$ and $w_f(x(k)) = B\eta(x(k))$ represents the state disturbance produced by the quantization error.

The above allows to define the terminal region in (7.22) as:

$$\mathbb{X}_f = \{x \in \mathbb{R}^n : Kx \in \bar{\mathbb{U}}\}$$

To guarantee stability of the FCS-MPC loop (7.26) we propose to design the cost function in (7.15) considering the (sufficient) stabilizing conditions presented in the following theorem.

Theorem 7.5.1 *Let $\mathcal{D}_{\delta_N} \triangleq \{x \in \mathbb{X}_f : |x| \leq \delta_N\}$ be a neighbourhood of the origin, where*

$$\delta_N^2 \triangleq \left(\frac{1 + (1-\rho)N}{\lambda_{\min}(Q)(1-\rho)}\right)|W|\Delta_q^2. \tag{7.31}$$

in which $\rho = 1 - \frac{\lambda_{\min}(Q)}{\lambda_{\max}(P)} \in (0,1)$. If the cost function is designed such that the terminal cost satisfies that:

1. *matrix P is the solution to the algebraic Riccati equation*

$$A_K^T P A_K - P + Q^* = 0, \quad Q^* = Q + K^T RK, \tag{7.32}$$

2. *there exists a local controller, $\kappa_f(x)$, which satisfies the following condition in the terminal region:*

$$V_f(f(x,\kappa_f(x))) - V_f(x) + \ell(x,\kappa_f(x)) < \gamma \tag{7.33}$$

for all $x \in \mathbb{X}_f$ and some $\gamma \geq 0$,

then system (7.26) *is PAS with $\mathcal{D}_{\delta_N}$ as an ultimately invariant set.* ■

The proof of this theorem can be found in [12]. A more rigorous analysis of stability of MPC with finite control sets is given in [37, 85, 122].

7.5.2 FCS-MPC Convergence

It is clear that the cost function, $V_N(x)$ in (7.15), is always positive, becoming zero only at the origin, i.e., $V_N(0) = 0$. Therefore, the system state will be led to the origin (system reference) if the cost $V_N(x)$ decreases. For this reason, we will next study the convergence of the cost function, when designed as per (7.32).

Terminal Condition

We first analyze the practical stability condition (7.33), presented in Theorem 7.5.1, for our problem.

$$\begin{aligned} &V_f(Ax + \kappa_f(x)) - V_f(x) + \ell(x,\kappa_f(x)) \\ &\quad = |A_K x + B\eta|_P^2 - |x|_P^2 + |x|_Q^2 + |Kx + \eta|_R^2, \\ &\quad = x^T\big(A_K^T P A_K - P + Q^*\big)x + 2x^T(A_K^T P B + K^T R)\eta + \eta^T W \eta, \end{aligned}$$

Since matrix P is chosen to be the solution to the discrete Riccati equation in (7.32), we have that

$$\begin{aligned} A_K^T P A_K - P + Q^* = 0, \\ A_K^T P B + K^T R = A^T P B + K^T W = 0. \end{aligned}$$

Consequently, considering that the quantization error is bounded by $|\eta| \leq \Delta_q$, it follows that

$$V_f(Ax + Bu_f) - V_f(x) + \ell(x, u_f) \leq |W|\Delta_q^2, \tag{7.34}$$

for all $x \in \mathbb{X}_f$.

Monotonicity of the Cost Function

Let $x'(0) = x(k) = x \in X_N$ be the current system state. Consider that the optimal input sequence obtained at the current instant is

$$\vec{u}_{op}(x) = \left[\ (\kappa_N(x))^T \ (u'_{op}(1))^T \ \dots \ (u'_{op}(N-1))^T \right]^T,$$

Thus, the optimal value of the cost function is given by

$$V_N^{op}(x) = V_N(x, \vec{u}_{op}(x)). \tag{7.35}$$

Afterwards, for the next sampling instant $k+1$ the optimal input sequence, say $\vec{u}_{op}(x(k+1))$, gives us the optimal value

$$V_N^{op}(x) = V_N(x(k+1), \vec{u}_{op}(x(k+1))). \tag{7.36}$$

It is important to emphasize that $\vec{u}_{op}(x(k+1))$ may not have any common elements when compered to $\vec{u}_{op}(x)$. Thus, comparing (7.35) with (7.36) may be hard task. To study this problem, we take into account the proposed stabilizing local controller, $\kappa_f(x)$, in order to adopt the shifted sequence approach [12] and use the following feasible input sequence,

$$\tilde{u} = \left[\ (u'_{op}(1))^T \ \dots \ (u'_{op}(N-1))^T \ \kappa_f(x'(N))^T \right]^T,$$

which considers the elements of $\vec{u}_{op}(x)$ and the local controller $\kappa_f(x'(N))$. Notice that, by constraint (7.22), $x'(N) \in \mathbb{X}_f$. Thus, by optimality, we obtain the bound

$$V_N^{op}(x(k+1)) \leq V_N(x(k+1), \tilde{u}). \tag{7.37}$$

Comparing (7.35) with (7.37), and taking into account (7.15), we obtain that (with $x(k) = x$)

$$\begin{aligned}\Delta V_N(x) =& V_N^{op}(x_{k+1}) - V_N^{op}(x)\\ \leq& V_N(x_{k+1}, \tilde{u}) - V_N^{op}(x)\\ =& -\ell(x, \kappa_N(x)) + V_f\left(Ax'(N) + B\kappa_f(x'(N))\right) + \ell(x'(N), \kappa_f(x'(N))) - V_f(x'(N)).\end{aligned}$$

Therefore, considering (7.34) and that $\ell(x,u) > |x|_Q^2$, it follows that

$$\Delta V_N(x) \leq -a_3|x|^2 + \sigma,\ \forall x \in X_N. \tag{7.38}$$

where $a_3 = \lambda_{\min}(Q)$ and $\sigma = |W|\Delta_q^2$.

Consequently, the cost function, $V_N(x)$, will monotonically decrease, until the system state reaches a value of $|x|^2 < \frac{\sigma}{a_3}$.

Practical CLF

We first notice that

$$V_N(x, \vec{u}) \geq \ell(x, \kappa_N(x)) \geq |x|_Q^2. \tag{7.39}$$

Afterwards, using $\kappa_f(x)$ in (7.28), we can obtain the following feasible input sequence (see also [79])

$$\tilde{u}(x) = [(\kappa_f(x))^T\ (\kappa_f(x'(1)))^T\ \ldots\ (\kappa_f(x'(N-1)))^T]^T.$$

Thus, it is possible to derive the following relationship

$$|x'(N-1)|_Q^2 + |\kappa_f(x'(N-1))|_R^2 + |x'(N)|_P^2 = |x'(N-1)|_P^2 + |\eta_\nu(x(N-1))|_W^2.$$

By iterating this procedure for the remaining elements of $\tilde{u}(x)$ and using optimality, we obtain the bound (with $x(k) = x$)

$$V_N(x, \vec{u}_{op}(x)) \leq V_N(x, \tilde{u}(x)) = |x|_P^2 + \sum_{j=0}^{N-1} |\eta_\nu(x'(j))|_W^2, \quad \forall x \in \mathbb{X}_f. \tag{7.40}$$

Consequently, tacking into account (7.38)-(7.40) and considering Definition 7.2.2, we obtain that $V_N(x)$ is a practical CLF for the system (7.13) which satisfies

$$\begin{aligned} V_N(x) &\geq a_1|x|^2, \qquad \forall x \in X_N \\ V_N(x) &\leq a_2|x|^2 + d, \quad \forall x \in \mathbb{X}_f \\ \Delta V_N(x) &\leq -a_3|x|^2 + \sigma, \end{aligned} \tag{7.41}$$

for all $x \in X_N$, where

$$\begin{aligned} a_1 = a_3 = \lambda_{\min}(Q), \quad a_2 = \lambda_{\max}(P), \\ d = N|W|\Delta_q^2, \quad \sigma = |W|\Delta_q^2. \end{aligned}$$

Exponential Convergence

It follows from (7.41) that

$$V_N(x(k+1)) \leq V_N(x(k)) - a_3|x(k)|^2 + \sigma.$$

Considering that $V_N(x) < a_2|x|^2 + d$, we obtain that

$$\begin{aligned} V_N(x(k+1)) \leq & V_N(x(k)) - \frac{a_3}{a_2}(V_N(x(k) - d) + \sigma \\ \leq & \rho V_N(x(k)) + (1-\rho)d + \sigma, \end{aligned}$$

where $\rho = 1 - a_3/a_2 \in (0, 1)$.

By iterating this relationship we can derive the following bound for the evolution of the cost function, starting for a initial state $x(0) = x_0$

$$V_N(x(k)) \leq \rho^k V_N(x_0) + a_1 \left(1 - \rho^k\right) \delta_N^2, \tag{7.42}$$

for all $k > 0, x_0 \in \mathbb{X}_f$.

Thus, since $\rho \in (1, 0)$, the cost function will be ultimately bounded by

$$\lim_{k \to \infty} |V_N(x(k))| \leq \gamma_N = a_1 \delta_N^2$$

Considering that $V_N(x) > a_1|x|^2$, we can derive the following quadratic bound for the system state:

$$|x(k)|^2 \leq \frac{1}{a_1}\rho^k V_N(x_0) + \left(1-\rho^k\right)\delta_N^2,$$

Finally, as was stated in Theorem 7.5.1, the system state will be ultimately bounded by

$$\lim_{k\to\infty} |x(k)| \leq \delta_N$$

Consequently, the optimal control law, $\kappa_N(x)$, obtained from FCS-MPC strategy will steer the initial system state $x_0 \in X_N$ into the terminal region $\mathbb{X}_f$ and then exponentially into the ultimately invariant set $\mathcal{D}_{\delta_N}$ where finally the system will be confined.

7.6 Case Studies

In this section we illustrate the Lyapunov-based stability and performance analysis presented in this work when it is applied to two classes of power converters, a buck converter and a 2-level inverter.

7.6.1 Buck DC-DC converter

For this simulation study, we focus on a three-level buck dc-dc converter presented in Section 7.3.1, see also Fig. 7.2. The electrical parameters of this dc-dc converter are chosen as $V_{dc} = 100\ V$, $r = 5\ \Omega$, $L = 5\ mH$ and $C = 40\ \mu F$. The desired output voltage reference is set as $v_o^\star = 37.5\ V$, thus, $\alpha = 0.375$, see Section 7.3.1.

The predictive controller was implemented using a sampling period of $h = 200\ \mu s$. To design the cost function, we chose a weighting factor $\omega_x = 1$ which gives us a trade off between the inductor current tracking error, x_1, and the output voltage tracking error, x_2. In addition, a weighting factor for the control input $\omega_u = 0.1$ is considered. Thus, the

stage cost becomes

$$\begin{aligned}\ell(x(j), u(j)) &= |x(j)|_Q^2 + |u(j)|_R^2 \\ &= (i_{L,pu}(j) - \alpha)^2 + \omega_x(v_{o,pu}(j) - \alpha)^2 + \omega_u(v_{i,pu}(j) - \alpha)^2\end{aligned}$$

where

$$Q = \begin{bmatrix} 1 & 0 \\ 0 & 1 \end{bmatrix}, \quad R = 0.1.$$

Afterwards, we can solve the Riccati equation presented in (7.32) in order to set the terminal cost. Thus, we obtain that:

$$P = \begin{bmatrix} 3.2271 & -0.2591 \\ -0.2591 & 1.0563 \end{bmatrix}, \quad K = \begin{bmatrix} -2.5912 & 0.5635 \end{bmatrix}.$$

Finally, considering a prediction horizon of $N = 1$, the cost function (7.15) becomes:

$$V_N(x, \vec{u}) = |x(k)|_Q^2 + |u(k)|_R^2 + |x(k+1)|_P^2.$$

From this design, we can say that the cost function will be exponentially bounded as shown in (7.42), with a decay rate of:

$$\rho = 1 - a_2/a_3 = 0.6930,$$

and final value

$$\gamma_N = 0.0573.$$

Thus, one can anticipate that the system state deviation, x, will be led by the predictive controller to the ultimately invariant set, $\mathcal{D}_{\delta_N}$, characterized via, see (7.31),

$$\mathcal{D}_{\delta_N} = \{x \in \mathbb{R}^n : |x| \leq \delta_N = 0.2394\}.$$

The evolution of the buck converter under FCS-MPC, starting from $v_{o,pu} = i_{L,pu} = 0$, is depicted in Fig. 7.4. Here, one can see that the predictive controller leads the system state to the invariant set $\mathcal{D}_{\delta_N}$. The per-unit system state (inductor current $i_{L,pu}$ and output voltage $v_{o,pu}$) and the finite control input (input voltage $v_{i,pu}$) behaviour, over the time, are shown in Fig. 7.5. It is clear that the steady-state system trajectories are bounded around of the desired reference.

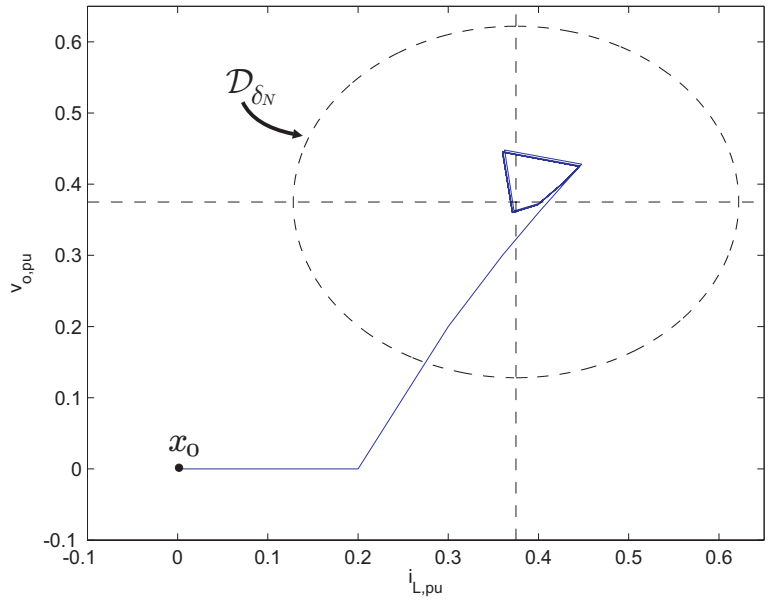

Figure 7.4: Convergence of the buck converter to the ultimate invariant set $\mathcal{D}_{\delta_N}$; $\delta_N = 0.2394$.

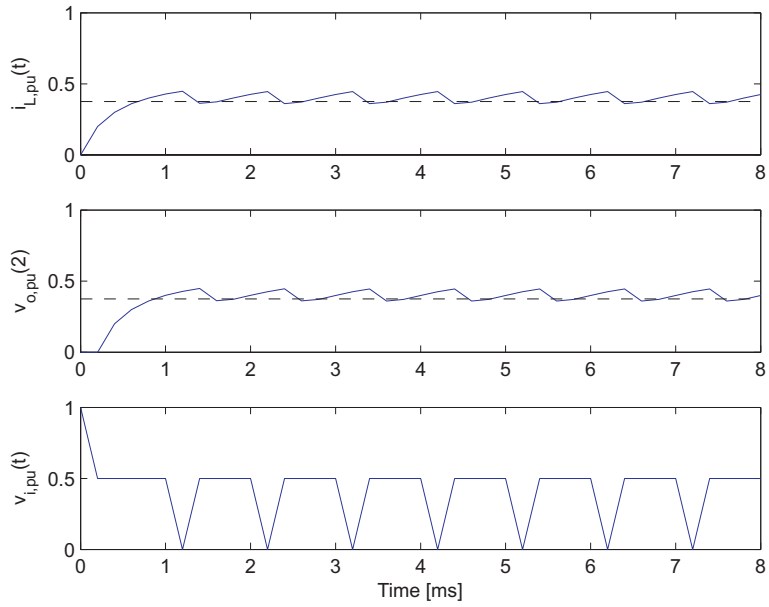

Figure 7.5: System state and input behaviour over time.

Due to the design of the cost function, $V_N(x)$, one can see in Fig. 7.6 that $V_N(x)$ is exponentially bounded as defined in (7.42). Hence, it decreases exponentially until the

system state deviation, x, reaches the ultimately invariant set $\mathcal{D}_{\delta_N}$. Inside this region, the cost function, $V_N(k)$, presents an oscillating behaviour bounded by γ_N. This is attributable to the fact that due to the switching action which occurs at discrete time-instants the system cannot reach an equilibrium point for the given reference.

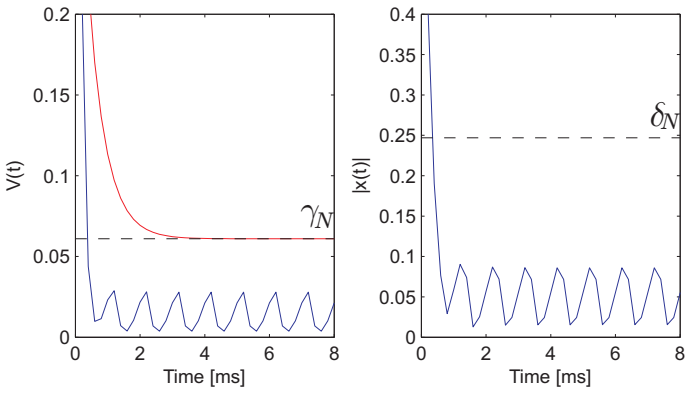

Figure 7.6: Cost function $V_N(x)$ and norm of the state deviation $|x|$ over time.

To show how the cost function design affects the system behaviour, we carried out simulations for the buck converter using a different matrix R. In this case we propose to set matrix $R = 0.01$. Following the same procedure used previously, we obtain

$$P = \begin{bmatrix} 2.22401 & -0.0441 \\ -0.0441 & 1.00090 \end{bmatrix}, \quad K = \begin{bmatrix} -4.4057 & 0.8990 \end{bmatrix}.$$

Consequently, under this new setting the cost function satisfies the bound (7.42) with a decay factor $\rho = 0.5507$ and a final value of $\gamma_N = 0.0247$.

Finally, the ultimately invariant set for the system state deviation under this new scenario is given by:

$$\mathcal{D}_{\delta_N} = \{x \in \mathbb{R}^n : |x| \leq \delta_N = 0.1572\}.$$

The system state deviation behaviour, x, with this new cost function parameters, is presented in Figures 7.7 and 7.8 Here one can observe that the system trajectories produce a smaller tracking error than in the previous case. This is achieved by incrementing the commutations between the available inputs. Furthermore, in Fig. 7.9 one can clearly see that the cost function decreases faster than in the previous case.

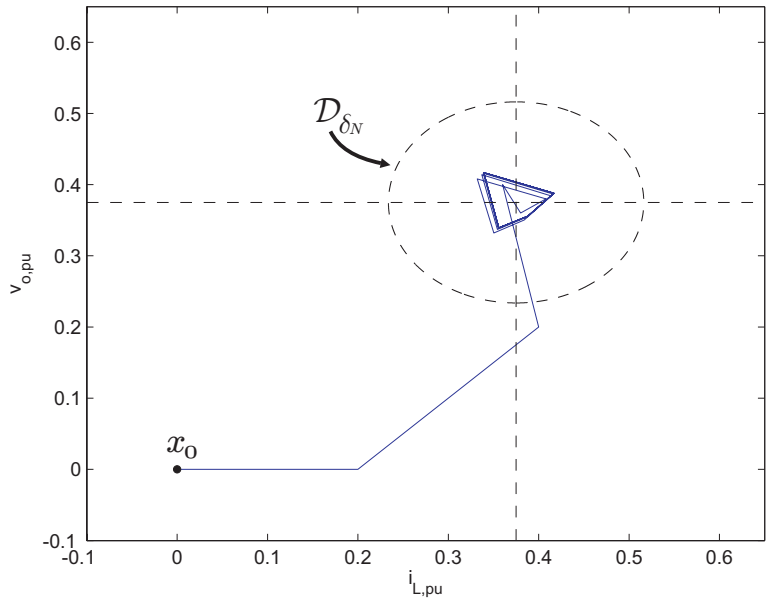

Figure 7.7: Convergence of the buck converter to the ultimate invariant set $\mathcal{D}_{\delta_N}$; $\delta_N = 0.1572$.

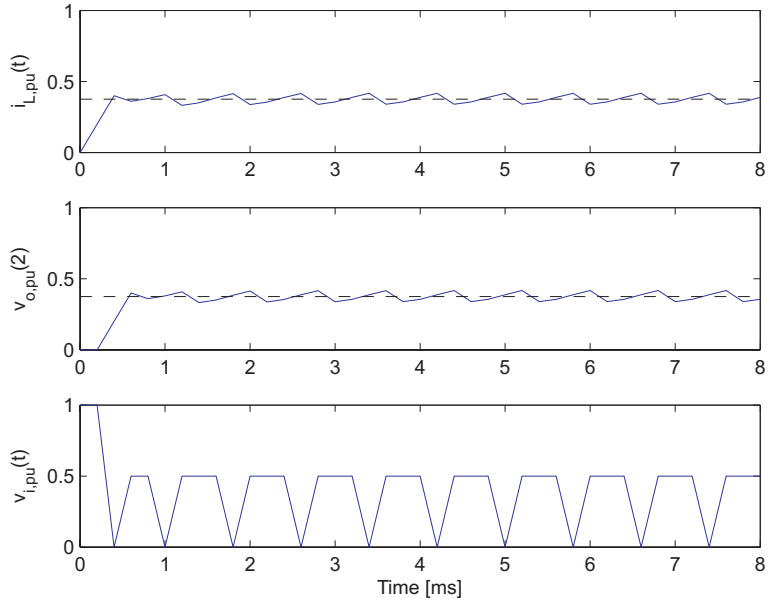

Figure 7.8: System state and input behaviour over time.

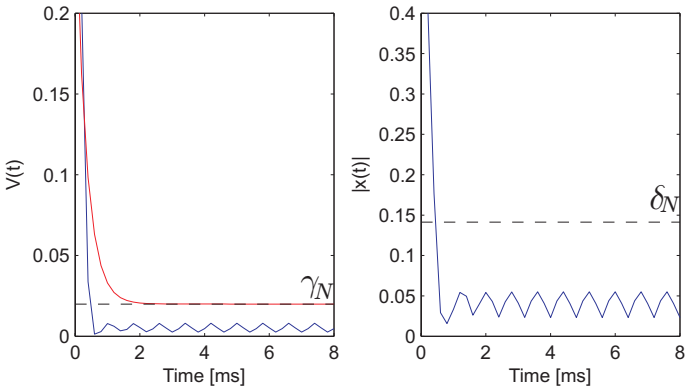

Figure 7.9: Cost function $V_N(x)$ and norm of the state deviation $|x|$ over time.

7.6.2 2-Level Inverter

Here, experimental results of the performance of FCS-MPC when applied to the 2-level inverter are presented. The inverter prototype was built based on discrete insulated-gate bipolar transistors (IGBTs) IRG4PC30KD. The electrical parameters of the converter-load system are $V_{dc} = 200\ V$, $r = 5\ \Omega$ and $L = 17\ mH$, see Fig. 7.3. The predictive strategy was implemented in a standard TMS320C6713 DSP considering a sampling period of $h = 100\ \mu s$. Then, the optimal input was applied to the converter by using an XC3S400 FPGA. The desired amplitude for the output current is $I^\star = 5\ A$ with a frequency of $f_0 = 50\ Hz$. For this converter, the associated nominal input set is chosen to be

$$\bar{\mathbb{U}} \triangleq \{\bar{u} \in \mathbb{R} : |\bar{u} + s^\star_{dq}| \leq 1/2\}.$$

A key observation is that the set $\bar{\mathbb{U}}$ can be used for the analysis of $\mathbb{U}(k)$. This follows directly from (7.12). In fact, since $\Gamma(k)\mathbb{S} \in [-1, 1]$ for all $k \geq 0$, from (7.27), we obtain that

$$|\eta(x)| \leq \Delta_q = \frac{1}{2}, \quad \forall x \in \mathbb{X}_f.$$

The cost function was set with $N = 1$, $Q = I_{2x2}$ and $R = 0_{2x2}$. Thus, following the stabilizing design presented in Theorem 7.5.1, we obtain that

$$P = \begin{bmatrix} 2.1554 & 0 \\ 0 & 2.1554 \end{bmatrix}, \quad K = \begin{bmatrix} -0.2030 & -0.0066 \\ 0.0066 & -0.2030 \end{bmatrix}.$$

Consequently, the cost function satisfies the bound (7.42) with a decay factor $\rho = 0.5360$ and a final value of $\gamma = 2.3533$. Thus, the ultimately invariant set, where the system state deviation, x, will be confined, is given by:

$$\mathcal{D}_\delta = \{x \in \mathbb{R}^n : |x| \leq \delta = 1.5340\}.$$

The behaviour of the state deviation of the 2-level inverter is shown in Fig. 7.10. Here, the controller leads the system to the desired reference, in terms of amplitud (dq frame). Consequently, a sinusoidal behaviour of the output currents, i_{abc}, is obtained, see Fig. 7.11. This is generated by the optimal input voltage, v_{abc}, applied to the load. Phase-a inverter voltage, v_a, and the line-to-line voltage, v_{ab}, are also presented in Fig. 7.11. As expected for FCS-MPC, the inverter voltage spectrum is spread as can be observed in Fig. 7.11, yielding a distortion of $\text{THD}_\text{v} = 2.2802$ %. The evolution of the cost function, $V(x)$, is shown in Fig. 7.12. This is exponentially bounded by (7.42). A similar behaviour can be observed in the norm of the system state $|x(k)|$.

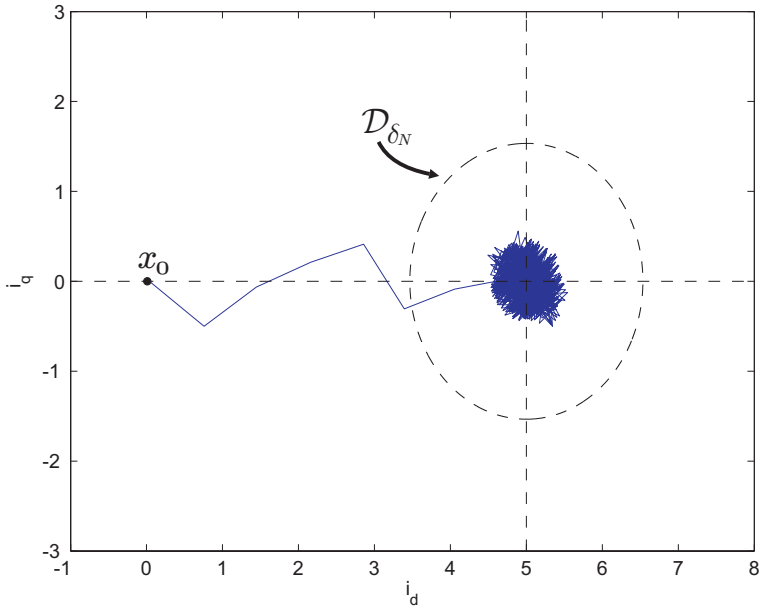

Figure 7.10: Convergence of the 2-level inverter in dq frame to the ultimate invariant set $\mathcal{D}_{\delta_N}$; $\delta_N = 1.5340$.

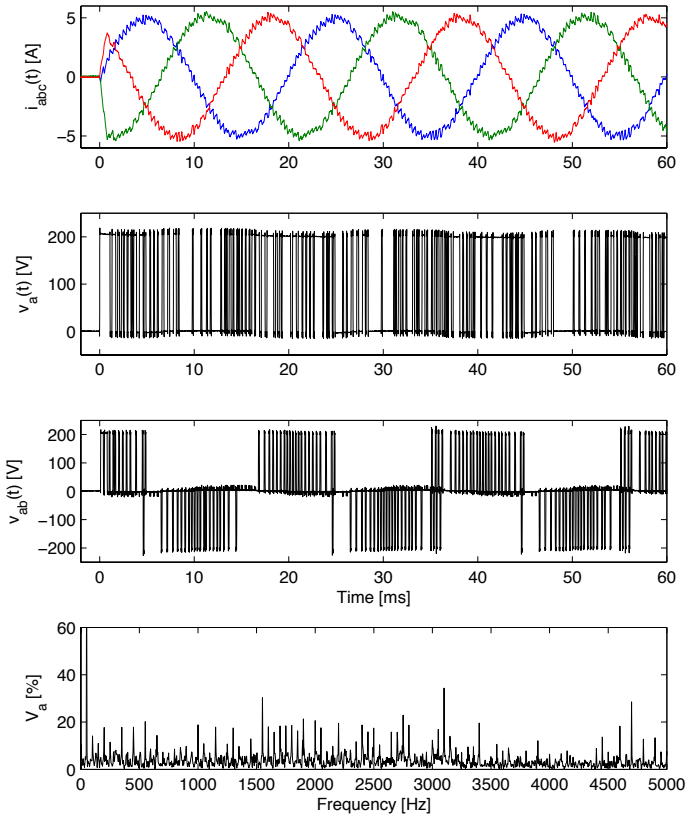

Figure 7.11: Output current and inverter voltage in abc frame.

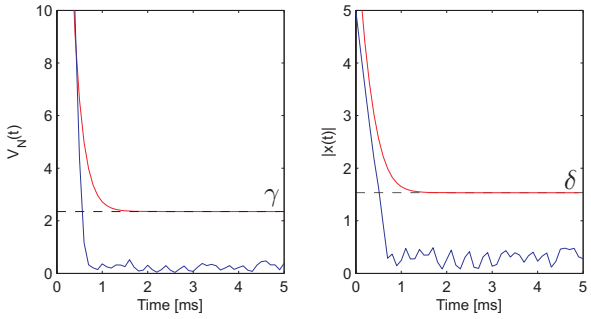

Figure 7.12: Cost function $V_N(x)$ and norm of the state deviation $|x|$ over time.

Similar to the buck converter, here we change the value of matrix R to see how this setting affects the loop. In this case, this setting is chosen to be $R = 2I_{2x2}$. Thus, we obtain that

$$P = \begin{bmatrix} 2.3332 & 0 \\ 0 & 2.3332 \end{bmatrix}, \quad K = \begin{bmatrix} -0.2030 & -0.0066 \\ 0.0066 & -0.2030 \end{bmatrix}.$$

Consequently, for this new controller setting, the cost function will be exponentially bounded with a decay rate of $\rho = 0.5242$ and a final value of $\gamma = 4.3576$. Thus, the ultimately invariant set is given by: $\mathcal{D}_\delta = \{x \in \mathbb{R}^n : |x| \leq \delta = 2.0875\}$.

The behaviour of the system state under this new scenario is depicted in Figures 7.13 and 7.14. In the latter, one can observe that the inverter voltage patten is different to the one presented in Fig 7.11. It is important to emphasize that the inverter voltage pattern is a direct consequence of the optimization. This is due to the fact that the matrix R directly affects the control input. Since in this case $R > Q$, the predictive controller gives more preference to minimize the input action, u, than the state tracking error, x. Consequently, the harmonic pollution in the inverter voltage is reduced, as depicted in Fig. 7.14, obtaining a distortion of $\text{THD}_\text{v} = 1.3367$ %. The evolution of the cost function,

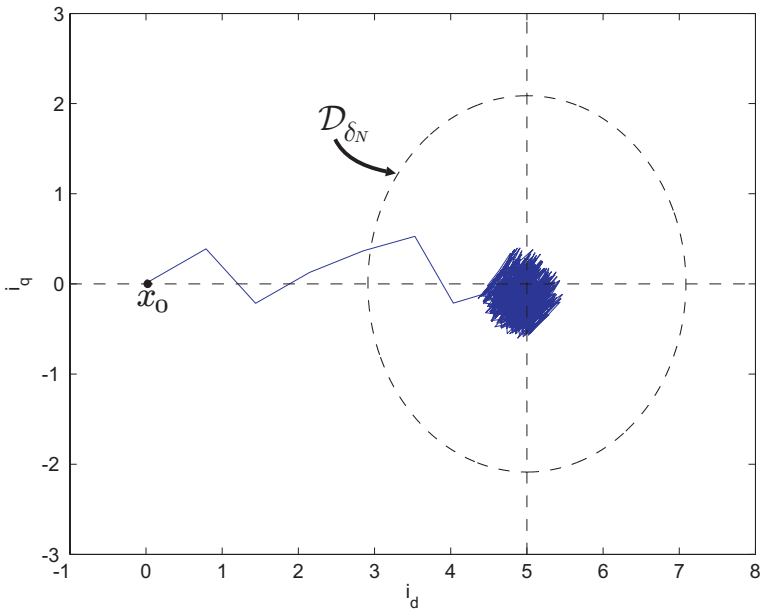

Figure 7.13: Convergence of the 2-level inverter in dq frame to the ultimate invariant set $\mathcal{D}_{\delta_N}$; $\delta_N = 2.0875$.

$V_N(x)$ as well as the norm of the system state are presented in Fig, 7.15.

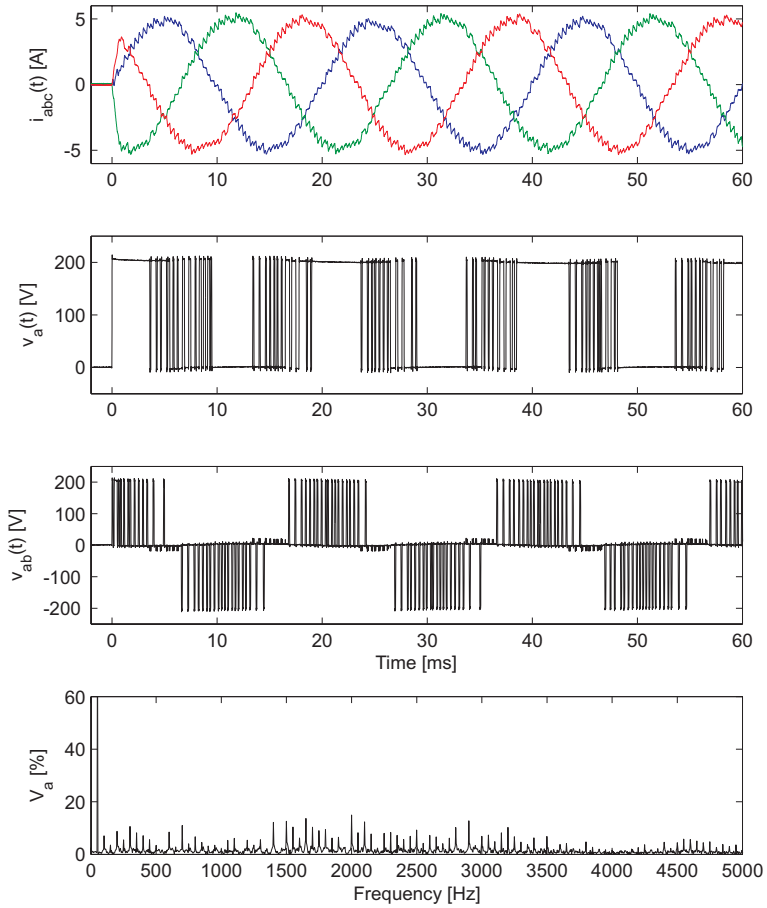

Figure 7.14: Output current and inverter voltage in abc frame.

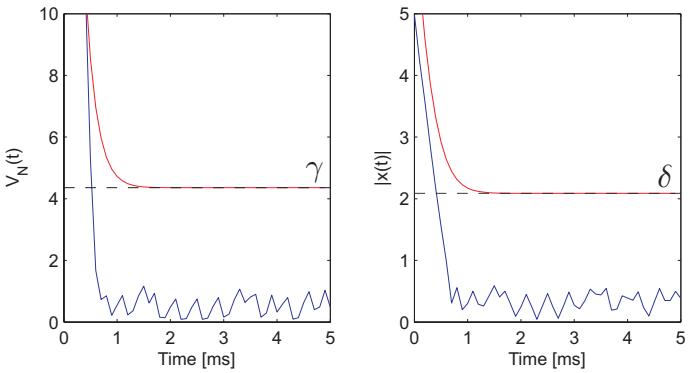

Figure 7.15: Cost function $V_N(x)$ and norm of the state deviation $|x|$ over time.

7.7 Conclusions

When controlling solid-state power converters in discrete-time, in general, voltages and currents will not converge to the desired steady-state values. This motivates the analysis of such converters from a practical stability viewpoint, i.e., by studying convergence of state variables to a bounded invariant set. The present work has applied, in a semi-tutorial fashion, Lyapunov-stability concepts to study local practical stability of FCS-MPC when applied to a class of power converters. Our results show how the cost function can be designed to guarantee practical stability. We also provide bounds on the associated invariant sets. As was established, this analysis can be used to track both constant and sinusoidal references. Future work may focus on extending the results presented in this work to more complex power converter topologies and also to develop novel high-performance controllers. Another interesting topic is to further investigate the effect of the input weighting matrix R on the switching frequency and spectrum. Additionally, based on this work, robustness of FCS-MPC when external disturbances or model uncertainties are present can be analyzed.

8

Conclusions

In this thesis we have investigated practical and theoretical issues regarding the use of FCS-MPC to handle power converters. We have shown that this predictive control paradigm can improve the performance of some classes of power converters, in terms of power quality and dynamic response, when compared to traditional modulation-based control methodologies. We have presented a stability analysis of MPC for linear time-invariant (LTI) systems with discrete input alphabets. Based on our theoretical results, we also analysed stability and performance of power converters when governed by FCS-MPC. The latter study is focused on power converters that can be modelled as LTI systems with quantised inputs. We believe that our results can be used as a framework in order to develop new predictive control formulations for power converters.

8.1 Summary of Contributions

Chapter 2 In this chapter we implemented an FCS-MPC strategy to extend the number of output voltage levels of a three-cell FCC. The predictive method developed gives excellent performance obtaining a fast dynamic in the control of the floating capacitor voltages and a reduced output current distortion. We also showed that it is possible to achieve a maximum of 8-level in the output voltage even when a high power factor load is considered. This clearly improves upon previously reported operation limits obtained with PWM-based techniques. However, the best output currents, in terms of waveform distortion, were obtained for the 6-level operation.

Chapter 3 An FCS-MPC formulation for AFE was presented in this chapter. The key novelty of the proposed approach lies in the way that dynamic references are handled. To do this, a careful examination of electrical properties of the rectifier was carried out allowing us to derive compatible references for the active power and the dc-voltage. The introduction of a reference prediction horizon, which may differ from the switching horizon, has proven useful allowing the system designer to trade-off tracking band-width for control effort. Our proposal does not require any additional control-loop. Moreover, saturation of the source current are also included in the control formulation to ensure safe operation of the converter.

Chapter 4 In this chapter, we studied the continuous-time performance of power converters when governed by FCS-MPC. We showed analytically and experimentally that existing FCS-MPC strategies give, in general, a non-zero steady-state error even when models and parameter values are exactly known. To address this issue, two different modifications to the existing FCS-MPC strategy have been proposed. The first one, IS-MPC, is based on taking measurements in the middle of the sampling period while the second one, IE-MPC, considers the predicted continuous-time behaviour in the cost function. In both cases, a higher ripple in the load current is obtained when compared to standard FCS-MPC. Therefore, there is a trade-off between the ripple in the variable to be controlled and its average steady-state error. An important characteristic of our proposals is that they do not affect the dynamic response obtained with standard FCS-MPC. The approaches only improve the steady-state performance.

Chapter 5 A predictive control strategy to achieve robustness to faults has been proposed in this chapter. This methodology is applied to a three-phase three-cell FCC. Faults are identified by using output voltages measurements. To do this, constraints on the switch sequence transitions are imposed. As remedial action, in case of faults, the proposed controller adapts the capacitor voltage references in order to maintain the original number of output voltage levels. The most important benefit of this predictive control strategy is the good performance achieved in the tracking of the capacitor voltages and the three-phase

currents even when a fault occurs. We believe that our proposal expands the possibilities of predictive control in industrial application not only to achieve good performance in the tracking errors, but also to achieve fault tolerant operation of power converters.

Chapter 6 In this chapter, sufficient conditions to ensure practical stability of LTI systems with a discrete input alphabet have been presented. We have shown that stabilization of a neighbourhood of the origin (system reference) when using the discrete alphabet MPC loop is possible if the cost function is designed as per our results. Thus, our framework can be used to establish practical stability of any LTI system in which the inputs are affected by a quantisation processes.

Chapter 7 Motivated by the results presented in Chapter 6, in this chapter we analysed power converters when governed by FCS-MPC from a practical stability viewpoint, i.e., by studying convergence of voltages and currents to a bounded invariant set. This analysis extends the study presented in Chapter 6 by achieving practical stability when tracking both constant and sinusoidal references. As an illustrative example, we have applied our results to the control of two kinds of converter, namely, a dc-dc buck converter and a two-level inverter.

8.2 Future Work

The results of this thesis have the potential to be extended in several directions:

Extending Prediction Horizon It is well known that choosing lager prediction horizons, in general, gives better closed-loop performance than shorter ones. Unfortunately, for FCS-MPC to obtain the optimal input sequence requires one to solve a combinatorial optimisation problem. This limits the use of larger horizons in practical applications. To address this problem, it would be useful to obtain a suboptimal solution based on the stability results presented in this thesis, which can be used to reduced the search space to obtain the optimal one. Thus, one can develop more efficient algorithms which allow us to use larger horizons in the optimal problem.

Weighting Matrices Design Another key element in the performance of the resulting closed-loop is the selection of the weighting factors. We showed that adding a weighting matrix for the input allows us to improve the output current spectrum. Nevertheless, these key elements in MPC are normally chosen by trial and error. It would be interesting to obtain an accurate analytical framework which allows one to design these parameters in order to achieve desired performance objectives.

Robustness Analysis An important aspect that can be investigated in the future is the analysis of the performance of FCS-MPC when external disturbances and/or model uncertainties are present. In this thesis, specifically in Chapters 2 and 3, we have shown that FCS-MPC can tolerate some level of uncertainties. However, it has not been rigorously studied how these uncertainties can affect the predictive closed-loop stability and performance. This may be done by including the uncertainties in the stability analysis presented in Chapters 6 and 7.

Stability Analysis for Complex Converters The stability analysis presented in this work is limited to power converters which can be modeled as LTI systems with quantised inputs. Therefore, this study does not cover all existing topologies. This opens the door to extend this study to more complex power converters by considering stability techniques for non-linear systems governed by MPC.

A

Appendix

Statements of Contribution of Others

In this appendix, the statements from each co-author attesting to the contribution of the author's thesis to a joint publication included as part of this thesis are included.

Statement of Authorship

I, Dr. Daniel E. Quevedo, attest that Research Higher Degree candidate Ricardo Patricio Aguilera contributed in the conception, development and analysis of the research results, as well as the writing of the manuscripts of all the following publications:

R. P. Aguilera, D. E. Quevedo, T. J. Summers, and P. Lezana, "Predictive control algorithm robustness for achieving fault tolerance in multicell converters," *in the 34th Annual Conference of IEEE Industrial Electronics Society (IECON),* Orlando, Florida, Nov. 2008.

P. Lezana, R. P. Aguilera, and D. E. Quevedo, "Model Predictive Control of an Asymmetric Flying Capacitor Converter," *IEEE Transactions on Industrial Electronics,* vol. 56, no. 6, pp. 1839–1846, 2009.

D. E. Quevedo, R. P. Aguilera, M. Pérez, P. Cortés, and R. Lizana, "Model Predictive Control of an AFE Rectifier with Dynamic References," *IEEE Transactions on Power Electronics,* to appear 2012.

R. P. Aguilera and D. E. Quevedo, "Stability Analysis of Quadratic MPC with a Discrete Input Alphabet," submitted for journal publication.

R. P. Aguilera and D. E. Quevedo, "Finite Control Set MPC for Power Converters: Stability and Performance," submitted for journal publication.

R. P. Aguilera, P. Lezana, and D. E. Quevedo, "Finite-Control-Set Model Predictive Control with Improved Steady-State Performance," submitted for journal publication.

Dr. Daniel E. Quevedo
School of Electrical Engineering & Computer Science
The University of Newcastle, Australia
Date: 28/3/2012

Ricardo P. Aguilera, PhD Candidate
School of Electrical Engineering & Computer Science
The University of Newcastle, Australia
Date: 28/03/2012

A/Prof. Richard Merifield
Assistant Dean Research Training (ADRT)
Faculty of Engineering and Built Environment
The University of Newcastle, Australia
Date: 28/3/2012

Statement of Authorship

I, Dr. Terrence Summers, attest that Research Higher Degree candidate Ricardo Patricio Aguilera contributed in the conception, development and analysis of the research results, as well as the writing of the manuscripts of the following publication:

R. P. Aguilera, D. E. Quevedo, T. J. Summers, and P. Lezana, "Predictive control algorithm robustness for achieving fault tolerance in multicell converters," *in the 34th Annual Conference of IEEE Industrial Electronics Society (IECON),* Orlando, Florida, Nov. 2008.

Dr. Terrence Summers
School of Electrical Engineering & Computer Science
The University of Newcastle, Australia
Date:

Ricardo P. Aguilera, PhD Candidate
School of Electrical Engineering & Computer Science
The University of Newcastle, Australia
Date: 27/03/2012

A/Prof. Richard Merifield
Assistant Dean Research Training (ADRT)
Faculty of Engineering and Built Environment
The University of Newcastle, Australia
Date: 28/3/2012

Statement of Authorship

I, Dr. Pablo Lezana, attest that Research Higher Degree candidate Ricardo Patricio Aguilera contributed in the conception, development and analysis of the research results, as well as the writing of the manuscripts of all the following publications:

R. P. Aguilera, D. E. Quevedo, T. J. Summers, and P. Lezana, "Predictive control algorithm robustness for achieving fault tolerance in multicell converters," *in the 34th Annual Conference of IEEE Industrial Electronics Society (IECON),* Orlando, Florida, Nov. 2008.

P. Lezana, R. P. Aguilera, and D. E. Quevedo, "Model Predictive Control of an Asymmetric Flying Capacitor Converter," *IEEE Transactions on Industrial Electronics,* vol. 56, no. 6, pp. 1839–1846, 2009.

R. P. Aguilera, P. Lezana, and D. E. Quevedo, "Finite-Control-Set Model Predictive Control with Improved Steady-State Performance," submitted for journal publication.

Dr. Pablo Lezana
Departamento de Ingeniería Eléctrica
Universidad Técnica Federico Santa María, Chile
Date: 26/03/2012

Ricardo P. Aguilera, PhD Candidate
School of Electrical Engineering & Computer Science
The University of Newcastle, Australia
Date: 26/03/2012

A/Prof. Richard Merifield
Assistant Dean Research Training (ADRT)
Faculty of Engineering and Built Environment
The University of Newcastle, Australia
Date: 28/3/2012

Statement of Authorship

I, Dr. Marcelo Pérez, attest that Research Higher Degree candidate Ricardo Patricio Aguilera contributed in the conception, development and analysis of the research results, as well as the writing of the manuscripts of the following publication:

D. E. Quevedo, R. P. Aguilera, M. Pérez, P. Cortés, and R. Lizana, "Model Predictive Control of an AFE Rectifier with Dynamic References," *IEEE Transactions on Power Electronics,* to appear 2012.

Dr. Marcelo Pérez
Departamento de Electrónica
Universidad Técnica Federico Santa María, Chile
Date:

Ricardo P. Aguilera, PhD Candidate
School of Electrical Engineering & Computer Science
The University of Newcastle, Australia
Date: 26/03/2012

A/Prof. Richard Merifield
Assistant Dean Research Training (ADRT)
Faculty of Engineering and Built Environment
The University of Newcastle, Australia
Date: 28/3/2012

Statement of Authorship

I, Dr. Patricio Cortés, attest that Research Higher Degree candidate Ricardo Patricio Aguilera contributed in the conception, development and analysis of the research results, as well as the writing of the manuscripts of the following publication:

D. E. Quevedo, R. P. Aguilera, M. Pérez, P. Cortés, and R. Lizana, "Model Predictive Control of an AFE Rectifier with Dynamic References," *IEEE Transactions on Power Electronics,* to appear 2012.

Dr. Patricio Cortés
Departamento de Electrónica
Universidad Técnica Federico Santa María, Chile
Date: 26/03/2012

Ricardo P. Aguilera, PhD Candidate
School of Electrical Engineering & Computer Science
The University of Newcastle, Australia
Date: 26/03/2012

A/Prof. Richard Merifield
Assistant Dean Research Training (ADRT)
Faculty of Engineering and Built Environment
The University of Newcastle, Australia
Date: 28/3/2012

Statement of Authorship

I, Mr. Ricardo Lizana, attest that Research Higher Degree candidate Ricardo Patricio Aguilera contributed in the conception, development and analysis of the research results, as well as the writing of the manuscripts of the following publication:

D. E. Quevedo, R. P. Aguilera, M. Pérez, P. Cortés, and R. Lizana, "Model Predictive Control of an AFE Rectifier with Dynamic References," *IEEE Transactions on Power Electronics,* to appear on 2012.

Mr. Ricardo Lizana
Departamento de Electrónica
Universidad Técnica Federico Santa María, Chile
Date: 03/21/2012

Ricardo P. Aguilera, PhD Candidate
School of Electrical Engineering & Computer Science
The University of Newcastle, Australia
Date: 26/03/2012

A/Prof. Richard Merifield
Assistant Dean Research Training (ADRT)
Faculty of Engineering and Built Environment
The University of Newcastle, Australia
Date: 28/3/2012

Bibliography

[1] D. Jones, "Electrical engineering: the backbone of society," in *Science, Measurement and Technology, IEE Proceedings A*, 1991, pp. 1–10.

[2] M. H. Rashid, *Power Electronics Handbook*. Academic Press, Sep. 2001.

[3] B. K. Bose, *Modern Power Electronics and AC Drives*. Prentice Hall PTR, 2002.

[4] J. Sun, X. Ding, M. Nakaoka, and H. Takano, "Series resonant ZCS-PFM DC-DC converter with multistage rectified voltage multiplier and dual-mode PFM control scheme for medical-use high-voltage X-ray power generator," in *Electric Power Applications, IEE Proceedings*, 2000, pp. 527–534.

[5] J. Carrasco, L. Franquelo, J. Bialasiewicz, E. Galvan, R. Guisado, M. Prats, J. Leon, and N. Moreno-Alfonso, "Power-Electronic Systems for the Grid Integration of Renewable Energy Sources: A Survey," *Industrial Electronics, IEEE Transactions on*, vol. 53, no. 4, pp. 1002–1016, 2006.

[6] B. Kroposki, C. Pink, R. DeBlasio, H. Thomas, M. Simões, and P. Sen, "Benefits of Power Electronic Interfaces for Distributed Energy Systems," *Energy Conversion, IEEE Transactions on*, vol. 25, no. 3, pp. 901–908, 2010.

[7] A. Luo, C. Wu, J. Shen, Z. Shuai, and F. Ma, "Railway Static Power Conditioners for High-speed Train Traction Power Supply Systems Using Three-phase V/V Transformers," *Power Electronics, IEEE Transactions on*, vol. 26, no. 10, pp. 2844–2856, 2011.

[8] H. Huang, J. Bao, and L. Zhang, "A MASH-Controlled Multilevel Power Converter for High-Efficiency RF Transmitters," *Power Electronics, IEEE Transactions on*, vol. 26, no. 4, pp. 1205–1214, 2011.

[9] B. Parkhideh, S. Bhattacharya, J. Mazumdar, and W. Koellner, "Utilization of Supplementary Energy Storage Systems in High Power Mining Converters," *Industry Applications Society Annual Meeting, 2008. IAS '08. IEEE*, pp. 1–7, 2008.

[10] P. Cortés, M. P. Kazmierkowski, R. M. Kennel, D. E. Quevedo, and J. Rodríguez, "Predictive Control in Power Electronics and Drives," *Industrial Electronics, IEEE Transactions on*, vol. 55, no. 12, pp. 4312–4324, Dec. 2008.

[11] J. Rodríguez and P. Cortés, *Predictive Control of Power Converters and Electrical Drives*, 1st ed. Wiley-IEEE Press, May 2012.

[12] J. Rawlings and D. Mayne, *Model Predictive Control: Theory and Design.* Nob Hill Publishing, 2009.

[13] G. C. Goodwin, M. Serón, and J. De Doná, *Constrained control and estimation: an optimization approach.* Springer Verlag, 2005.

[14] S. Kouro, P. Cortés, R. Vargas, U. Ammann, and J. Rodríguez, "Model Predictive Control—A Simple and Powerful Method to Control Power Converters," *Industrial Electronics, IEEE Transactions on*, vol. 56, no. 6, pp. 1826–1838, Jun. 2009.

[15] J. Holtz, "Power Electronics-A Continuing Challenge," *Industrial Electronics Magazine, IEEE*, vol. 5, no. 2, pp. 6–15, 2011.

[16] B. Bose, "Power Electronics and Motor Drives Recent Progress and Perspective," *Industrial Electronics, IEEE Transactions on*, vol. 56, no. 2, pp. 581–588, 2009.

[17] S. Kouro, M. Malinowski, K. Gopakumar, J. Pou, L. Franquelo, B. Wu, J. Rodríguez, M. A. Pérez, and J. Leon, "Recent Advances and Industrial Applications of Multilevel Converters," *Industrial Electronics, IEEE Transactions on*, vol. 57, no. 8, pp. 2553–2580, 2010.

[18] M. P. Kaźmierkowski and R. Krishnan, *Control in Power Electronics: Selected Problems* . Academic Press, Aug. 2002.

[19] D. G. Holmes, T. A. Lipo, and T. A. Lipo, *Pulse Width Modulation for Power Converters: Principles and Practice* . Wiley-IEEE Press, 2003.

[20] V. Raviraj and P. Sen, "Comparative study of proportional-integral, sliding mode, and fuzzy logic controllers for power converters," *Industry Applications, IEEE Transactions on*, vol. 33, no. 2, pp. 518–524, 1997.

[21] B. Bose, "Fuzzy logic and neural networks in power electronics and drives," *Industry Applications Magazine, IEEE*, vol. 6, no. 3, pp. 57–63, 2000.

[22] S.-C. Tan, Y. Lai, and C. Tse, "A unified approach to the design of PWM-based sliding-mode voltage controllers for basic DC-DC converters in continuous conduction mode," *Circuits and Systems I: Regular Papers, IEEE Transactions on*, vol. 53, no. 8, pp. 1816–1827, 2006.

[23] B. K. Bose, "Neural Network Applications in Power Electronics and Motor Drives—An Introduction and Perspective," *Industrial Electronics, IEEE Transactions on*, vol. 54, no. 1, pp. 14–33, 2007.

[24] S. Bolognani, S. Bolognani, L. Peretti, and M. Zigliotto, "Design and Implementation of Model Predictive Control for Electrical Motor Drives," *Industrial Electronics, IEEE Transactions on*, vol. 56, no. 6, pp. 1925–1936, 2009.

[25] A. Linder, R. Kanchan, R. Kennel, and P. Stolze, "Model-Based Predictive Control of Electrical Drives," Cuvillier Verlag Göttingen, 2010.

[26] T. Geyer, "A Comparison of Control and Modulation Schemes for Medium-Voltage Drives: Emerging Predictive Control Concepts Versus PWM-Based Schemes," *Industry Applications, IEEE Transactions on*, vol. 47, no. 3, pp. 1380–1389, 2011.

[27] R. Kennel, A. Linder, and M. Linke, "Generalized predictive control (GPC)-ready for use in drive applications?" in *Power Electronics Specialists Conference, 2001. PESC. 2001 IEEE 32nd Annual*, 2001, pp. 1839–1844.

[28] T. Geyer, G. Papafotiou, R. Frasca, and M. Morari, "Constrained Optimal Control of the Step-Down DC–DC Converter," *Power Electronics, IEEE Transactions on*, vol. 23, no. 5, pp. 2454–2464, Sep. 2008.

[29] T. Geyer, G. Papafotiou, and M. Morari, "Hybrid Model Predictive Control of the Step-Down DC–DC Converter," *Control Systems Technology, IEEE Transactions on*, vol. 16, no. 6, pp. 1112–1124, 2008.

[30] D. P. Bertsekas, *Dynamic programming and optimal control*, 2nd ed. Athena Scientific, 2000.

[31] R. H. Wilkinson, T. A. Meynard, and H. du Toit Mouton, "Natural Balance of Multicell Converters: The General Case," *Power Electronics, IEEE Transactions on*, vol. 21, no. 6, pp. 1658–1666, 2006.

[32] B. McGrath and D. Holmes, "Analytical Modelling of Voltage Balance Dynamics for a Flying Capacitor Multilevel Converter," *Power Electronics, IEEE Transactions on*, vol. 23, no. 2, pp. 543–550, 2008.

[33] A. Bouafia, J.-P. Gaubert, and F. Krim, "Predictive Direct Power Control of Three-Phase Pulsewidth Modulation (PWM) Rectifier Using Space-Vector Modulation (SVM)," *Power Electronics, IEEE Transactions on*, vol. 25, no. 1, pp. 228–236, 2010.

[34] P. Cortés, J. Rodríguez, P. Antoniewicz, and M. Kazmierkowski, "Direct Power Control of an AFE Using Predictive Control," *Power Electronics, IEEE Transactions on*, vol. 23, no. 5, pp. 2516–2523, 2008.

[35] C. Turpin, P. Baudesson, F. Richardeau, F. Forest, and T. A. Meynard, "Fault management of multicell converters," *Industrial Electronics, IEEE Transactions on*, vol. 49, no. 5, pp. 988–997, 2002.

[36] B. Picasso, S. Pancanti, A. Bemporad, and A. Bicchi, "Receding–horizon control of LTI systems with quantized inputs," in *Analysis and design of hybrid systems 2003: a proceedings volume from the IFAC conference.* Elsevier, 2003, pp. 259–264.

[37] D. E. Quevedo, G. C. Goodwin, and J. A. De Doná, "Finite constraint set receding horizon quadratic control," *International Journal of Robust and Nonlinear Control*, vol. 14, no. 4, pp. 355–377, Jan. 2004.

[38] J. Rodríguez, J.-S. Lai, and F. Z. Peng, "Multilevel inverters: a survey of topologies, controls, and applications," *Industrial Electronics, IEEE Transactions on*, vol. 49, no. 4, pp. 724–738, 2002.

[39] A. Nabae, I. Takahashi, and H. Akagi, "A New Neutral-Point-Clamped PWM Inverter," *Industry Applications, IEEE Transactions on*, no. 5, pp. 518–523, 1981.

[40] T. A. Meynard and H. Foch, "Multi-level choppers for high voltage applications," *Journal of European Power Electronics and Drives*, vol. 2, no. 1, pp. 45–50, 1992.

[41] P. Hammond, "A new approach to enhance power quality for medium voltage AC drives," *Industry Applications, IEEE Transactions on*, vol. 33, no. 1, pp. 202–208, 1997.

[42] L. Tolbert, F. Z. Peng, and T. Habetler, "Multilevel converters for large electric drives," *Industry Applications, IEEE Transactions on*, vol. 35, no. 1, pp. 36–44, 1999.

[43] J. Rodríguez, J. Pontt, G. Alzarnora, N. Becker, O. Einenkel, and A. Weinstein, "Novel 20-MW downhill conveyor system using three-level converters," *Industrial Electronics, IEEE Transactions on*, vol. 49, no. 5, pp. 1093–1100, 2002.

[44] J. Pontt, J. Rodríguez, R. Huerta, P. Newman, W. Michel, and C. Argandona, "High-power regenerative converter for ore transportation under failure conditions," *Industry Applications, IEEE Transactions on*, vol. 41, no. 6, pp. 1411–1419, 2005.

[45] S. Alepuz, S. Busquets-Monge, J. Bordonau, J. Gago, D. Gonzalez, and J. Balcells, "Interfacing Renewable Energy Sources to the Utility Grid Using a Three-Level Inverter," *Industrial Electronics, IEEE Transactions on*, vol. 53, no. 5, pp. 1504–1511, 2006.

[46] Q. Song, W. Liu, and Z. Yuan, "Multilevel Optimal Modulation and Dynamic Control Strategies for STATCOMs Using Cascaded Multilevel Inverters," *Power Delivery, IEEE Transactions on*, vol. 22, no. 3, pp. 1937–1946, 2007.

[47] C. Rech and J. Pinheiro, "Hybrid Multilevel Converters: Unified Analysis and Design Considerations," *Industrial Electronics, IEEE Transactions on*, vol. 54, no. 2, pp. 1092–1104, 2007.

[48] J. Huang and K. Corzine, "Extended operation of flying capacitor multilevel inverters," *Power Electronics, IEEE Transactions on*, vol. 21, no. 1, pp. 140–147, 2006.

[49] A. M. Lienhardt, G. Gateau, and T. A. Meynard, "Digital Sliding-Mode Observer Implementation Using FPGA," *Industrial Electronics, IEEE Transactions on*, vol. 54, no. 4, pp. 1865–1875, 2007.

[50] E. Silva, B. McGrath, D. E. Quevedo, and G. C. Goodwin, "Predictive Control of a Flying Capacitor Converter," in *American Control Conference, 2007. ACC '07*, 2007, pp. 3763–3768.

[51] L. Malesani, P. Mattavelli, and S. Buso, "Robust dead-beat current control for PWM rectifiers and active filters," *Industry Applications, IEEE Transactions on*, vol. 35, no. 3, pp. 613–620, 1999.

[52] M. Nemec, D. Nedeljkovic, and V. Ambrozic, "Predictive Torque Control of Induction Machines Using Immediate Flux Control," *Industrial Electronics, IEEE Transactions on*, vol. 54, no. 4, pp. 2009–2017, 2007.

[53] P. Zanchetta, D. Gerry, V. Monopoli, J. Clare, and P. Wheeler, "Predictive Current Control for Multilevel Active Rectifiers With Reduced Switching Frequency," *Industrial Electronics, IEEE Transactions on*, vol. 55, no. 1, pp. 163–172, 2008.

[54] M. A. Pérez, P. Cortés, and J. Rodríguez, "Predictive Control Algorithm Technique for Multilevel Asymmetric Cascaded H-Bridge Inverters," *Industrial Electronics, IEEE Transactions on*, vol. 55, no. 12, pp. 4354–4361, 2008.

[55] S. Muller, U. Ammann, and S. Rees, "New time-discrete modulation scheme for matrix converters," *Industrial Electronics, IEEE Transactions on*, vol. 52, no. 6, pp. 1607–1615, 2005.

[56] J. Rodríguez, J. Pontt, C. Silva, P. Correa, P. Lezana, P. Cortés, and U. Ammann, "Predictive Current Control of a Voltage Source Inverter," *Industrial Electronics, IEEE Transactions on*, vol. 54, no. 1, pp. 495–503, 2007.

[57] P. Cortés, J. Rodríguez, D. E. Quevedo, and C. Silva, "Predictive Current Control Strategy With Imposed Load Current Spectrum," *Power Electronics, IEEE Transactions on*, vol. 23, no. 2, pp. 612–618, 2008.

[58] R. Vargas, P. Cortés, U. Ammann, J. Rodríguez, and J. Pontt, "Predictive Control of a Three-Phase Neutral-Point-Clamped Inverter," *Industrial Electronics, IEEE Transactions on*, vol. 54, no. 5, pp. 2697–2705, 2007.

[59] X. Kou, K. Corzine, and Y. Familiant, "Full binary combination schema for floating voltage source multilevel inverters," *Power Electronics, IEEE Transactions on*, vol. 17, no. 6, pp. 891–897, 2002.

[60] J. Dai, D. Xu, B. Wu, and N. Zargari, "Unified DC-Link Current Control for Low-Voltage Ride-Through in Current-Source-Converter-Based Wind Energy Conversion Systems," *Power Electronics, IEEE Transactions on*, vol. 26, no. 1, pp. 288–297, 2011.

[61] J. Dai, D. Xu, and B. Wu, "A Novel Control Scheme for Current-Source-Converter-Based PMSG Wind Energy Conversion Systems," *Power Electronics, IEEE Transactions on*, vol. 24, no. 4, pp. 963–972, 2009.

[62] Y. W. Li, M. Pande, N. Zargari, and B. Wu, "An Input Power Factor Control Strategy for High-Power Current-Source Induction Motor Drive With Active Front-End," *Power Electronics, IEEE Transactions on*, vol. 25, no. 2, pp. 352–359, 2010.

[63] J. Rodriguez, J. Dixon, J. Espinoza, J. Pontt, and P. Lezana, "PWM regenerative rectifiers: state of the art," *Industrial Electronics, IEEE Transactions on*, vol. 52, no. 1, pp. 5–22, 2005.

[64] S. Kwak and H. Toliyat, "Design and rating comparisons of PWM voltage source rectifiers and active power filters for AC drives with unity power factor," *Power Electronics, IEEE Transactions on*, vol. 20, no. 5, pp. 1133–1142, 2005.

[65] M. Malinowski, M. P. Kazmierkowski, and A. Trzynadlowski, "A comparative study of control techniques for PWM rectifiers in AC adjustable speed drives," *Power Electronics, IEEE Transactions on*, vol. 18, no. 6, pp. 1390–1396, 2003.

[66] M. P. Kazmierkowski, M. Jasinski, and G. Wrona, "DSP-Based Control of Grid-Connected Power Converters Operating Under Grid Distortions," *Industrial Informatics, IEEE Transactions on*, vol. 7, no. 2, pp. 204–211, 2011.

[67] J. Hu, L. Shang, Y. He, and Z. Zhu, "Direct Active and Reactive Power Regulation of Grid-Connected DC/AC Converters Using Sliding Mode Control Approach," *Power Electronics, IEEE Transactions on*, vol. 26, no. 1, pp. 210–222, 2011.

[68] C. Hou and P. Cheng, "Experimental verification of the active front-end converters dynamic model and control designs," *Power Electronics, IEEE Transactions on*, no. 99, p. 1, 2010.

[69] Y. Xie, R. Ghaemi, J. Sun, and J. Freudenberg, "Implicit Model Predictive Control of a Full Bridge DC–DC Converter," *Power Electronics, IEEE Transactions on*, vol. 24, no. 12, pp. 2704–2713, 2009.

[70] R. Vargas, U. Ammann, B. Hudoffsky, J. Rodríguez, and P. Wheeler, "Predictive Torque Control of an Induction Machine Fed by a Matrix Converter With Reactive Input Power Control," *Power Electronics, IEEE Transactions on*, vol. 25, no. 6, pp. 1426–1438, 2010.

[71] T. Geyer, "Computationally Efficient Model Predictive Direct Torque Control," *Power Electronics, IEEE Transactions on*, vol. 26, no. 10, pp. 2804–2816, 2011.

[72] P. Lezana, R. Aguilera, and D. E. Quevedo, "Model Predictive Control of an Asymmetric Flying Capacitor Converter," in *Industrial Electronics, IEEE Transactions on*, 2009, pp. 1839–1846.

[73] T. Geyer, G. Papafotiou, and M. Morari, "Model Predictive Direct Torque Control—Part I: Concept, Algorithm, and Analysis," *Industrial Electronics, IEEE Transactions on*, vol. 56, no. 6, pp. 1894–1905, 2009.

[74] K. J. Åström and T. Hägglund, *PID controllers: Theory, Design and Tuning*, 2nd ed. Instrument Society of America, 1995.

[75] R. Burgos, E. Wiechmann, and J. Holtz, "Complex state-space modeling and nonlinear control of active front-end converters," *Industrial Electronics, IEEE Transactions on*, vol. 52, no. 2, pp. 363–377, 2005.

[76] E. F. Camacho and C. Bordons, *Model predictive control*, 2nd ed. New York: Springer Verlag, Jul. 2004.

[77] J. M. Maciejowski, *Predictive Control with Constraints*, ser. with constraints. London: Prentice Hall, 2002.

[78] D. E. Quevedo, C. Müller, and G. C. Goodwin, "Conditions for optimality of Naive quantized finite horizon control," *International Journal of Control*, vol. 80, no. 5, pp. 706–720, May 2007.

[79] C. Müller, D. E. Quevedo, and G. C. Goodwin, "How Good is Quantized Model Predictive Control With Horizon One?" *Automatic Control, IEEE Transactions on*, vol. 56, no. 11, pp. 2623–2638, 2011.

[80] M. Nagahara and D. E. Quevedo, "Sparse representations for packetized predictive networked control," in *Proceedings of the 18th IFAC World Congress*, Milano, Italy, Aug. 2011.

[81] R. P. Aguilera and D. E. Quevedo, "On stability and performance of finite control set MPC for power converters," in *Predictive Control of Electrical Drives and Power Electronics (PRECEDE), 2011 Workshop on*, Oct. 2011, pp. 55–62.

[82] A. Bemporad, "Reference governor for constrained nonlinear systems," *Automatic Control, IEEE Transactions on*, vol. 43, no. 3, pp. 415–419, 1998.

[83] J. De Doná A, G. C. Goodwin, and M. M. Serón, "Anti-windup and model predictive control: Reflections and connections," *European Journal of Control*, vol. 6, no. 5, pp. 467–477, 2000.

[84] P. Lezana, R. Aguilera, and D. Quevedo, "Steady-state issues with finite control set model predictive control," in *Industrial Electronics, 2009. IECON '09. 35th Annual Conference of IEEE*, 2009, pp. 1776–1781.

[85] R. P. Aguilera and D. E. Quevedo, "On the stability of MPC with a Finite Input Alphabet," in *Proceedings of the 18th IFAC World Congress*, Milano, Italy, Aug. 2011, pp. 7975–7980.

[86] ——, "Capacitor voltage estimation for predictive control algorithm of flying capacitor converters," in *Industrial Technology, 2009. ICIT 2009. IEEE International Conference on*, Melbourne, Australia, Feb. 2009.

[87] J.-S. Hu and K.-Y. Chen, "Analysis and design of the receding horizon constrained optimization for class-D amplifier driving signals," *Digital Signal Processing*, vol. 20, no. 6, pp. 1511–1525, Dec. 2010.

[88] S.-H. Yu and M.-H. Tseng, "Optimal Control of a Nine-Level Class-D Audio Amplifier Using Sliding-Mode Quantization," *Industrial Electronics, IEEE Transactions on*, vol. 58, no. 7, pp. 3069–3076, 2011.

[89] M. Malinowski, K. Gopakumar, J. Rodríguez, and M. Pérez, "A Survey on Cascaded Multilevel Inverters," *Industrial Electronics, IEEE Transactions on*, vol. 57, no. 7, pp. 2197–2206, 2010.

[90] F. Richardeau, P. Baudesson, and T. A. Meynard, "Failures-tolerance and remedial strategies of a PWM multicell inverter," *Power Electronics, IEEE Transactions on*, vol. 17, no. 6, pp. 905–912, 2002.

[91] T. A. Meynard, H. Foch, P. Thomas, J. Courault, R. Jakob, and M. Nahrstaedt, "Multicell converters: basic concepts and industry applications," *Industrial Electronics, IEEE Transactions on*, vol. 49, no. 5, pp. 955–964, 2002.

[92] R. Chokhawala, J. Catt, and L. Kiraly, "A discussion on IGBT short-circuit behavior and fault protection schemes," *Industry Applications, IEEE Transactions on*, vol. 31, no. 2, pp. 256–263, 1995.

[93] S. Lefebvre, Z. Khatir, and F. Saint-Eve, "Experimental behavior of single-chip IGBT and COOLMOS devices under repetitive short-circuit conditions," *Electron Devices, IEEE Transactions on*, vol. 52, no. 2, pp. 276–283, 2005.

[94] T. A. Meynard, M. Fadel, and N. Aouda, "Modeling of multilevel converters," *Industrial Electronics, IEEE Transactions on*, vol. 44, no. 3, pp. 356–364, 1997.

[95] D. C. Tarraf, A. Megretski, and M. A. Dahleh, "A Framework for Robust Stability of Systems Over Finite Alphabets," *Automatic Control, IEEE Transactions on*, vol. 53, no. 5, pp. 1133–1146, Jun. 2008.

[96] G. Goodwin and D. Quevedo, "Finite alphabet control and estimation," *International Journal of Control, Automation, and Systems*, vol. 1, no. 4, pp. 412–430, Dec. 2003.

[97] D. E. Quevedo, H. Bölcskei, and G. C. Goodwin, "Quantization of Filter Bank Frame Expansions Through Moving Horizon Optimization," *Signal Processing, IEEE Transactions on*, vol. 57, no. 2, pp. 503–515, 2009.

[98] D. E. Quevedo, J. Østergaard, and D. Nešić, "Packetized Predictive Control of Stochastic Systems Over Bit-Rate Limited Channels With Packet Loss," *Automatic Control, IEEE Transactions on*, vol. 56, no. 12, pp. 2854–2868, 2011.

[99] J. Østergaard, D. E. Quevedo, and J. Jensen, "Real-Time Perceptual Moving-Horizon Multiple-Description Audio Coding," *Signal Processing, IEEE Transactions on*, vol. 59, no. 9, pp. 4286–4299, 2011.

[100] A. Gersho and R. M. Gray, *Vector quantization and signal compression*, ser. Kluwer international series in engineering and computer science. Kluwer Academic Publishers, 1992.

[101] D. Liberzon, "Hybrid feedback stabilization of systems with quantized signals," *Automatica*, vol. 39, no. 9, pp. 1543–1554, Sep. 2003.

[102] T. Kameneva and D. Nešić, "On l2 Stabilization of Linear Systems With Quantized Control," *Automatic Control, IEEE Transactions on*, vol. 53, no. 1, pp. 399–405, Feb. 2008.

[103] N. Elia and S. K. Mitter, "Stabilization of linear systems with limited information," *Automatic Control, IEEE Transactions on*, vol. 46, no. 9, pp. 1384–1400, 2001.

[104] D. Coutinho, M. Fu, and C. de Souza, "Input and Output Quantized Feedback Linear Systems," *Automatic Control, IEEE Transactions on*, vol. 55, no. 3, pp. 761–766, 2010.

[105] G. C. Goodwin, D. Q. Mayne, K. Chen, C. Coates, G. Mirzaeva, and D. E. Quevedo, "An introduction to the control of switching electronic systems," *Annual Reviews in Control*, vol. 34, no. 2, pp. 209–220, Dec. 2010.

[106] W. Langson, I. Chryssochoos, S. V. Raković, and D. Q. Mayne, "Robust model predictive control using tubes," *Automatica*, vol. 40, no. 1, pp. 125–133, Jan. 2004.

[107] D. Q. Mayne, M. Serón, and S. V. Raković, "Robust model predictive control of constrained linear systems with bounded disturbances," *Automatica*, vol. 41, no. 2, pp. 219–224, 2005.

[108] D. Limón, T. Álamo, F. Salas, and E. F. Camacho, "Input to state stability of min–max MPC controllers for nonlinear systems with bounded uncertainties," *Automatica*, vol. 42, no. 5, pp. 797–803, May 2006.

[109] M. Lazar, D. Muñoz de la Peña, W. P. M. H. Heemels, and T. Álamo, "On input-to-state stability of min–max nonlinear model predictive control," *Systems & control letters*, vol. 57, no. 1, pp. 39–48, Jan. 2008.

[110] H. Khalil, *Nonlinear Systems (3rd Edition)*. Prentice Hall, 2001.

[111] Z.-P. Jiang and Y. Wang, "Input-to-state stability for discrete-time nonlinear systems," *Automatica*, vol. 37, no. 6, pp. 857–869, Jun. 2001.

[112] D. M. Raimondo, D. Limón, M. Lazar, L. Magni, and E. F. Camacho, "Min-max model predictive control of nonlinear systems: A unifying overview on stability," *European Journal of Control*, vol. 15, pp. 1–17, 2009.

[113] D. Limón, T. Álamo, D. Raimondo, D. de la Peña, J. Bravo, A. Ferramosca, and E. Camacho, "Input-to-state stability: a unifying framework for robust model predictive control," in *Nonlinear Model Predictive Control*, L. Magni, D. Raimondo, and F. Allgöwer, Eds. Springer Berlin / Heidelberg, 2009, pp. 1–26.

[114] L. Magni, D. M. Raimondo, and R. Scattolini, "Regional Input-to-State Stability for Nonlinear Model Predictive Control," *Automatic Control, IEEE Transactions on*, vol. 51, no. 9, pp. 1548–1553, Sep. 2006.

[115] D. M. Raimondo, D. Limón, M. Lazar, L. Magni, and E. F. Camacho, "Regional input-to-state stability of min-max model predictive control," in *Proceedings of the 7th IFAC Symposium on Nonlinear Control Systems*, Pretoria, South Africa, Aug. 2007, pp. 116–121.

[116] Z.-P. Jiang and Y. Wang, "A converse Lyapunov theorem for discrete-time systems with disturbances," *Systems & control letters*, vol. 45, pp. 49–58, 2002.

[117] L. Grüne and J. Pannek, *Nonlinear Model Predictive Control: Theory and Algorithms*, ser. Communications and Control Engineering. Springer Verlag, Apr. 2011.

[118] D. Liberzon, "Quantization, time delays, and nonlinear stabilization," *Automatic Control, IEEE Transactions on*, vol. 51, no. 7, pp. 1190–1195, 2006.

[119] E. Agrell, T. Eriksson, A. Vardy, and K. Zeger, "Closest point search in lattices," *Information Theory, IEEE Transactions on*, vol. 48, no. 8, pp. 2201–2214, 2002.

[120] H. Lin and P. J. Antsaklis, "Stability and Stabilizability of Switched Linear Systems: A Survey of Recent Results," *Automatic Control, IEEE Transactions on*, vol. 54, no. 2, pp. 308–322, Feb. 2009.

[121] D. E. Quevedo, R. P. Aguilera, M. A. Pérez, P. Cortés, and R. Lizana, "Model Predictive Control of an AFE Rectifier With Dynamic References," *Power Electronics, IEEE Transactions on*, vol. 27, no. 7, pp. 3128–3136, 2012.

[122] R. P. Aguilera and D. E. Quevedo, "Stability Analysis of Quadratic MPC with a Discrete Input Alphabet," *Automatic Control, IEEE Transactions on*, under review, 2012.

[123] D. Mayne, J. Rawlings, and C. Rao, "Constrained model predictive control: Stability and optimality," *Automatica*, vol. 36, pp. 789–814, 2000.